Title
Micromagnetic Ratcheting Manipulation for Bioengineering Research Applications

Author
Murray, Coleman Tyler

Publication Date
2015

Peer reviewed|Thesis/dissertation

UNIVERSITY OF CALIFORNIA

Los Angeles

Micromagnetic Ratcheting Manipulation for Bioengineering Research Applications

A dissertation submitted in partial satisfaction of the requirements for the degree Doctor of Philosophy in Mechanical Engineering

by

Coleman Tyler Murray

2015

ABSTRACT OF THE DISSERTATION

Micromagnetic Ratcheting Manipulation for Bioengineering Research Applications

by

Coleman Tyler Murray

Doctor of Philosophy in Mechanical Engineering

University of California, Los Angeles, 2015

Professor Dino Di Carlo, Co-Chair

Professor Pei-Yu Chiou, Co-Chair

Richard Feynman in his famous address “There’s plenty of room at the bottom” illuminated the potential that nano and micro technologies had in extending our reach into the microscopic world. Specifically, his vision of “a hundred tiny hands” where motions at the human scale can be de-amplified to the micro scale are alluring because biological systems, such as cells and bacteria, occupy this scale. Indeed the ability to achieve microscopic motion control is essential for developing miniaturized systems for biological assays.

Magnetic ratcheting serves as a superior technique for high throughput micromanipulation to develop miniaturized systems due to its specificity, biocompatibility, and highly parallelized nature. Ratcheting manipulation uses an external magnetic field combined with arrays of micro-pillars composed of a magnetically soft alloy to generate localized potential minima in which superparamagnetic particles become trapped. When the external field is directionally cycled in a ratcheting manner, the particles follow the shifting potential minima and traverse across the micro pillar array with piconewton scale forcing. Using this

technique we have developed a high force (67pN) architecture to achieve highly parallelized manipulation (~$3x10^5$ manipulations/mm^2) for transporting magnetically labeled cells and or probing subcellular phenomena with magnetic particles. Using a mechatronic system to generate the ratcheting field, magnetic particles can be automatically or manually piloted via a joystick interface. We have demonstrated highly resolved particle mediated interface with cells and also automated manipulation of magnetically labeled cells for performing automated single cell assays.

The system's high force envelop also allows rapid transport and concentration of immunomagnetically labeled cells using nanoscale particles, enabling higher labeling efficiency and specificity. Using a funneling ratcheting array, endothelial cells labeled with 500nm particles were concentrated in a little as 15 minutes, showing potential as a point of care diagnostic and also operability in complex solutions such as blood. Additionally, our ratcheting manipulation system was used to achieve quantitative magnetic separation on micro-pillar arrays with gradient pitch. Here ratcheting was used to separate and concentrate cells based on surface expression but also enrich circulating tumor cells from clinical blood samples.

In addition to in vitro applications, we demonstrated a therapeutic use case in treatment of bacterial biofilm infections of intravenous catheters. Staphylococcus aureus biofilms gown on ratcheting substrates could be mechanically disrupted using magnetic particles combined with both static and dynamic forcing, potentially increasing antibiotic penetration into the biofilm matrix. Using this ratcheting "scrubbing" approach, a majority (~91%) of S. aureus biofilms were removed. This method of mechanically

perturbing the adhered biofilm shows promise as a minimally invasive treatment for biofilm infected catheters.

Magnetic ratcheting is a powerful tool which can be used to construct miniaturized systems for high throughput single cell operations or for therapeutic use to provide localized force in a minimally invasive manner. Ratcheting provides a vehicle to extend our reach into the microscopic length scale to solve problems or gain knowledge; providing us a million tiny hands to reach into, explore, and engineer in the microscale world.

The dissertation of Coleman Tyler Murray is approved

Chang-Jin Kim

Jeffery Eldredge

Pei-Yu Chiou, Committee Co-Chair

Dino Di Carlo, Committee Co-Chair

University of California, Los Angeles

2015

I would like to dedicate this work to some very special people who have helped me and supported me along the way. First I would like to give due credit to my Lord and Savior Jesus Christ who makes all things possible. He has carried me through tough times and has celebrated with me in victories. By Him and through Him all things were made and find their purpose. I would like to recognize my beautiful wife, Dayna, who has been my strength and my joy. She has been with me through thick and thin, bearing the burdens of life alongside me. I cannot begin to describe how thankful I am to have her. I also want to thank my mom and dad for I derive so much strength and encouragement from them. My mom has always covered me in love and prayer and my dad has always given me strength and shown me how to be a man of honor. My mom and dad have shown strength in the face of adversity and continue to inspire me today in their love and dedication to each other. I am also so thankful for my Grandee and Grandad, for their constant prayer on my behalf and unconditional love. I am blessed to have loving in-laws who have provided such amazing support for me. Finally I would like to recognize David Stroud for his amazing faith and grace in the face of extreme challenge. Dave fought a long battle against cancer which ultimately brought him home to the Lord. Though short, Dave's life inspired me to join the cause of serving others in developing new medical technologies. I hope that someday this work can be used to help others like Dave. I am so thankful for the people in my life and the wisdom they have given me. I am blessed with so much, and above all, I am blessed with a life full of rich relationships.

Table of Contents

Biographical Sketch

Coleman Murray has a background in mechanical design, robotics, and microelectromechanical systems (MEMS). He received his bachelor's degree in mechanical engineering from the University of California Santa Barbara with emphasis on mechatronics, fluid mechanics, and MEMS. He was accepted into the mechanical engineering program at UCLA and has worked under the guidance of Professor Dino Di Carlo in the department of bioengineering where he received his masters and continues to work as a Ph.D. student. His research focus is on implementing magnetic micro-technologies into high throughput and automated clinical research tools.

Chapter 1 Magnetic MEMS in Bioengineering Applications

In his famous address “Plenty of Room at the Bottom” [1], Richard Feynman conceptualized the idea of “a hundred tiny hands” where a set of robotic arms pilots a sequentially smaller and smaller set for the purpose of extending control from the human scale to the microscopic scale. This notion of miniaturized control has been and continues to be a driving current in many innovation frontiers, particularly in those relating to health and biological sciences. Due to the extremely complex and interconnected nature of biological systems, miniaturized and parallelized tools that operate with single cell resolution are essential for expedited biological discovery [2,3]. Indeed lab-on-a-chip (LOC) technologies have substantially increased the capabilities of biological research, enabling investigators to rapidly extract data and construct models with extremely high information granularity.

In order to develop fully integrated systems capable of carrying out automated biological assays, LOC systems require robust and specialized sample handling and manipulation. For one, these systems are often required to perform operations involving complex samples such as blood or tissue digests. Therefore, selective manipulation or integrated filtration platforms which can isolate and sequentially manipulate only desired cell types from the biosamples are advantageous. Additionally, high resolution and high fidelity manipulations are important for use cases involving subcellular interrogation as many cellular activities, such as immune synapses or cellular polarization, occur at nanometer length scales. Therefore, manipulation systems with nanometer scale resolution are needed to probe and stimulate these phenomena. Finally, manipulation throughput is a major system requirement in order to

generate statistically relevant data with high granularity ideally with operational performance in the MHz to GHz regimes. Generally lab on a chip systems perform manipulation operations through a variety of methods the most popular being: microstructure, optic, electric, and magnetic force fields (Figure 1-1).

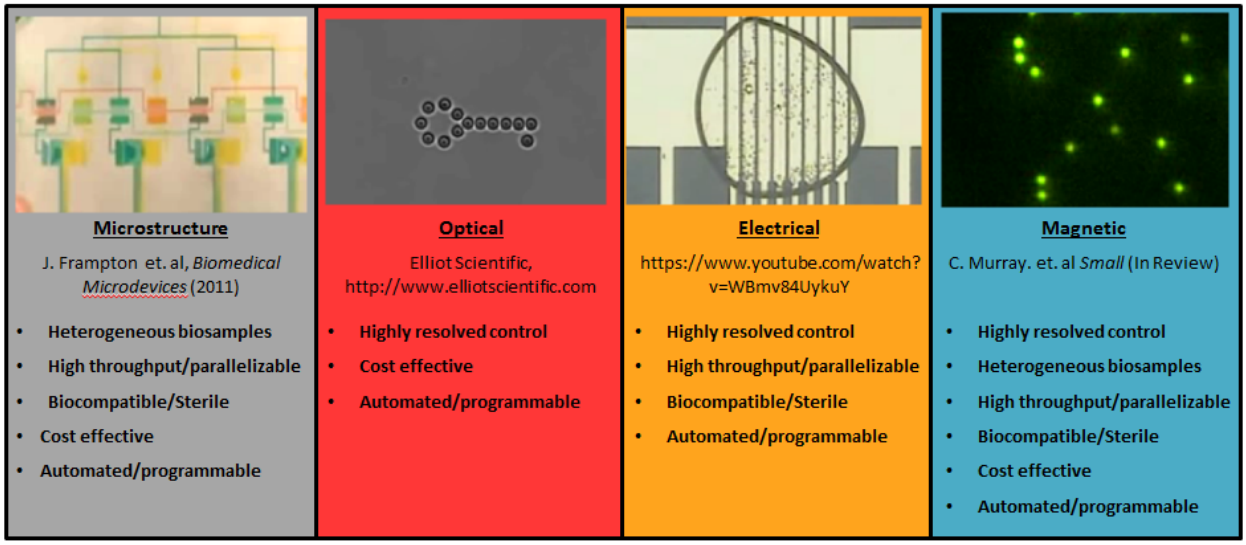

Figure 1-1: Manipulation platforms for lab-on-a-chip systems include but are not limited to microstructure based manipulation such as pneumatically deformed PDMS channels, optical manipulations such as optical tweezers, electrical manipulations such as electro-wetting on dielectric, and magnetic manipulation such as magnetic tweezers. Magnetic manipulation offers many advantages over other platforms as it can achieve nanometer scale manipulations, work with complex biosamples, is highly parallelizable, can enact forces in sealed/sterile systems, can be produced inexpensively, and can be easily automated.

Of these architectures, magnetic manipulation platforms are of advantageous for several reasons. Primarily, magnetic systems can achieve highly resolved, nanometer scale control allowing users interface at subcellular length scales. Secondly, magnetic architectures work well in heterogeneous biosamples as manipulation can be specific to a desired cell population using immunomagnetic labeling. Additionally magnetic techniques have excellent biocompatibility and are routinely used in biomedical

applications as research tools, such as magnetic activated cell sorting (MACS)[4], and diagnostic instruments, such as CellSearch[5]. Using magnetic microstructures, these systems can be highly parallelized enabling high throughput capabilities in the GHz ranges. Furthermore, many magnetic LOC techniques can be produced monolithically, in a cost effective manner and can also be easily automated for reliable assay development. In addition to the platform advantages, magnetic particles are excellent vehicles for microscopic interface due to their ability to conjugate functional groups to their surface. Magnetic particles are used for a myriad of applications including tagging cells based on a receptor/ligand interaction[6], force or biochemical mediated cell stimulation[7,8], and MRI contrast agents[9] for diagnostic uses. Because magnetic particles offer this "plug and play" like flexibility, they can be used powerfully in LOC operations.

Magnetic based LOC systems have been a research focus since the early two thousands[10] and have been integrated into numerous instruments and assays. While a few magnetic manipulation techniques operate through actuating magnetic structures[11,12], the vast majority achieve manipulation by the use of magnetic particles[13] or magnetic colloidal solutions[14]. Magnetic particles are widely in bioassays for diagnostic and therapeutic applications[5,15,16,17,18] due to their high biocompatibility, chemical stability and surface customizability. For example, magnetic particles can be used to exert mechanical force for microfluidic mixing applications[19] or exclude volume for size based particle separation and concentration[20]. Additionally, by functionalizing the magnetic particle surface with specific ligands, such as an antibody, targeted entities can be magnetically tagged, separated and concentrated upon application of a

magnetic field, a technique known as immunomagnetic labeling. Immunomagnetic labeling is a commonly used in research and industry applications for highly efficient capture and concentration of target antigens or cells[4,21,22]. One of the most well-known methods for precipitating magnetically labelled cells or bacteria is magnetic activated cell sorting (MACS)[23] which has since developed into several commercial products[4]. This method involves generating a high intensity magnetic field localized to specific points on a sample reservoir, usually a centrifuge tube, in order to extract magnetically labeled targets from the bulk solution (Appendix A). MACS is commonly used to capture specific populations of cells or bacteria but also can be used to deplete a sample of an unwanted population such as apoptotic sperm for in vitro fertilization procedures[24]. While powerful, traditional MACS systems have some significant drawbacks. Traditional MACS techniques utilize macroscale magnetic fields and macroscale field gradients for extraction which is important due to the fact that magnetophoretic force magnitude is dependent on the magnetic field strength, the field gradient and the volume of magnetic content within each particle. Shown in Equation 1 is the derived magnetic force, $\boldsymbol{F_{mag}}$, on a superparamagnetic particle in an aqueous environment where $\boldsymbol{V_p}$ is the volume of the particle, $\boldsymbol{\chi_p}$ is the difference in magnetic susceptibility between the particle and the surrounding medium, $\boldsymbol{\mu_o}$ is the magnetic permeability of free space, and $\boldsymbol{B}$ is the magnetic flux density of a local magnetic field[25].

$$\boldsymbol{F_{mag}} = \frac{\boldsymbol{V_p}\,\boldsymbol{\chi_p}}{\boldsymbol{\mu_o}}\,(\boldsymbol{B}\cdot\boldsymbol{\nabla})\boldsymbol{B} \qquad \textbf{Equation 1}$$

For macroscale systems (characteristic length≥ 1mm) the field length scale is large relative to the micro or nano scale particles, resulting in a weak field gradient and a limited magnetophoretic force envelope. This is usually compensated by using larger

particles (diameter ≥ 3μm) to amplify the magnetophoretic force. However, large particles have limited binding efficiency due to their small diffusion lengths and therefore must be used in high concentrations[26] to ensure effective binding. However, this leads to extremely high particle backgrounds as well as high off target labeling leading which leads to an impure separation. Therefore, miniaturization of MACS systems is advantageous as scaling down magnetic systems can potentially yield more efficient and high purity separations. Indeed many microfluidic MACS systems have been developed for efficient separation of immunomagnetically labeled targets. For example Pamme et. al 2006 developed a microfluidic MACS system for continuous separation of magnetically labeled cells in a microfluidic channel using an externally applied magnetic field applied orthogonal to a flow cell[27]. Cells with varying amount of bound or internalized magnetic particles would migrate across streamlines and end up in different outlets depending on their bound magnetic content. Here the characteristic length scale was on the order of ~100μm enabling more rapid separation compared to traditional MACS due to the reduction in required distance of separation. However, most of these systems still utilize a bulk field gradient and therefore must be processed at low throughput on the order of mL per hour, especially when using smaller particles.

In order to amplify the magnetophoretic force, several LOC systems have employed the scaling characteristics of magnetics to drastically increase the magnetic force envelope via the use of magnetic microstructures. By introducing magnetically permeable microstructures, most often composed of nickel, iron or permalloy, the magnetic field gradient can be increased several orders of magnitude compared to the bulk field as shown by the gradient term in Equation 1. Indeed many technologies

utilize thin films structures with high magnetic permeability to collect of guide immunomagnetically labeled targets. For example, Adams et. al. 2008 ferromagnetic strips into a continuous flow microfluidic device to locally amplify the magnetic field gradient near the strips and achieve higher force and flow throughput[28,29,30]. Additionally, integrated current carrying wires have been used to supply high gradient magnetic micro-fields to manipulate magnetic particles for LOC applications[31,32]. In addition to continuous flow bases systems, many technologies using static magnetic microstructures have been used for LOC applications. Tseng et. al. utilized high aspect ratio permalloy microstructures to explore intracellular force application of adherent cells with internalized superparamagnetic iron oxide nanoparticles (SPIONs)[8] and Kunze et. al utilizes a similar platform to study intracellular forcing in cortical neurons[7]. Chen et. al. 2015, utilized thin film magnetic structures to extract colon carcinomas spiked into blood[33]. While these methods are powerful they have limitations for use in performing dynamic lab-on-a-chip operations such as manipulation or sorting.

An altogether different magnetic manipulation technology which shows applicability in LOC systems is magnetic ratcheting. Magnetic ratcheting (Movie S1), also known as magnetic domain wall manipulation, has been extensively studied as a method to discretely transport magnetic particles or magnetically labeled cells with high precision and accuracy[34,35,36,37,38,39,40]. Magnetic ratcheting utilizes arrays of magnetically soft microstructures combined with a directionally cycled magnetic field create dynamic potential energy wells that can trap and manipulate magnetic particles or labeled cells. Most often, these arrays are assemblies of micro-pillars composed of a magnetically permeable metal or alloy such as nickel or permalloy. Upon application of

a magnetic field the micro-pillars magnetize according to their shape and applied field direction thereby modifying the magnetic potential energy landscape introducing dynamic potential wells in which superparamagnetic particles become trapped (Figure 1-2a). The location of these potential wells relative to the micro-pillars is dependent upon the applied orientation of the bulk field and the micro-pillar geometry. For example, when the applied magnetic field runs parallel to the array plane, the micro-pillars will magnetize radially creating a potential well at the edge of the micro-pillar (Figure 1-2b). In plane rotation of the applied magnetic field causes the potential well to migrate around the edge of the pillar yielding angular transport of the magnetic particles[41]. When the applied field is reset, or ratcheted, the nearest potential well will be located at the edge of the next pillar and can therefore be transported across the array. This method of magnetic ratcheting has been most commonly utilized as the micro-pillar elements are thin and have a magnetization bias in the radial direction. Similarly, the rotation of the applied magnetic field can be performed orthogonal to the array plane where particles can be transported across the diameter of the pillar (Figure 1-2c). Of note however that ratcheting orthogonal to the array plane can only be achieved by micro-pillars with a close 1:1 aspect ratio, which will be covered in the next chapter.

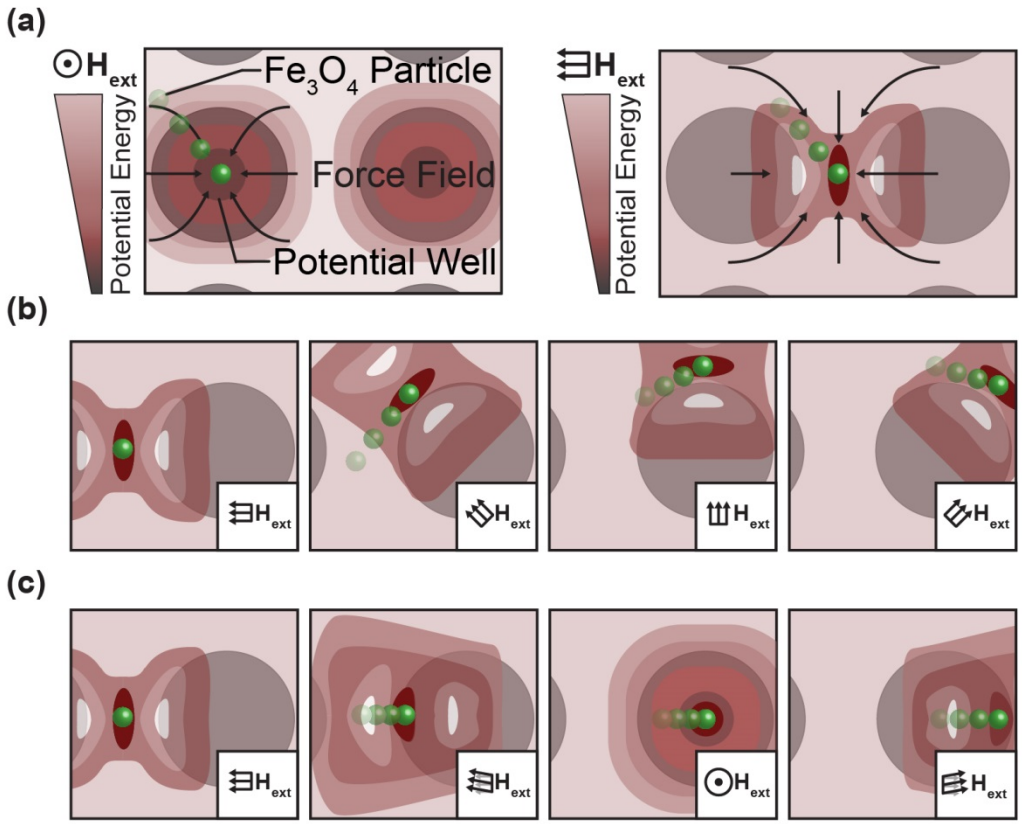

Figure 1-2: Magnetic ratcheting arrays consisting of micro-pillars of soft magnetic material with high relative permeability. (a) In the presence of an applied magnetic field, the micro-pillars modify the magnetic potential energy landscape introducing local minima which superparamagnetic particles magnetophoretically migrate to. The magnetic properties, shape and direction of the applied field determine the location of the potential wells. (b) In plane rotation and ratcheting of the applied field causes particles to migrate around the edge of the micro-pillar where it can be transferred to the neighboring pillar and translate through the array. (c) Similarly, the field can be cycled normal to the array plane causing particles to ratchet across the micro-pillars.

Magnetic ratcheting is advantageous as a LOC manipulation technology for several reasons. First, the presence of the magnetically soft micro-pillars amplifies the field gradient several orders of magnitude enabling a substantial magnification of magnetophoretic force as shown in Equation 1. The ability to apply larger magnetophoretic force not only speeds up processing time but also enables the use of small magnetic particles, such as superparamagnetic nanoparticles (SPIONS), which have significant advantages over larger particles (≥3μm) particularly in cell labeling

efficiency and minimal particle background. Additionally, macro scale rotations in the applied magnetic field de-amplify to nanoscale shifts in particle equilibrium positions allowing for precise positioning without the use of complex gearing or mechanical coupling. Finally, magnetic ratcheting techniques can be massively parallelized where millions of manipulations can be carried out simultaneously which is required of multiplexed and high throughput systems.

Indeed magnetic ratcheting offers many advantages and has been the focus of this work in implementing this technique for biomedical research applications. Chapter 2 will focus on the specific design rationale, numerical simulations and governing equations for our novel magnetic ratcheting system. Additionally, mechatronic system components design and construction will be discussed and finally, system ratcheting forcing and transport behavior will be described. Chapter 3 outlines a preliminary biomedical implementation of our ratcheting system where endothelial cells can be magnetically labeled and rapidly purified with high efficiency and purity. In Chapter 4 we demonstrate the power of the system to quantitatively separate particles based on magnetic content and cell populations based on surface marker expression. Finally, in Chapter 5 we show the system's ability to impart highly localized forces in order to scrub surfaces of bacterial biofilms for therapeutic uses.

Potential Market Impact for Magnetic Ratcheting LOC Systems

Before moving on, the potential impact of ratcheting technology should be discussed as a potential commercial product. Transition of technology from academic labs to a commercial enterprise is often the most direct path for a technology to benefit society, especially in biomedical and clinical settings. Lab on a chip technologies are

part of rapidly growing global market that was valued at $3.4 billion in 2012 and is expected to reach $14.4 billion in 2018[42]. Figure 1-3 shows the total addressable market (TAM) of biochip based technologies showing substantial growth in all market segments. Specifically the lab on a chip market segment occupies of 33% of the TAM and was valued at $2.1 billion in 2014.

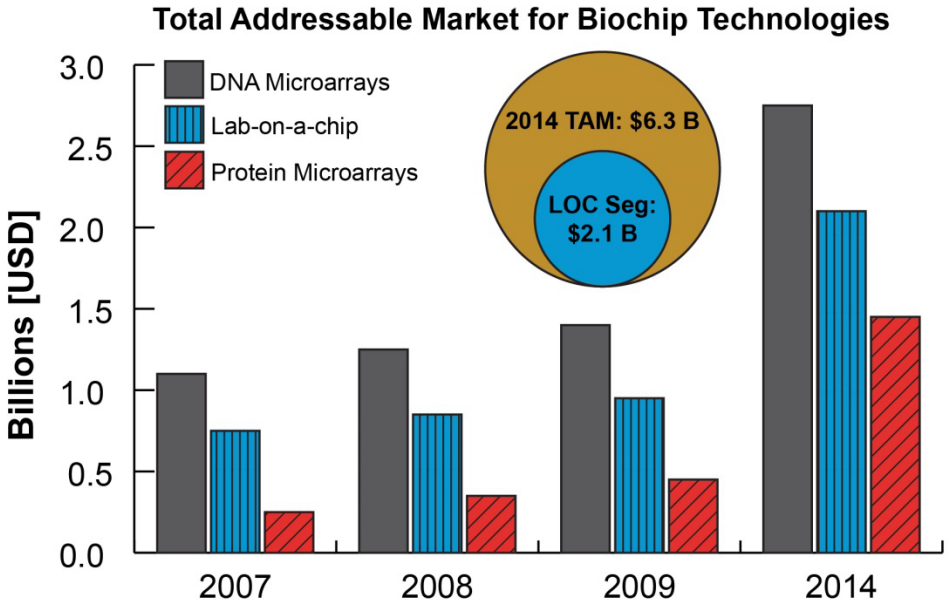

Figure 1-3: Total addressable market for biochip technologies consisting of DNA microarray, Lab-on-a-chip, and protein microarray market segments. In 2014, the TAM was valued at $6.3 billion and the LOC segment valued at $2.1 billion, occupying approximately 33% of the market share. Adapted from *Global Biochip Markets: Microarrays and Lab-on-a-Chip* market report[42].

The LOC market segment is further broken into proteomic, structural proteomic, electrophoretic separation, polymerase chain reaction (PCR), immunoassay, and sequencing chip based products. Almost all of the current product offerings utilize fluid, electrical or microstructure based cell manipulation architectures to perform operations. However, one of the large challenges faced by current LOC technologies is the production cost and complexity of operation. For example, one of the most successful

LOC technologies has been the Biomark™ HD single-cell sequencing system from Fluidigm® which utilizes microstructure manipulation to isolate single cells and perform sequencing operations. While powerful, this system has significant unit cost of approximately $1000 per chip[43] and a base instrument cost of approximately $100,000. Another LOC product from Silicon Biosystems, known as the DEP Array™, relies on dielectrophoretic forces to manipulate cells. This system also has a high per chip cost and a base instrument cost of $400,000. Both of these systems are fairly complex where chip production consists of several lithographic, etching and alignment processes to produce, not to mention the complex quality control required for these integrated systems. Indeed the complexity of these systems is one of the main cost drivers, increasing prices and also decreasing system robustness.

As stated earlier, magnetic ratcheting can provide a superior manipulation architecture compared to the commonly utilized techniques today for several reasons. Primarily, ratcheting chip production cost is quite low compared to other cleanroom produced LOCs as they can be produced monolithically (not including overlaid fluid channels) and can be scaled up to high volume production easily. Finally they are robust, as the magnetic field is the sole driver of manipulation, and do not require physical or electrical connections; nor do they have any moving parts. This robustness and seamless integration into current working practices makes magnetic ratcheting a powerful tool for developing LOC products, addressing many of the technical and economic shortcomings of current technologies.

Chapter 2 : Ratcheting Transport through Permalloy Micro-pillar Arrays

As described in Chapter 1, ratcheting transport of magnetic particles is achieved using arrays of magnetically soft micro-pillars combined with a directionally cycled magnetic field to dynamically modify the potential energy landscape and translate particles through the array. This transport is dependent on several variables including the local magnetic flux density $\boldsymbol{B}$, the pillar diameter, $\boldsymbol{D_{pillar}}$, the pillar aspect ratio, $\boldsymbol{AR_{pillar}}$, the micro-pillar's relative permeability, $\boldsymbol{\mu_{pillar}}$, the pillar pitch, $\boldsymbol{P}$, the differential susceptibility between the particle and the medium, $\Delta\boldsymbol{\chi_p}$ **,** and the particle geometry in terms of volume and diameter, $\boldsymbol{V_p}$ & $\boldsymbol{D_p}$. The key parameter of the ratcheting system is the force density, $(\boldsymbol{B}\cdot\boldsymbol{\nabla})\boldsymbol{B}$, which drives the magnetic forcing behavior for a given particle size and magnetic content (Equation 1). The force density is a time dependent vector field which is a function of $\boldsymbol{B}$ which is in turn a function of $\boldsymbol{D_{pillar}}$, $\boldsymbol{AR_{pillar}}$, $\boldsymbol{\mu_{pillar}}$,$\boldsymbol{P}$, and the applied magnetic field $\boldsymbol{H_{ext}}$. Essentially, the force density breaks down into two key factors; that is, the magnitude of the magnetic flux density and the flux density gradient. Firstly, magnetic ratcheting amplifies the force density by the flux density magnitude due to the fact that that $\boldsymbol{\mu_{pillar}}$ is large compared to the permeability of free space, $\boldsymbol{\mu_o}$, by approximately 8500 fold (Appendix B). Therefore, upon application of a magnetic field, $\boldsymbol{H_{ext}}$, the local magnetic flux density is substantially amplified (Equation 2).

$$\boldsymbol{B = \mu_{pillar}\mu_o\, H_{ext}} \qquad \textbf{Equation 2}$$

Secondly, the force density is amplified by scaling the magnetic field to the microscale. For example, a field with a micron characteristic length scale will have a relatively enormous gradient compared to a field with a centimeter characteristic length scale. In

this way, the scaling laws of magnetics can be exploited to impart highly resolved manipulative control on magnetic particles but also amplify force approximately three orders of magnitude higher than possible with a bulk magnetic field.

The Importance of Pillar Aspect Ratio in Magnetic Ratcheting

A subtle but important characteristic that has challenged previous ratcheting platforms is resultant from array geometry, specifically the aspect ratio of the micro-pillars themselves. Traditional ratcheting arrays are produced by first photolithographically patterning a stencil on a glass or silicon substrate and depositing magnetically soft metals such as nickel, cobalt, or permalloy using a sputterer or e-beam evaporator[36,44]. Once deposited the photolithographic layer can be stripped producing micro-pillar arrays of magnetically soft material. However, metal deposition via evaporation is limited to producing thin films (>1μm) due to time and cost barriers and result in pillars with an extremely low aspect ratio usually on the order of 0.05. While functional, these low aspect ratio elements have several limitations. First, the force applicability is low for these substrates, on the order of 5-10pN[41], (Figure 2-1) which limits the throughput capability. To compensate, thin film ratcheting systems often utilize larger particles (≥3μm), however larger particles are often cumbersome to work for several reasons. Large particles have small diffusion lengths yielding low binding efficiency to target cells and also cannot be used to easily probe subcellular phenomena. Additionally, thin film ratcheting pillars can only be magnetized radially due to high shape anisotropy (Appendix C) and can therefore only generate potential minima along the pillar edge. This limits the system resolution as there exists large

"dead zones" (Figure 2-2) where manipulations cannot be performed which can prove problematic if the zone of interest lies in one of these zones.

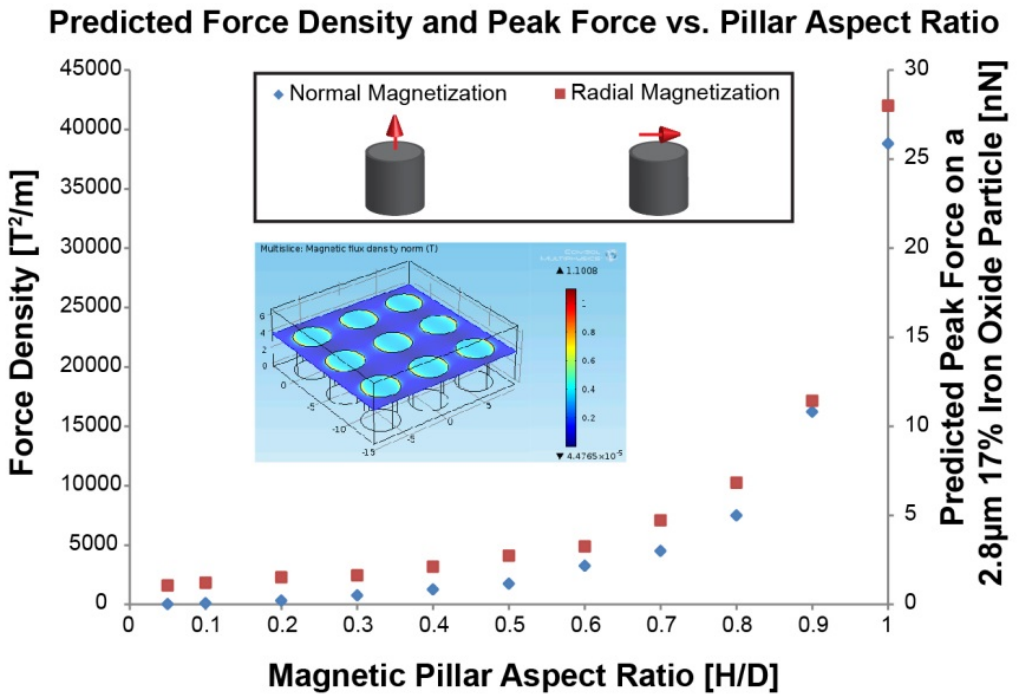

Figure 2-1: Predicted force density, ($B \bullet \nabla B$, and peak force on a 2.8µm magnetic particle (V_p=1.95µm^3, 17% Fe_3O_4, χ_p=0.65,μ_o=4π 1e-7 Tm/A) as a function of pillar aspect ratio was simulated using Comsol 4.2 Magnetostatics module. In the simulation the pillars were set to have a relative magnetic permeability of 8500, a diameter of 4µm, an orthogonal pitch of 6µm and a height derived from the corresponding aspect ratio. Boundary conditions included a 300mT inward flux density with either a normal (parallel to the pillar axis) or radial (parallel to the pillar radii) orientation. The force density was numerically calculated at the surface of each pillar and the magnetic force derived for a 2.8µm magnetic particle.

However, increasing micro-pillar aspect ratio to near unity amplifies the predicted force applicability by one to two orders of magnitude for both normal and radial magnetizations (Figure 2-1). This higher force envelope not only extends the transport throughput of particles and cells but also enables the use of nanoscale particles for higher labeling efficiency and precise biological interfacing. Furthermore, due to the

near isotropic shape, AR≈1 ratcheting arrays can achieve near continuous manipulation at nanometer scales for probing subcellular phenomena (Figure 2-2).

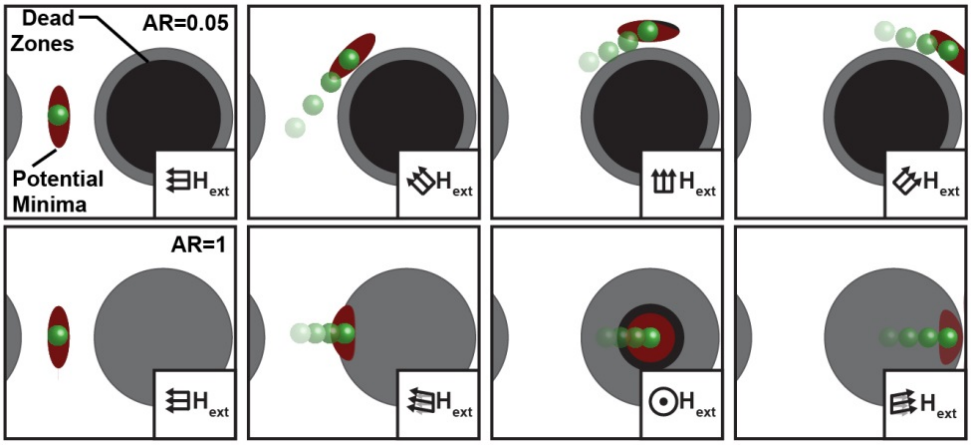

Figure 2-2: Thin film ratcheting arrays can only generate potential minima at the pillar edge, thereby yielding large dead zones in the middle of the pillars where particles cannot be manipulated. AR=1 ratcheting arrays can achieve high manipulation resolution due to the fact that the magnetization can occur in any direction due to a more isotropic shape. Particles can be manipulated around or through the pillars.

As such, ratcheting manipulation is best achieved when $\boldsymbol{AR_{pillar}}$≈1, enabling higher force applicability and higher manipulation resolution. Though subtle, it is this characteristic that distinguishes this body of work from previous ratcheting platforms, enabling highly parallelized and high force magnetic ratcheting manipulation to be better implemented high throughput transport and nanometer scale manipulation.

Modeling Magnetic Ratcheting Manipulation on Unity Aspect Ratio Arrays

Ratcheting transport on unity aspect ratio arrays can be performed in multiple modalities, either around the pillar edge but also through the pillar radius (Figure 2-2) to achieve rapid transport or finely tuned manipulation. To determine the force envelope we developed a 1 dimension transport model using Comsol® numerical simulations to determine the average force density.

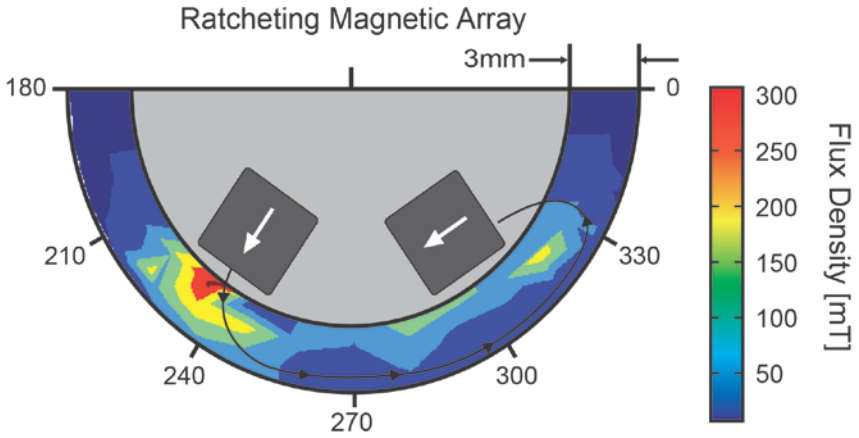

Figure 2-3: Magnetic wheel with a partial halbach array of N-52 grade rare earth magnets. As shown the peak flux density is 300mT with an average flux density of ~ 100mT with a radial distance of 3mm from the surface of the drum.

To provide physically relevant input to the numerical simulations, a magnetic wheel was fabricated using 3/8" rare earth cube magnets (N-52 grade) arranged into a quasi halbach array. As measured by a gauss meter and shown in Figure 2-3, the field provided by the magnetic wheel ranged between 50 - 300 mT in strength with a ratcheting field direction encoded by angular location. Field values at 2mm radial distance and 10 degree intervals across the wheel circumference were used as boundary conditions for the numerical simulations using Comsol® Magnetostatics Module (Figure 2-3 & Appendix D).

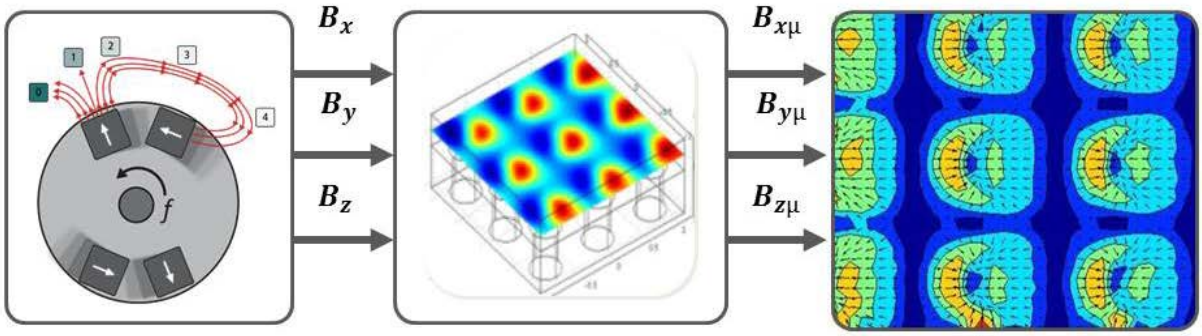

Figure 2-4: Process flow for numerical simulations of ratcheting on AR_{pillar}**≈1** arrays. (i) First, the magnetic wheel with partial halbach array was constructed and measured to confirm ratcheting field generation. Field measurements, B_x, B_y, B_z, were taken at 10º intervals across the ratcheting cycle and used as boundary conditions for numerical simulations of the ratcheting arrays. (ii) From the numerical simulations the three dimensional micro-magnetic field, $B_{\mu x}, B_{\mu y}, B_{\mu z}$**,** was calculated and the (iii) force density was calculated at varying z slices.

Key assumptions and design constraints in the modeling included: pillar pitch, P**,** ranged from 6 to 8μm, D_{pillar}=4μm and AR_{pillar}=1. An array of three by three micro-pillars was simulated with boundary conditions as measured from the magnetic wheel. Additionally, the pillar permeability μ_{pillar} was assumed to be constant with a value 8500 as previous work with permalloy electroplated microstructures which yields this value in fields ≤1 Tesla (Appendix B). From these simulations, the three dimensional micro-magnetic field within the arrays**,** $B_{\mu x}, B_{\mu y}, B_{\mu z}$, were determined for each design for each 10º interval on the magnetic wheel. The force density vector field was calculated numerically using Matlab® at cross sections at thickness, t**,** above the pillars (Movie S2) demonstrating translating and stable equilibrium positions through the ratcheting cycle (Figure 2-5).

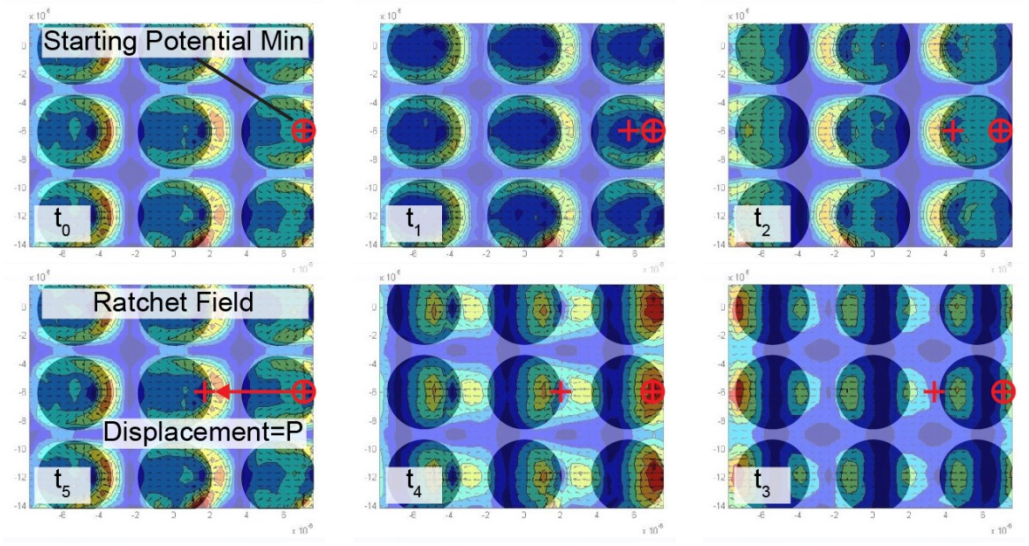

Figure 2-5: Time series of force density showing translating dynamic potential wells. Particle will displace by ***P*** every half cycle of the wheel or ***2P*** every full wheel cycle.

Setting an origin at the center of the middle pillar in the array, the average force density value was derived by sampling values along the horizontal axis. The average force density was calculated by averaging the values between stable equilibrium positions at sequential cycles and then averaged over the entire ratcheting cycle. Figure 2-6b shows the total averaged force density over the ratcheting cycle for three designs with 6, 7, and 8μm pitches at varying thicknesses above the pillar. Averaged force density did not substantially vary with modulating pitch between 6-8μm but was extremely sensitive to the thickness above the pillars. Therefore, ensure that the thickness above the pillars remained minimal in design and fabrication of these chips, ideally 1μm or less to ensure maximum forcing capabilities.

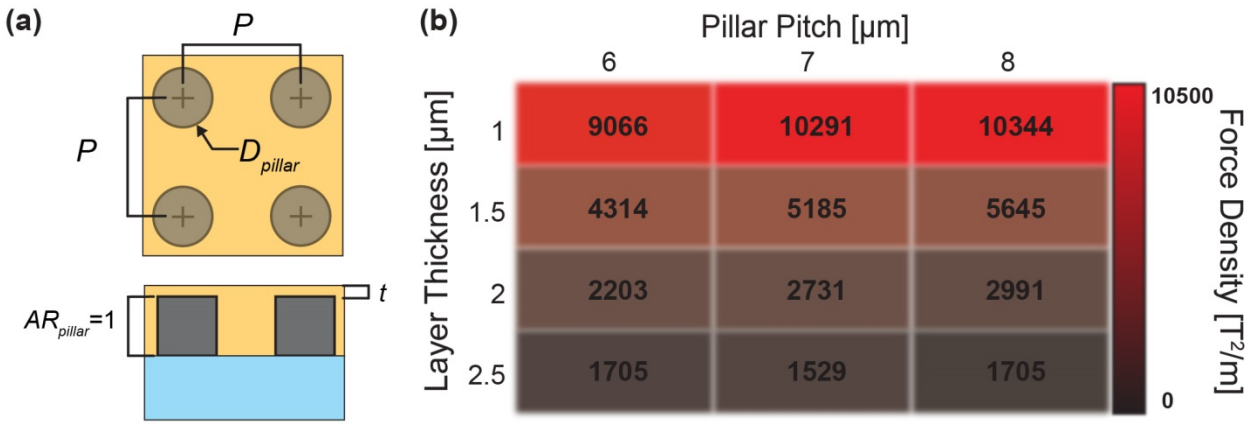

Figure 2-6: (a) Ratcheting array geometry can be characterized in terms of pitch ($\boldsymbol{P}$), pillar diameter ($\boldsymbol{D_{pillar}}$), pillar aspect ratio ($\boldsymbol{AR_{pillar}}$), and thickness of planarizing layer ($\boldsymbol{t}$). (b) Force density values averaged over a ratcheting cycle ranged from 1500-10,000T^2/m depending on thickness.

Assuming a 1.5µm layer above the pillars, the model predicts an average force density of 5185 T^2/m which correlates to a 3µm particle with 17% iron oxide content will experience a 59pN force (assuming $\boldsymbol{P}$= 7µm and $\boldsymbol{\Delta\chi_p}$=0.007). To put this in perspective a 59pN force can move a cell (~25µm diameter) at a speed of 250µm/s or 10 cell diameters per second. Assuming 50% of the ratcheting array is occupied by cells, the system can achieve approximately 11GHz/cm^2 of manipulation. This demonstrates the power of magnetic ratcheting to achieve extremely high throughput operations on single cells.

Using the average force density values, an analytical model for ratcheting transport was derived to develop operational intuition and design rules. Based on previously published model from Lim et. al. 2014[41], one dimensional ratcheting transport of particles can be modeled as a traveling wave.

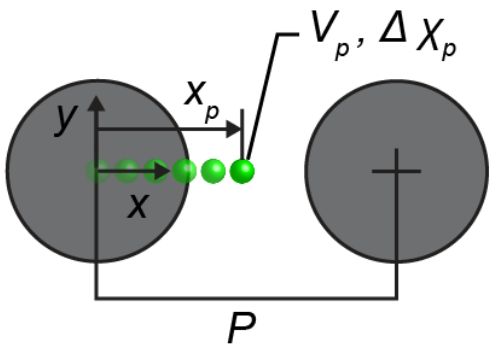

Figure 2-7: Modeling of ratcheting transport through an array with pitch ***P*** traversing along the x axis through the pillar radii. The particle distance is denoted as x_p and has volume V_p and magnetic susceptibility $\Delta\chi_p$.

Assuming a particle is being ratcheted from left to right along the x axis (Figure 2-7), the force experienced by the particle, F_x, can be described in terms of the particle volume, particle susceptibility, averaged force density, the particle location, the ratcheting frequency, and time (V_p, $\Delta\chi_p$, F_{den}, x_p, ω_{ext} , and t respectively). As shown in Equation 3, the force amplitude is a proportional to V_p, $\Delta\chi_p$, and F_{den} and the particle location is modeled in traveling wave form.

$$F_x = \frac{V_p \Delta\chi_p}{\mu_o} F_{den} \sin\left(\frac{2x_p}{P} - 2\omega_{ext} t\right) \qquad \textbf{Equation 3}$$

The magnetic force is balanced by fluidic drag and can be approximated using Stokes drag equation (Equation 4). The Stokes drag assumption is valid due to the fact that the particle's Reynolds Number and Stokes number are <<1 for the operating frequency and pitch range. Here μ_f represents the fluid viscosity, r_p is the particle radius, and $\overline{u_p}$ is the particle speed.

$$F_{drag} = 6\pi\mu_f r_p \overline{u_p} \qquad \textbf{Equation 4}$$

By equating the forces, a value for the particle speed can be derived which is dependent the balance of the particle magnetic properties and size as well as the array geometry.

$$\overline{u_p} = \frac{V_p \Delta\chi_p}{\mu_o} F_{den} \frac{1}{6\pi\mu_f r_p} \sin\left(\frac{2x_p}{P} - 2\omega_{ext} t\right)$$ **Equation 5**

Making the transformation (Equation 6) into traveling wave notation Equation 5 can be transformed into Equation 7, where Ω represents the phase lag of the particle within the traveling wave of the ratcheting field.

$$\Omega = \frac{x_p}{P} - \omega_{ext} t$$ **Equation 6**

$$\frac{d\Omega}{dt} = -\omega_{ext} + \omega_c \sin(2\Omega)$$ **Equation 7**

Here ω_c represents the critical frequency of the particle and is described in Equation 8.

$$\omega_c = \frac{V_p \Delta\chi_p F_{den}}{\mu_o 6\pi\mu_f r_p P}$$ **Equation 8**

As shown, the critical frequency is governed by the particle size and magnetic properties but also the averaged force density and array geometry. When $\omega_{ext} \leq \omega_c$ then $\Omega \leq \frac{\pi}{2}$ and there exists a homogeneous solution for Equation 7 where the particle can find a stable phase within the traveling wave. This results in a linear transport behavior and the particle will traverse the array with an average speed of $\overline{u_p} = P\frac{\omega_{ext}}{2\pi}$ or $\overline{u_p} = Pf$, where $f = \frac{\omega_{ext}}{2\pi}$ and $f_{crit} = \frac{\omega_c}{2\pi}$ (Figure 2-8).

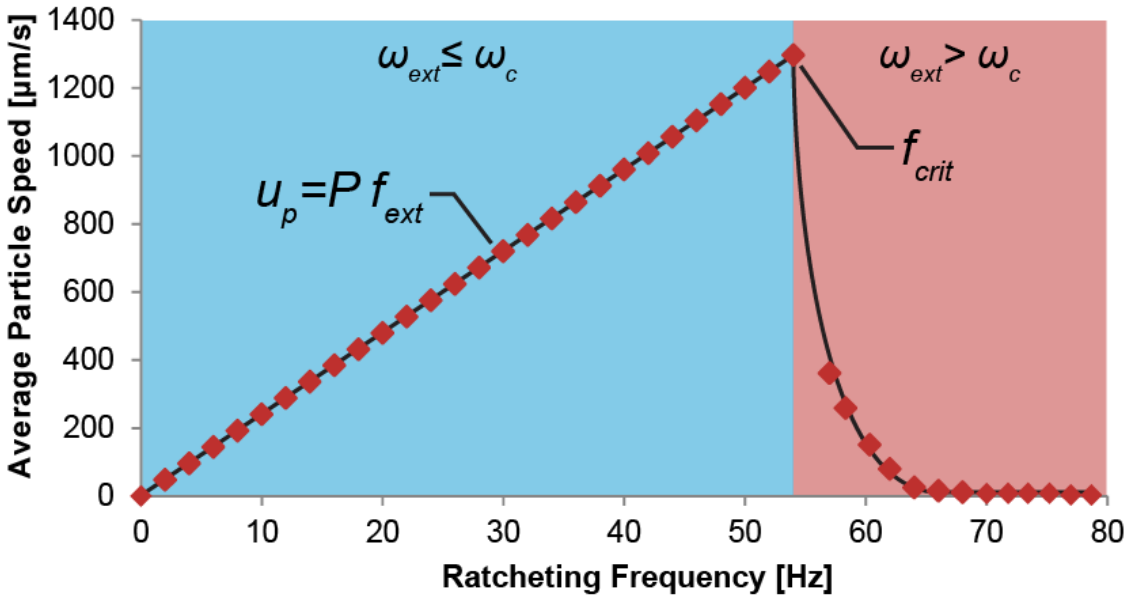

Figure 2-8: Analytical solution of Equation 7 shows predicted frequency response behavior of a 3µm particle as calculated by numerically solving Equation 7. When $\boldsymbol{\omega}_{ext} \leq \boldsymbol{\omega}_c$, the particle can find a stable phase within the traveling wave, thereby demonstrating a linear relationship between ratcheting frequency and particle speed. In this regime, the particle speed can be described as $u_p = P f_{ext}$ where f_{ext} is the ratcheting frequency in Hz. When $\boldsymbol{\omega}_{ext} > \boldsymbol{\omega}_c$, the particle begins to chase or lag behind the traveling wave and the particle speed decays quickly with increasing f_{ext} until the particle fails to traverse the array and oscillates on the pillar edge.

However when $\boldsymbol{\omega}_{ext} > \boldsymbol{\omega}_c$, $\boldsymbol{\Omega}$ becomes larger than $\frac{\pi}{2}$ and the particle fails to find a stable phase within the traveling wave, sometimes missing the translating equilibrium positions. When the external frequency is further increased, the particle will fail to transport altogether and will oscillate on the edge of the pillar. The predicted critical frequency for a 3µm particle ratcheting on a 7µm pitch array is approximately 51Hz meaning that the system can achieve speeds of 1.2mm/s or 171Hz if normalized to pillar pitch. Due to this rapid transport capability, rapid manipulation and processing of particles and cells can be achieved. Combining the high speed transport capabilities of

the ratcheting system combined with the highly parallelized nature demonstrates the power of the tool to carry out multiplexed lab-on-a-chip operations.

The critical frequency is a critical design parameter and can be used to intelligently design and operate ratcheting systems for biologically relevant applications. For example, the critical frequency is dependent upon both particle size and magnetic properties and therefore will exhibit different transport behavior trapping at critical frequencies depending on their size and magnetic content (Figure 2-9) and has been demonstrated in thin film ratcheting systems as well[34].

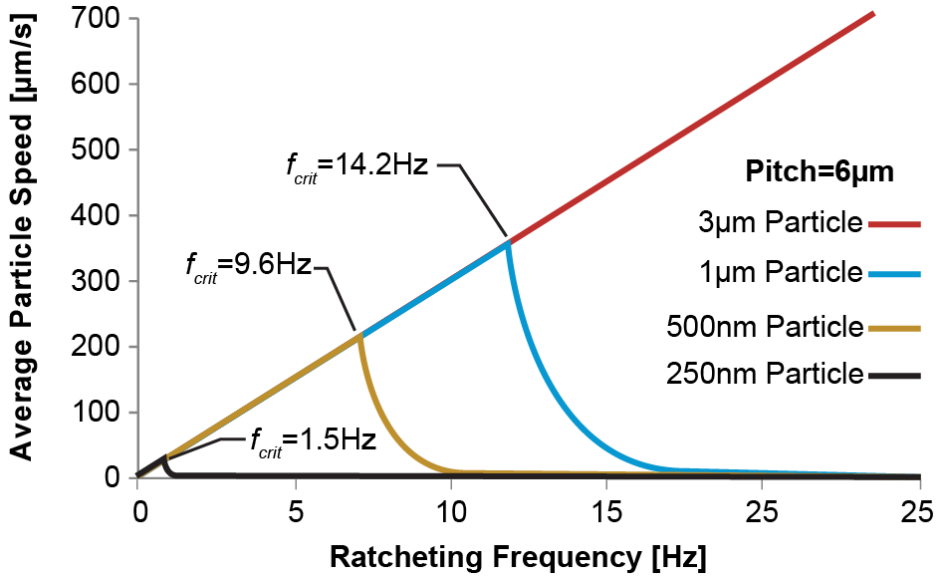

Figure 2-9: Predicted frequency response on a 6µm pitch for 3, 1, 0.5, and 0.25µm diameter particles with corresponding iron oxide volumes of 1.95, 0.19, 0.065, and 0.0042 μm^3. Note that transition from particle translation to trapping is dependent upon volume of iron oxide and particle size.

Additionally, the critical frequency can be written in terms of a critical pitch where a particle under a given driving frequency will traverse an array until trapping at a critical pitch. This method is more advantageous as particles with similar magnetic contents

and sizes can be separated and concentrated. This form of ratcheting behavior will be covered in more detail in Chapter 4.

Ratcheting Array Fabrication

Fabrication of magnetic ratcheting arrays with unity aspect ratios cannot be produced effectively using traditional metal evaporation methods. Utilizing previously developed methods of permalloy electroplating[8,7], magnetic structures with unity aspect ratios can be fabricated rapidly and at low cost. Figure 2-10 illustrates the fabrication process used to make the high force ratcheting arrays.

Beginning with a glass substrate, a metal seed layer of titanium, copper, and titanium is evaporated onto the substrate using e-beam evaporation with respective thicknesses of 50nm, 100nm, and 50nm. A photoresist layer is then spun on and array designs created using standard photolithography to produce electroplating molds. Before electroplating, the first titanium layer is etched away and the substrate is immersed in a custom permalloy electroplating bath to produce the permalloy structures. Both the current and the plating time are adjusted to achieve pillars with 1:1 aspect ratio.

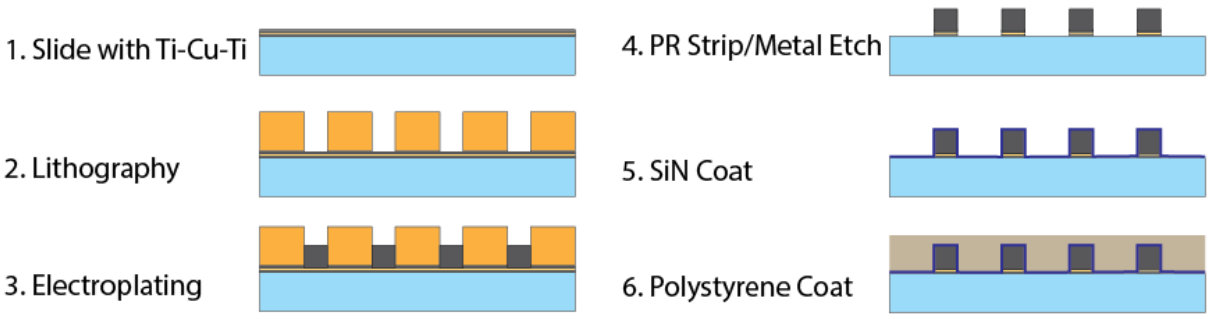

Figure 2-10: Fabrication of unity aspect ratio ratcheting arrays. (1) First a glass substrate is coated with a titanium-copper-titanium seed layer via e-beam evaporation with corresponding thicknesses of 50nm, 100nm, and 50nm. (2) Next array designs are produced photolithographically to create electroplating molds. (3) Before electroplating,

the topmost titanium layer is etched and the substrates are electroplated using a custom permalloy electroplater to a thickness of ~4μm (AR≈1). (4) Post plating, the photoresist and metal seed layers are etched and silicon nitride layer (5) is deposited to seal and protect the array. (6) Finally, a layer of polystyrene is spun on to a final thickness of ~0.8μm above the micro-pillars.

On average, plating takes between 30-60 minutes to create 4μm high, 4μm diameter pillars. Process optimization was performed for each array geometry and heights were characterized using a Dektak surface profilometer with an average height of 4.1±0.5μm. After electroplating, the photoresist layer is stripped and the metal layers are etched leaving the free standing permalloy array structures. The micro-pillars are then coated in ~200nm of silicon nitride using plasma enhanced chemical vapor deposition to protect and seal the arrays from oxidation. Finally, a planarizing layer of polystyrene is spun on to a final thickness of ~0.8μm above the array structures to ensure adequate magnetic reach of the micro-pillars.

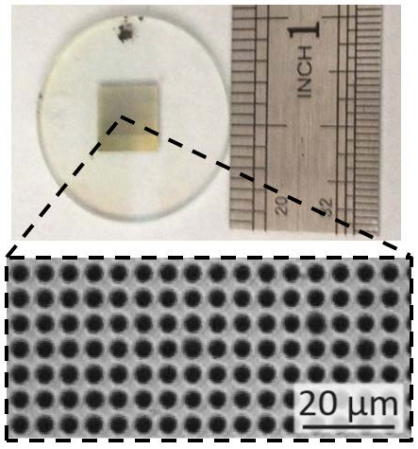

Figure 2-11: Ratcheting arrays produced via electroplating on 1 inch glass rounds. Arrays had a 4.0 ± 0.5 μm diameter and a height of 4.1 ± 0.5 μm. Final planarizing layer of polystyrene was spun to ~0.8μm above the pillar surfaces to a total height of 4.8-5μm.

The end result is a ratcheting array in the desired design with near unity aspect ratio (Figure 2-11) patterned on a transparent substrate.

Chapter 3 : Mechatronic System for High Force and High Resolution Ratcheting

Generating a ratcheting field with high strength and repeatability is a nontrivial task and is crucial to maintain robust manipulation. Previous ratcheting systems utilize electromagnets with 3-4 poles to generate the characteristic cyclic field (Figure 3-1a). However, electromagnets are bulky and have high power consumption, often requiring cooling infrastructure. A more compact and controllable method to generate a ratcheting field involves using high strength rare earth magnets (neodymium ferrite, N52 grade) arranged in a halbach array framed by a magnetic wheel (Figure 3-1b).

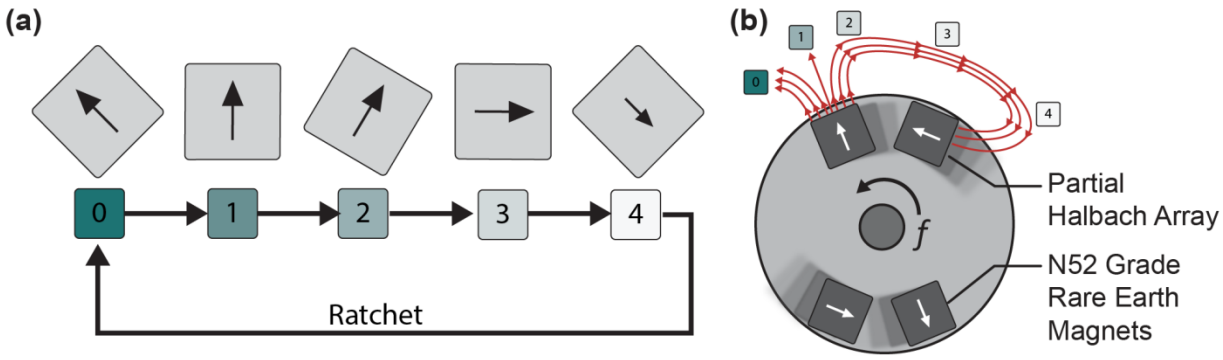

Figure 3-1: (a) Ratcheting field demonstrates a continuously changing angle to approximately 180º from starting orientation followed by a stepwise reset. (b) This cycle can be generated using a wheel of rare earth magnets arranged in a partial halbach array. Note that the wheel contains two ratcheting cycles.

Therefore, the ratcheting field is encoded into the angular position of the wheel and can achieve high field strengths which are challenging to produce with an electromagnet. Ratcheting using this technique has several advantages: first the field can be produced compactly, decreasing the system footprint and doesn't require specialized cooling infrastructure. Secondly, this method of ratcheting is can be easily integrated into automated systems and can be precisely controlled using electric motors and angular encoders. Finally, this technique can be used to generate high ratcheting

frequencies which can be challenging for electromagnets as higher frequencies generate increasing heat at constant field strength.

To produce ratcheting in a controllable manner we developed a mechatronic system to achieve automated manipulation. Several design constraints (Table 3-1) drove the system development which involved balancing technical constraints such as high field strength and ratcheting frequency control with experimental constraints such as visualization on an inverted scope and ease of use.

Table 3-1: Needs and related design constraints drive the design solution for the automated system.

Needs	**Design Constraint**	**Design Solution**
Strong ratcheting magnetic field	≥100mT field strength and 180º rotation and reset normal to array plane	Magnetic wheel with N 52 grade rare earth magnets in partial halbach array
Inverted Microscope: visualize chips from beneath	Magnetic wheel positioned above chip face-down on microscope	Cantilever system to hold magnetic wheel
Strong and repeatable ratcheting field	Magnetic wheel to be positioned between 1-3mm from back of chip	Precise vertical positioning control of the magnetic wheel
Large field of view microscopy imaging/image scanning	Need to lock relative movement between chip and magnetic wheel	Stage mounted system to lock relative motion between chip and magnetic wheel
Easy to use and automated system	Graphical user interface and physical input for commands	Labview® GUI and joystick based interface for intuitive manipulation

With these given design constraints, a mechatronic system to achieve automated ratcheting manipulation was designed and constructed (Figure 3-2). The mechatronic system consists of a scope mounted Cartesian stage with a cantilever arm supporting the ratcheting module (Figure 3-2 a & c). The ratcheting module housed the magnetic

wheel (Figure 3-2 d) initiating ratcheting via a computer controlled electric motor and gearing system. Additionally the ratcheting module can adjust the in plane angle to ratchet in any desired vector relative to the chip. The entire system can be piloted or automated by a user via a joystick and Labview® graphic user interface.

Once mounted onto an inverted florescence microscope, the ratcheting arrays can be placed facedown and the system can be piloted to position the magnetic wheel precisely above the arrays. This is crucial as generating a strong ratcheting field requires close proximity to the back side of the ratcheting array substrate. Using the joystick twisting, throttle and trigger functions ratcheting can be initiated in a desired direction with frequency ranges between 0.5-50 Hz (Movie S3). Using this system, ratcheting manipulation can be achieved reliably and in an intuitive manner, not requiring sophisticated training to operate. Additionally, manipulation can be automated through the graphic user interface (Figure 3-3) where a user can define a ratcheting frequency, in plane angle, and duration which can be executed once or looped.

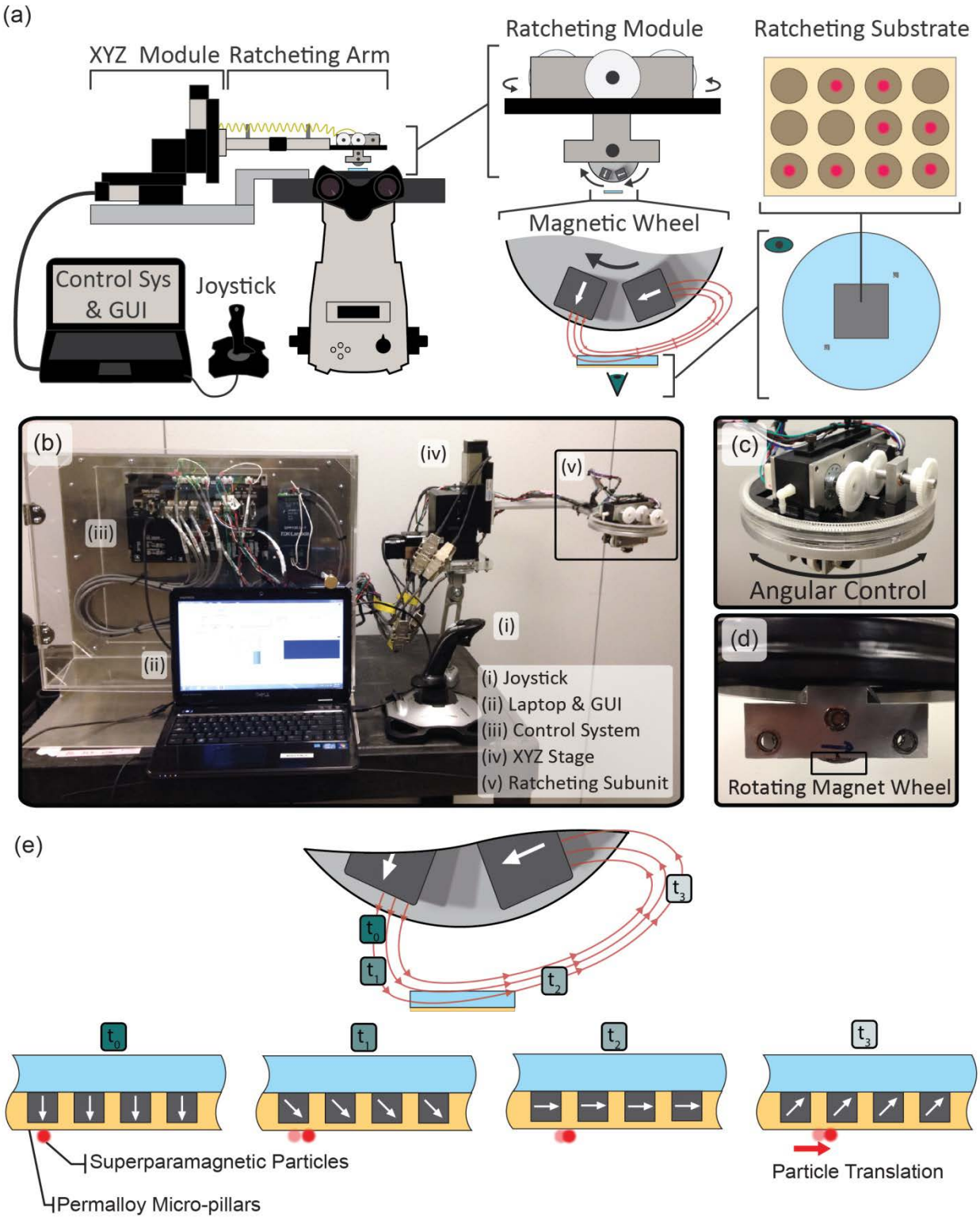

Figure 3-2: (a) Diagram showing mechatronic system for magnetic ratcheting system consisting of a scope mounted, Cartesian stage with a cantilever frame to hold a ratcheting module which generates a ratcheting field be spinning a magnetic wheel of

rare earth magnets. The ratcheting module also controls in plane angular control (parallel to the micro-pillar array) for ratcheting in any arbitrary vector. (b-d) The entire system is controlled via a joystick and laptop with Labview® graphic user interface. Pre-programmed ratcheting manipulations can also be achieved through the user interface as well. (e) The magnetic wheel, controlled by the ratcheting module, generates the desired directionally cycled magnetic field, enabling micromanipulation via the permalloy micro-pillar array.

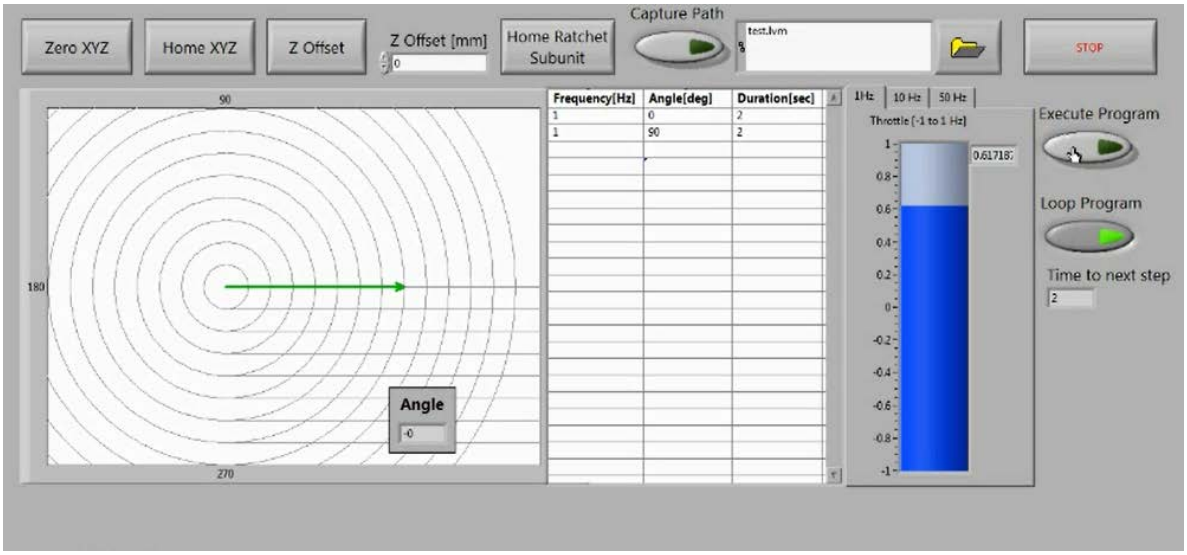

Figure 3-3: Automated ratcheting manipulations can be preprogrammed through graphic user interface. Users can define ratcheting frequency, in plane angle (relative to micro-pillar array), and duration of ratcheting for precise and automated manipulation control. The program can be executed once or looped continuously for repeated operations.

Massively Parallelized Manipulation of Particles and Cells on Ratcheting Arrays

Combining the unity aspect ratio micro-pillar arrays with the automated mechatronic system, we demonstrated highly parallelized manipulation of 2.8μm magnetic particles (Movie S4). Particle transport demonstrated the anticipated ratcheting behavior transitioning from pillar to pillar, but also was able to achieve finely tuned nanometer scale manipulations (Figure 3-4). We defined this bimodal manipulation as consisting of a “coarse mode,” where particle manipulations were

digitized by pillar pitch (*P*=6μm) and a “fine mode” where particles could be piloted within the pillar due to the ability to magnetize the pillar in any desired direction.

Coarse mode manipulations can be achieved manually via the joystick interface or automatically using the preprogrammed path functions to build any desired path (Figure 3-4a). The coarse mode transport was characterized by programming a square path with side lengths of 16 cycles or ~ 63 cm of circumferential distance with reference to the magnetic wheel (Figure 3-4b). Upon execution of the path, 3μm particles mirrored the trajectory in the microscale with high fidelity, demonstrating an averaged deviation from the path of 850nm. Furthermore, the coarse mode manipulation path resulted in a manipulation high success rate where 92% (N=100) of the particles across the substrate reached their intended pillar (Figure 3-4e). Even high resolution manipulation was achieved by manipulating particles within pillars (Figure 3-4b). The robustness and fidelity of this mode was also characterized using the automated programing functions where the robot executed a command to manipulate particles round the edges of a micro-pillar starting from a 0º point and rotating clockwise to the 90º location (Figure 3-4d). In response, the particles traversed the pillar perimeter with an averaged path deviation of 200nm. Of the particles manipulated (N=100), 83% ended the manipulation within ±500nm of the trajectory end point and 93% reached within ±1μm.

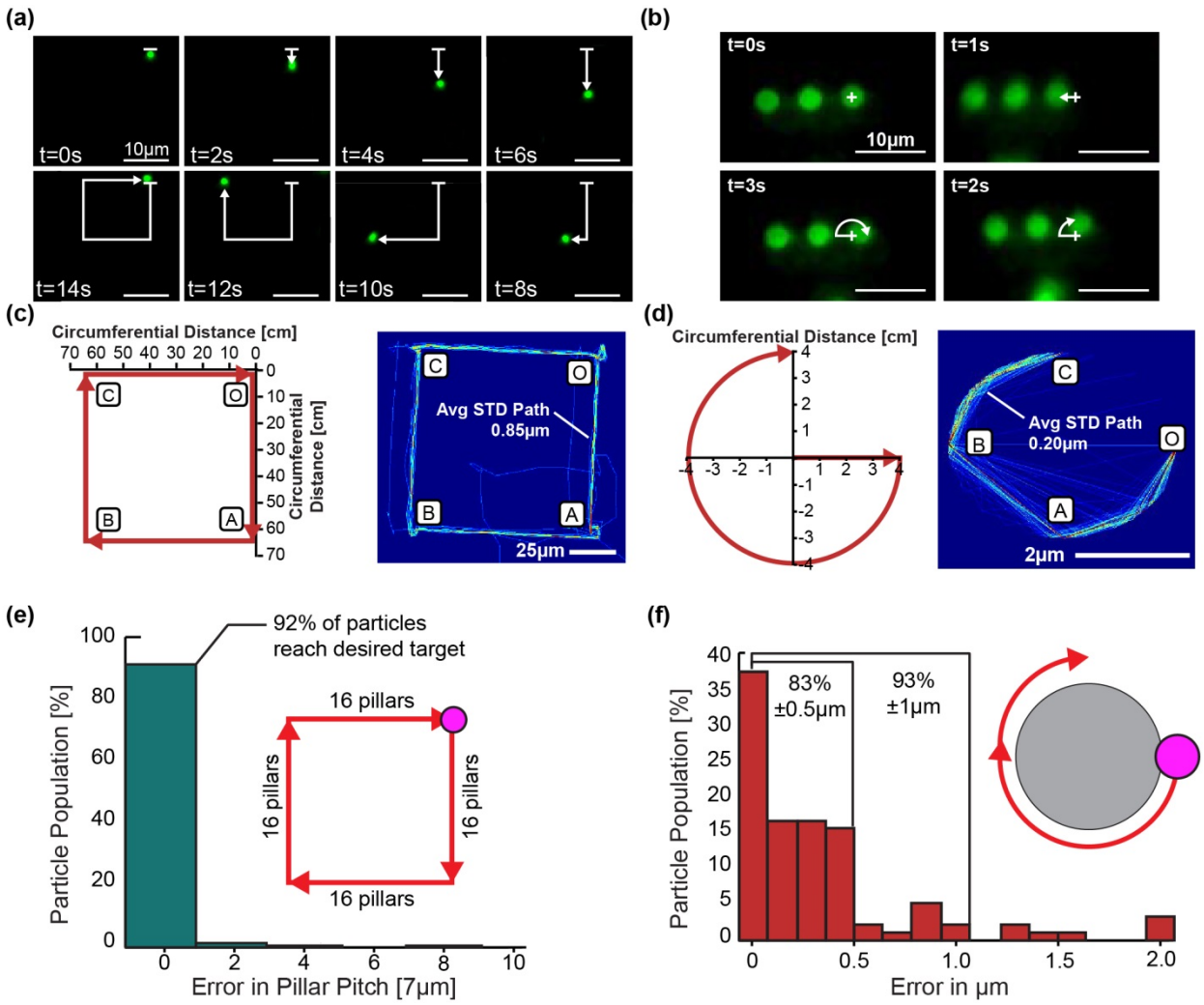

Figure 3-4: (a) “Coarse mode” manipulations, meaning manipulations digitized by pillar pitch, can be achieved in a highly parallelized manner. (b) Using the automated programming functions, the robot executed a square path with lengths of 16 ratcheting cycles, corresponding to ~63cm of circumferential distance of the magnetic wheel. The particles followed the expected trajectory with a side length of ~96μm, corresponding to 16 cycles of 6μm pitch with an averaged path deviation of 850nm. (d) “Fine mode” manipulations were also achieved using the automated path programming functions where the robot executed a path manipulating particles around the pillar edge with an averaged path deviation of 200nm. (e &f) Particle manipulations for both modes represented high fidelity motions. In coarse mode, 92% of the particles ratcheted the square trajectory successfully. In fine mode, 83% of the particles reached within 500nm of the target demonstrating the power and ease of the system for nanoscale interface.

It becomes apparent that this technique of magnetic ratcheting can be used for robust nanoscale manipulations for subcellular interface. In coarse mode the total path

of the robot de-amplifies from ~252cm to 200μm, a motion de-amplification of 6500 times. Fine mode manipulations show even higher resolution with a motion de-amplification of 20,000 times. To put this in perspective, this effectively makes a 25μm diameter cell into a 50 cm diameter cell at the human length scale.

Table 3-2: Robotic trajectories for coarse and fine mode manipulations can be de-amplified from cm scale to μm scale with corresponding de-amplification factors of 6500 & 20,000.

Mode	Total Robot Trajectory Length [cm]	Total Particle Trajectory Length [μm]	De-amplification Factor
Coarse	252	400	6500
Fine	18.9	9.42	20,000

Indeed high resolution ratcheting manipulation of this kind is only achievable due to the unity aspect ratio structures which enable a more isotropic magnetization and therefore represents a superior method of micromanipulation and lab-on-a chip control architecture.

High Force Applicability on Magnetic Particles

In addition to high resolution, the ratcheting system was able to produce large forces on smaller particles. As described in Chapter 2, the force on a magnetic particle is governed by the particle's magnetic content and size as well as the ratcheting array geometry. Using the model described previously we were able to characterize the force on a 3μm (17 % iron oxide, $\Delta\chi_p$=0.007) by ratcheting in glycerol solution at various frequencies and observing the critical frequency.

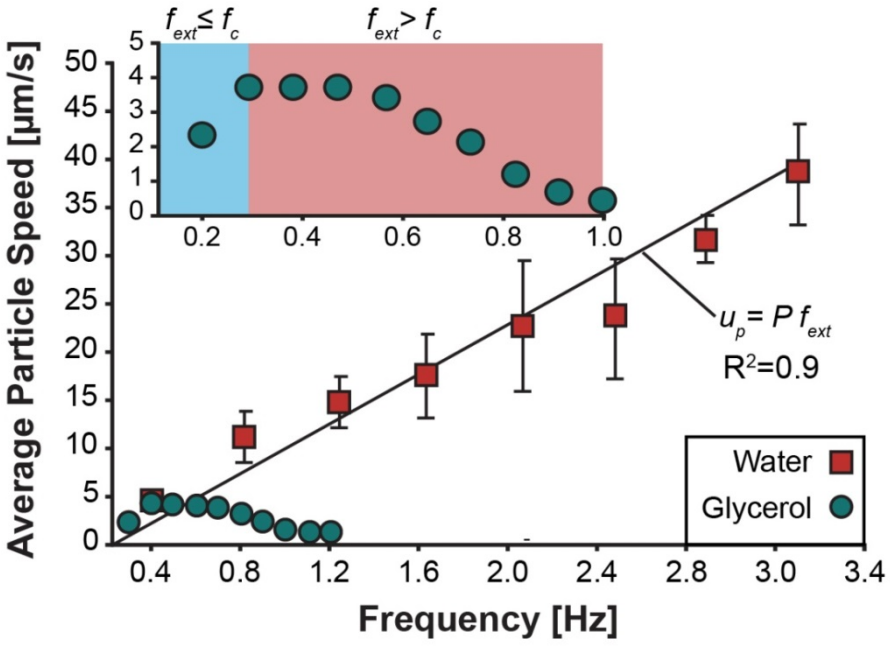

Figure 3-5: Frequency response of 3µm particles in water and glycerol solutions on a 6µm pitch array. The particles ratcheting in water have a high critical frequency (~51Hz) and therefore display a linear relationship between ratcheting frequency and particle speed. However, glycerol is highly viscous ($\boldsymbol{\mu}$=1410 cP) causing the particles to slip out of phase and stall at low frequencies. In glycerol solution, the critical frequency was approximately 3Hz corresponding to a drag force of 66.9 pN.

Ratcheting of 3µm particles in water has a high critical frequency on a 6µm pitch array (~51Hz). However, modulating frequency by ratcheting glycerol attenuates the critical frequency as the viscosity of the surrounding medium is 1410 times higher. In glycerol the critical frequency was observed to be approximately 0.3Hz (Figure 3-5). If balanced with drag, this shows that a 6µm pitch array under ~100mT applied field can impart 66.9pN of force on a 3µm particle (Equation 9).

$$\boldsymbol{F_{mag} = F_{drag} = 6\pi\mu_f r_p P f_{crit} = 66.9pN} \qquad \textbf{Equation 9}$$

The predicated critical pitch from the model slightly under predicts this value giving an estimated critical frequency of 0.15Hz and predicted force amplitude of 59.5pN.

The high force applicability of the system represents another advantage that this system has over other magnetic techniques and even existing ratcheting systems. Using bulk magnetic fields limits forces for a 3µm particle size to the femtonewton range which can be problematic for interfacing with cells and transporting cells. Thin film ratcheting systems can apply on the order of 5-6 pN while unity aspect ratio systems operate at an order magnitude higher enabling more rapid transport.

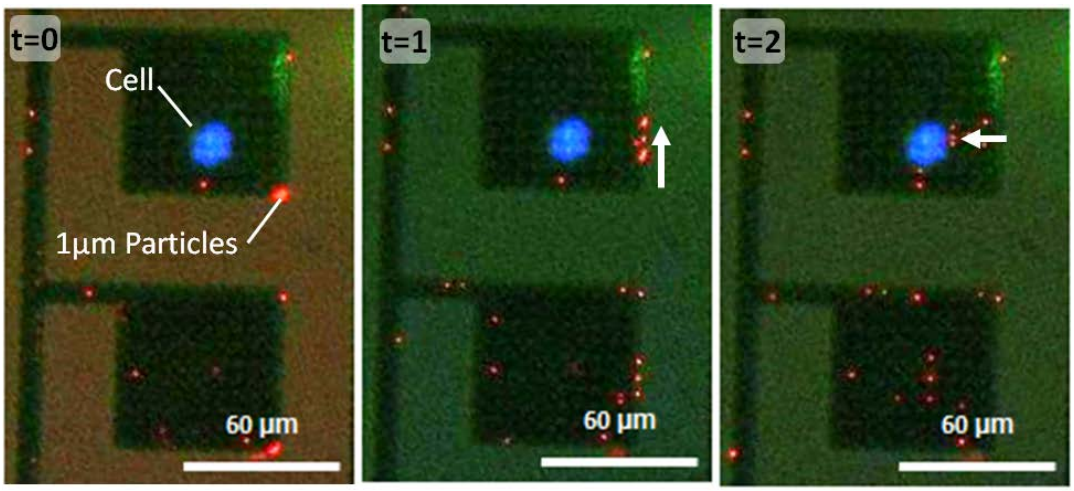

Figure 3-6: HeLa cell (blue) cultured on top of a magnetic ratcheting array with 1µm particles (red) being piloted to make contact with the cell. Functionalizing a desired stimulus to the particles surface can enable highly paralleled application of chemical stimuli to elucidate underlying biochemical phenomena.

This highly resolved manipulation architecture can be used in a variety of lab-on-a-chip applications. In particular this platform can be employed to probe stimulus at a subcellular length scale. Figure 3-6 shows a HeLa cell (blue) which has been cultured on top of a magnetic ratcheting array and seeded with 1µm particles (red). Using the system, particles can be manipulated to make contact at the cell surface. Using the particles as a vehicle of stimulus, cellular responses can be probed with nanoscale resolution.

Chapter 4 : Manipulation and Concentration of Magnetically Labeled Cells

Precise and high throughput manipulation of individual cells is an essential capability for lab-on-a-chip technologies executing single cell analysis. However, robust piloting of single cells to perform assay operations is a non-trivial task and faces many challenges. Often, the cell population of interest is hidden within a heterogeneous sample such as a blood or tissue biopsy, thereby requiring filtration of unwanted cell types (Negative Depletion) or specific manipulation of the target cell population (Positive Selection) for downstream processing. Additionally, manipulation operations need to be performed in high throughput to gain highly sampled, single cell resolved data sets to gain statistically relevant findings. Furthermore, manipulation operations should be performed rapidly in a biocompatible manner to reduce data loss due to cell death or biomolecule degradation. This is important as many biological assays, such as RNA analysis, are time sensitive which can result in data loss with lengthy processing times.

Magnetic ratcheting on unity aspect ratio arrays stands to address these needs and has potential to provide a completely integrated manipulation platform to meet these criteria. Using magnetic particles functionalized with specific ligands, cell populations within complex biosamples can be targeted either for negative depletion or positive selection. Additionally, magnetic based technologies are highly biocompatible where even high magnetic fields demonstrate minimal effect on underlying biological function. Finally, the unity aspect ratio structures enable high magnetic force, and therefore rapid transport, through complex biosamples with high viscosity. Using magnetic ratcheting, manipulation operations can be performed on specific cell types in a high throughput and biocompatible manner.

High Throughput Manipulation of Immunomagnetically Labeled Cells

Immunomagnetic labeling of cells is a household method to specifically label and extract a target cell population from mixed populations[23]. This technique involves functionalizing an antibody or other ligand to the surface of a magnetic particle which can specifically bind to a desired cell type even within mixed populations. Concentration and enrichment of the target population can be achieved using a magnet to precipitate magnetically tagged cells, a technique known as magnetic activated cell sorting (MACS). However one of the challenges faced by traditional magnetic separation and manipulation techniques is the inherent tradeoff between particle size and force applicability. High force leads to higher throughput operations which is proportional to the volume of magnetic content within the particle (Figure 4-1). However, increasing particle size results in decreasing diffusion due to the diffusion constant is inversely proportional to particle diameter.

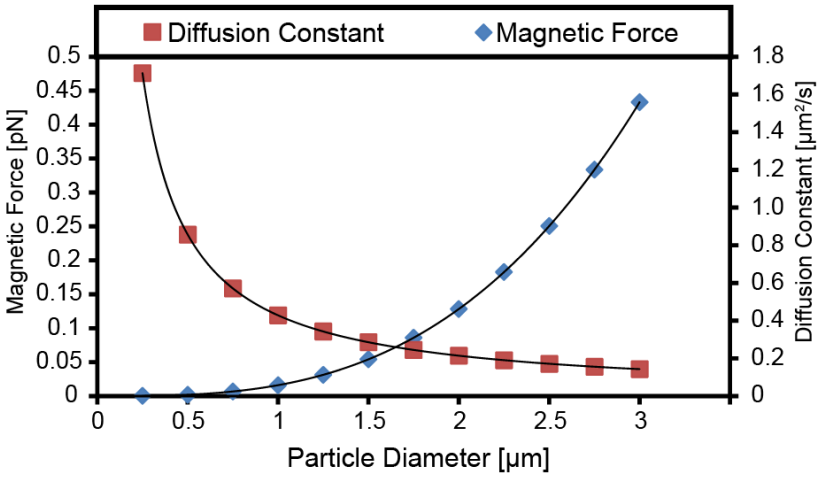

Figure 4-1: Predicted magnetic force in a bulk magnetic field gradient ($\boldsymbol{F_{den} = 5.5}$, $\boldsymbol{\Delta\chi_p = 0.007}$) as a function of particle diameter. Magnetic force is proportional to particle magnetic content and therefore particle volume. However, the diffusion

constant as approximated at 20ºC (Stokes–Einstein–Sutherland equation) is inversely proportional to particle diameter demonstrating a tradeoff between magnetic force and diffusion.

High diffusion is needed in order to effectively label cells with magnetic particles and high labeling efficiency is needed when target cell populations are rare. Though increasing the concentration of large particles can boost the magnetic labeling efficiency, the resultant magnetic extraction is crowded by high numbers of unbound particles and off target labeled cells. However magnetic ratcheting on unity aspect ratio structures provides high force capabilities and can be used to manipulate cells with small particles quickly. Figure 4-2 shows a LNCaP cell labeled with 1µm particles coated with anti-Epithelial Cell Adhesion Molecule (EpCAM) being manipulated in a square trajectory on a 6µm pitch ratcheting array.

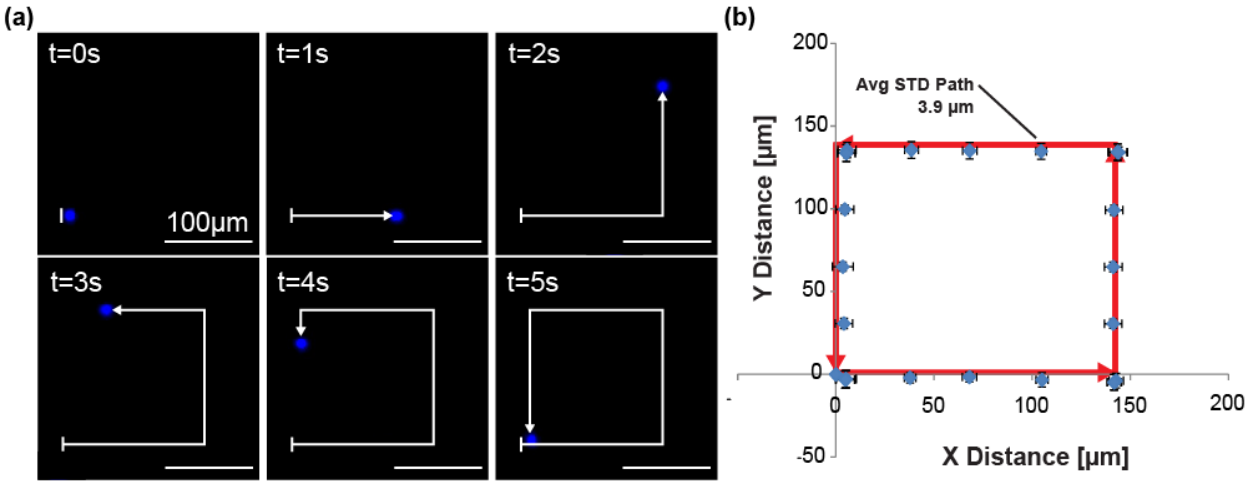

Figure 4-2: (a) LNCaP cell labeled with 1µm EpCAM functionalized magnetic particles being manipulated in a square trajectory on a 6µm pitch array (20 ratcheting cycles in length) using the magnetic system. The cells showed high fidelity manipulation with an averaged deviation from the path of 3.9µm (N=10).

Manipulation of labeled LNCaP cells demonstrated high parallelization and high fidelity with an average deviation from the trajectory path of 3.9µm and all cells made it

within 5µm of their intended destination. This highly resolved and highly parallelized cell manipulation can be employed powerfully for LOC technologies as cells can be manipulated rapidly into various fluid wells to perform staining or wash steps within micro-wells. Furthermore this manipulation can be made specific based on surface target expression, in this case EpCAM. In this way, manipulations can be cell type specific, allowing processing to be performed in mixed populations as long as the surface target is exclusive to the desired cell type.

Rapid Magnetophoretic Concentration of Magnetically Labeled Cells

Selective manipulation of target cells from bulk solutions is indeed a much needed capability to perform enrichment of a cell population which provide insight into a disease state. A good example is that of circulating endothelial cells (CECs) which are the focus of significant research focus[45,46] as a biomarker for coronary heart disease (CAD). CAD remains one of the leading causes of death affecting more than 12 million people worldwide[47]. Specifically, acute coronary syndromes (ACS) induced by the formation of atherosclerotic plaques and subsequent rupture of vasculature are particular deadly demonstrating a mortality rate between 18-23%[48]. Formation of atherosclerotic plaques induce endothelial cells desquamation; shedding cells into the circulatory system at low numbers (~10/mL) which increase as vascular damage worsens. Recovery and subsequent analysis of CECs is of extreme diagnostic and prognostic value due to the close temporal relationship between the CECs and the wound site. Isolation of CECs from peripheral whole blood has been achieved in a variety of ways including density gradient[49] and microfluidic[50,51] systems. However a majority of CEC enrichment techniques utilize immunomagnetic labelling of specific

CEC surface markers for magnetic mediated precipitation (refs). Magnetic assisted cell separation (MACS) of CECs is robust and efficient extraction technique particularly when combined with microfluidic systems. While powerful, MACS based systems have significant drawbacks including limited purity due to off target labelling as well as extremely high particle background which can outnumber the CECs 1 to 100,000. High off target labelling and particle backgrounds can introduce noise into the cell isolate, making downstream analysis problematic. Additionally, many microfluidic MACS based separation are highly sensitive to flow characteristics and most often rely on large magnetic particles (≥3μm diameter) to scale the magnetophoretic force with fluidic forces. Unfortunately, larger particles have limited binding efficiency due to their small diffusion length which must be compensated by adding large particle concentrations ($\geq 10^7$ pts/mL) leading to high particle background. However, magnetic ratcheting can enable the use of smaller particles to reduce particle background and also decrease processing time due to increased magnetic labeling efficiency and cell concentration. As shown in Figure 4-3 endothelial cells (ECs) labeled with both 1μm and 500nm particles functionalized with anti CD 146 demonstrate rapid ratcheting transport when ratcheted between 2-8 Hz.

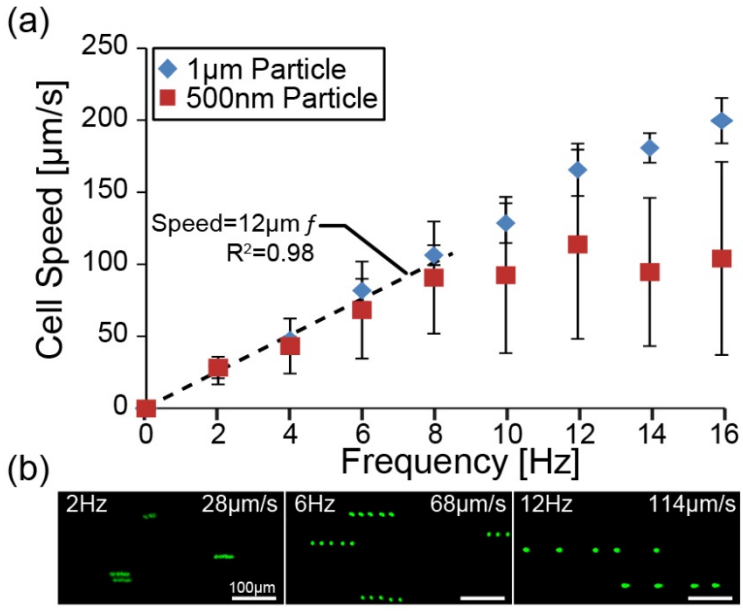

Figure 4-3: Frequency response of endothelial cells labeled with 1µm and 500nm magnetic particles functionalized with anti-CD 146 on a 6µm pitch array. Ratcheting frequencies ≤ 8Hz both display high linearity between driving frequency and cell speed. As the ratcheting frequency increases, the cells labeled with 500nm particles begin to slow while the 1µm labeled cells continue to display the linear transport trend due to high force capability.

Within the frequency regime the transport behavior between 1µm and 500nm particles is the same yielding a top speed of 101µm/s. However increasing frequencies show that the speed 500nm labeled cells begins to taper while the 1µm labeled cells continues to increase. Therefore, by using the high forcing capabilities of the unity aspect ratio enables smaller particles to be used without compromising on processing time.

A ratcheting array was constructed to achieve rapid magnetophoretic concentration of magnetically labeled endothelial cells from bulk solutions (Figure 4-4 a & b). The chip consisted of a large 3cmx3cm array with a 6µm pitch array upon which to extract magnetically labeled endothelial cells from bulk solution (Figure 4-4b). Here labeled ECs within liquid biosamples were flowed over or directly added over the

ratcheting array and transported out of the bulk solution. Eventually, the ECs will encounter the slanted arrays and will become concentrated down to a trapping zone, becoming dynamically entrained at a localized point.

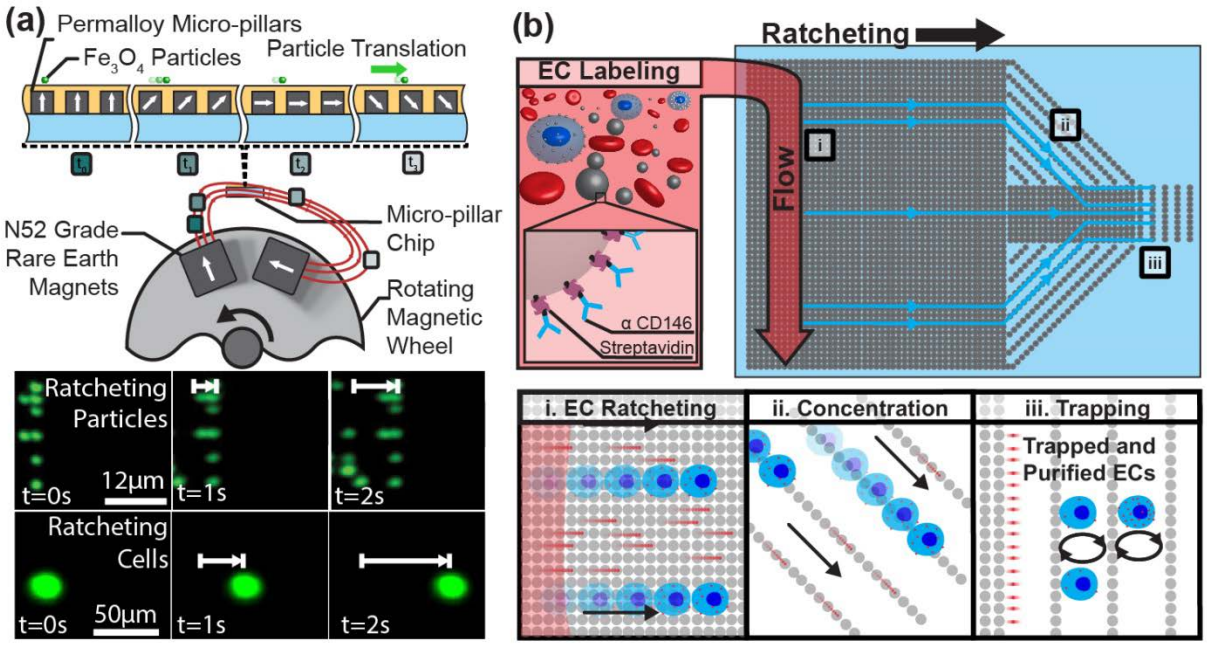

Figure 4-4: (a) High force magnetic ratcheting on unity aspect ratio arrays enables rapid magnetic transport of particles and magnetically labeled cells. (b) Magnetically labeled endothelial cells can be first extracted from a bulk solution by ratcheting on a large 3cmx3cm square array, concentrated using slanted rows of permalloy micro-pillars, and finally trap and concentrate at a small collection zone. The collection zone has a pitch of 40 µm of which cells will be unable to traverse and will therefore collect at the array edge.

Figure 4-5 shows the realization of this technology, were ECs magnetically labeled with 1µm magnetic particles are extracted, concentrated, and trapped on the ratcheting concentrator chip.

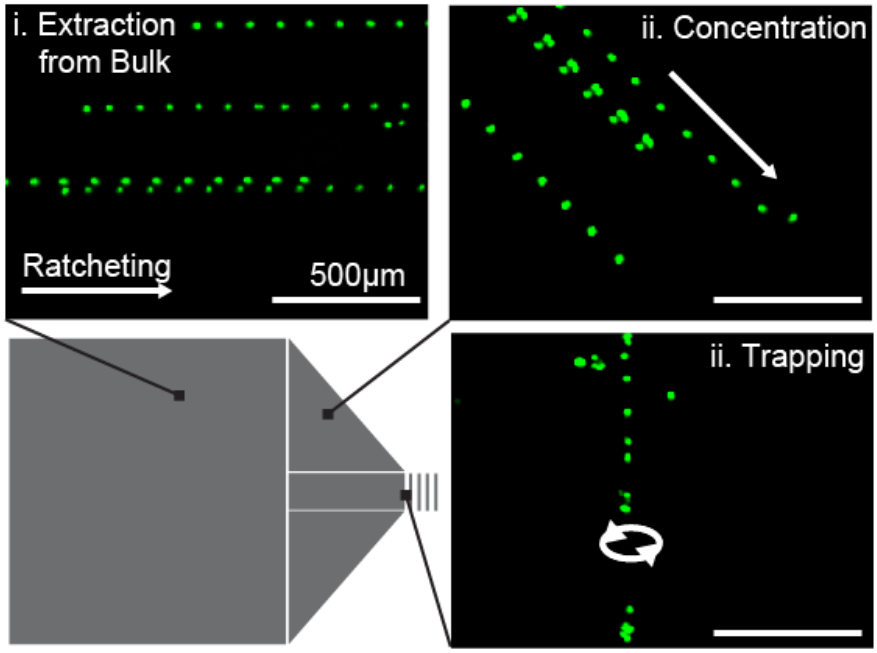

Figure 4-5: Endothelial cells labeled with 1µm particles ratcheted at 5Hz show rapid magnetophoretic collection at the trapping zone. (i) ECs are transported from the bulk solution where they encounter slanted arrays (ii) and concentrate to the trapping zone (iii). Extraction of cells from bulk solution averaged ~60µm/s showing full extraction in approximately 15 minutes.

Under a 5Hz ratchet, ECs exhibited an average ratcheting speed of ~60µm/s and thereby capable of traversing the entire chip in 12.5 minutes. This demonstrates the power of the ratcheting concentrator to quickly isolate magnetically labeled cells from bulk solutions. This is of particular interest for timely assays such as RNA sequencing or proteomic analysis. Furthermore, the speed of separation makes this platform a tenable option for point of care applications which is particularly impactful for patients with acute or chronic heart disease where answers are needed quickly. For instance, a patient demonstrating ACS symptoms can be tested for circulating endothelial cells in under an hour, allowing for a 15 min labeling incubation with magnetic particles followed by a 15 minute ratcheting concentration to extract circulating endothelial cells from the patient's blood. Paring with rapid genomic analysis could help surgeons identify where

the circulating endothelial cells are shedding from the wound site and develop a treatment plan in a matter of hours after patient admittance. Here magnetic ratcheting can be used powerfully to expedite diagnostics and potentially guide clinical decisions.

In addition to concentrating cells, particles can be rapidly concentrated using this platform as well. Magnetic nanoparticles, specifically super paramagnetic iron oxide nanoparticles (SPIONS), are widely used in many applications besides immunomagnetic labeling and often require surface functionalization with charged groups, therapeutic agents, ect. However, as shown in Figure 4-1 the applicable magnetic force is extremely low making it challenging to concentrate which can be an issue if the working chemistry is unstable or time sensitive. The magnetic ratcheting concentrator can enable rapid extraction of nanoparticles (Figure 4-6) which would normally take hours to fully concentrate.

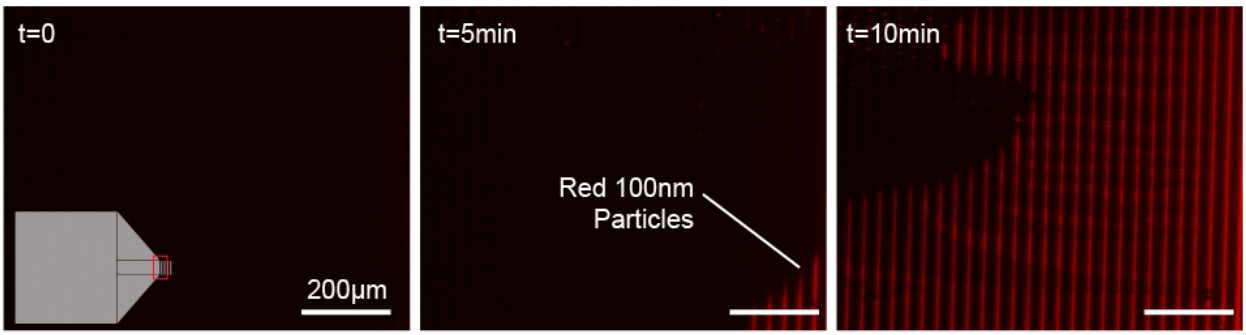

Figure 4-6: Ratcheting concentration of 100nm red florescent particles after 10 minutes of ratcheting at 5Hz.

Using this platform, processing steps for solid phase chemistry on SPIONS can be decreased or automated making particle manufacture quicker and automated.

Chapter 5 : Quantitative Separation of Particles & Cells on Gradient Pitch Arrays

Extraction of rare target cells from biosamples remains a cornerstone capability of cell biology research. Traditional rare cell separation techniques, such as magnetic activated cell sorting (MACS), are robust but can't achieve quantitative separation based surface antigen expression. We report a quantitative magnetic separation technology using high-force magnetic ratcheting over arrays of magnetically soft micro-pillars with gradient spacing, and use the system to separate and concentrate magnetic beads based on iron oxide content (IOC) and cells based on surface expression. The system consists of a microchip of permalloy micro-pillar arrays with increasing lateral pitch and a mechatronic device to generate a cycling magnetic field. Particles with higher IOC separate and equilibrate along the micro-pillar array at larger pitches. We develop a semi-analytical model that predicts behavior for particles and cells. Using the system, LNCaP cells were separated based on the bound quantity of 1μm anti-EpCAM iron oxide particles as a metric for expression. The ratcheting cytometry system achieved a ±13 particle resolution, successfully distinguishing LNCaP from PC3 cell populations based on EpCAM expression, correlating with flow cytometry analysis. In patient samples, we isolated EpCAM-labeled cells achieving a 74% purity and demonstrating the power of ratcheting cytometry for quantitative magnetic separation.

Introduction: Quantitative Magnetic Separation via Magnetic Ratcheting

Separating and concentrating cells from bulk solutions for analysis is a nontrivial task in life science research, diagnostics, and industrial processing. As such, various approaches based on physical[52] or biochemical[53] properties of cells have been developed to improve separation efficiency. Biochemical moieties on cell surfaces are

most commonly used to distinguish cell populations, in which a specific receptor or protein is targeted with a recognition element (e.g. antibody, aptamer, ligand) to yield a fluorescent or magnetic label enabling downstream sorting.

The most widely used cell sorting techniques of this nature are fluorescence-activated cell sorting (FACS) and magnetic activated cell sorting (MACS). In FACS, multiple cell populations can be separated from heterogeneous mixtures based on the quantity of fluorophore associated with the cell. Though effective, the FACS process is performed serially and each cell is analyzed individually, increasing processing times for large sample volumes. Comparatively, magnetic based approaches are advantageous due to their simplicity and robustness, not requiring sophisticated fluid handling. These approaches are also able to operate on minimal cell quantities and/or process larger volumes more rapidly[54]. However, magnetic separation approaches remain less quantitative than FACS, which can gate on the relative quantity of a biomarker. This lack of quantification from traditional MACS is due to the fact that these approaches cannot discriminate effectively based on the number of bound magnetic particles. Additionally, most magnetic particles available today are not tightly controlled in size or magnetic content, further exacerbating efforts for quantification of biomarker levels as correlated to number of bound particles.

Several microfluidics approaches have been developed to quantitatively separate cells based on bound or internalized magnetic content[28,29,55,27,56]. In general, these techniques involve generating a magnetophoretic force orthogonal to a fluid flow direction, inducing cell deflection across streamlines and separation into different outlets depending on magnetic content. However, these “kinetic” based separations require

precise tuning of flow rate, fluidic resistance, and magnetic field positioning. Additionally, many of these systems have low throughput as they rely on weaker bulk magnetic field gradients. Finally, the output from flow-through based systems often yields diluted solutions which may require concentration steps and is particularly challenging for isolating and locating rare cell types.

Magnetic ratcheting has the potential to achieve quantitative magnetic separations to both purify magnetic particle populations and separate cells based on bound number of particles. In magnetic ratcheting, arrays of magnetic micro-pillars combined with a directionally cycled magnetic field create dynamic potential energy wells that trap and manipulate superparamagnetic particles[34,35,36,37] in a magnetic-content and particle-size dependent manner. However, previous ratcheting platforms have utilized thin film magnetic structures (height ≤ 200nm), which have minimal force capacities on the order of 10pN, due to the low aspect ratio of the structures used (SI Text). To compensate, larger particles are used (~3-10μm) to maximize the force envelope. However, larger particles have reduced magnetic labeling efficiency for cell separations due to slow diffusive motions. This slow diffusive motion results in inefficient binding of large particles to cell surface targets and the large increment in magnetic content per bound particle makes it difficult to relate bead binding to target expression levels. The use of smaller magnetic particles is necessary to increase labeling efficiency as well as provide a sensitive metric to relate bound particle numbers with cell surface expression, but is not practically compatible with current ratcheting technology. Additionally, previous ratcheting platforms[34] rely on velocity differences between particles to achieve magnetic based separation. But again this is a “kinetic” separation

requiring initial sample concentration prior to process initiation, and time dependent collection functions. These challenges have limited use as a quantitative sorting tool. Ideally, an equilibrium separation could achieve reduced dependence on initial and final conditions of a sample yielding a more robust and quantitative separation.

To address these fundamental challenges we developed magnetic ratcheting arrays composed of 1:1 aspect ratio, electroplated magnetic structures, increasing the force capacity by 10 fold. Furthermore, the array was designed with increasing horizontal pitch enabling rapid magnetophoretic equilibrium separation of particles or cells, yielding concentrated “bands” which are quantized and proportional to magnetic content.

Our gradient magnetic ratcheting system (Movie S3) was able to rapidly separate and concentrate magnetic particles based on iron oxide (IO) content with high precision; yielding complete equilibrium separation of a particle batch in less than 60 seconds. The platform was then used to evaluate EpCAM expression on PC3 and LNCaP cells using the quantity of bound anti-EpCAM 1μm IO particles as a marker of expression. The system was able to successfully distinguish PC3 and LNCaP cell populations and was highly correlated with EpCAM expression as determined by flow cytometry of the two cell lines. We also demonstrated applicability as a rare cell cytometer achieving a capture efficiency of 26±4% and a purity of 67±35% of LNCaP cells spiked into 1mL of whole blood, which was comparable with other MACS-based systems[57,58] but with a substantially higher separation purity. Ratcheting cytometry was also evaluated as a clinical tool for capture and quantification of circulating tumor cells in three patients with metastatic castration resistant prostate cancer. In 2 of 3 patients, approximately 8-10

large nucleated CD45-negative cells were extracted and concentrated due to their large anti-EpCAM bound particle content with an average purity of 71%.

Theory: Modulating Pillar Pitch for Iron Oxide Content based Separation

Transport of magnetic particles by ratcheting is achieved using arrays of magnetically soft micro-pillars combined with a directionally cycled magnetic field to dynamically modify the potential energy landscape. This creates translating potential wells that trap and manipulate magnetic particles (Appendix E Figure S1). Upon application of a magnetic field from a mechatronically controlled magnetic system (Appendix E Figure S3 & Movie S3), the micro-pillars magnetize in alignment to the bulk field, introducing potential wells in which superparamagnetic magnetic particles become trapped. As the magnetic wheel is cycled, particles follow the potential wells and ratchet through the pillars based on their size and magnetic properties (Figure 5-1 a-b).

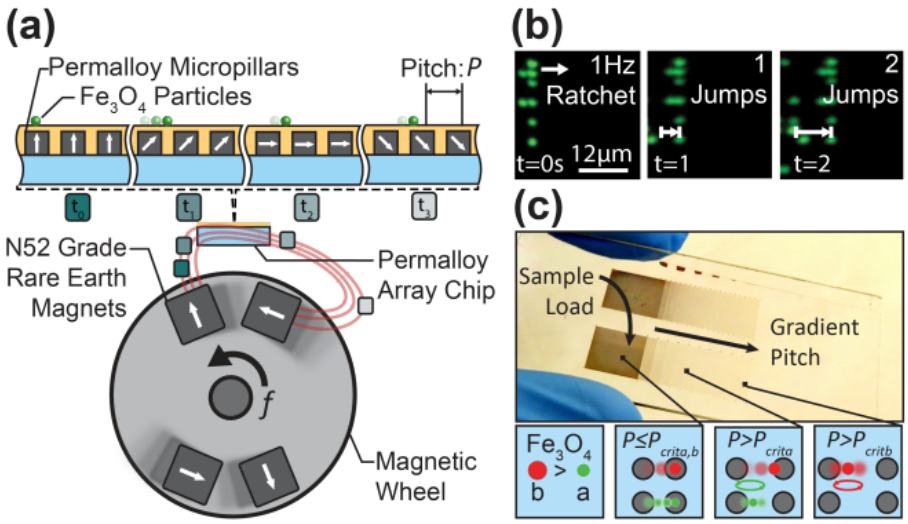

Figure 5-1: Magnetic ratcheting utilizes arrays of electroplated permalloy micro-pillars, of pitch ***P*****,** to create dynamic potential energy wells which can be used to trap and manipulate superparamagnetic particles. (a)The magnetic ratcheting system is comprised of a mechatronic instrument driving a rotating magnetic wheel as well as a microchip composed of permalloy micro-pillar arrays, with each pillar having a 1:1

aspect ratio. When proximal to the magnetic wheel, the micro-pillars magnetize in alignment to the bulk field; modifying the magnetic potential energy landscape and introducing potential wells in which superparamagnetic particles migrate. (b)As the wheel is cycled at frequency $\boldsymbol{f}$, particles will follow the potential wells and ratchet through the pillars based on size and iron oxide content. Using a chip consisting of micro-pillar arrays with gradient horizontal pitch (c), particles will traverse the array until reaching their critical pitch, $\boldsymbol{P_{crit}}$, where they will collect and oscillate. Particles with increasing magnetic content will have correspondingly higher critical pitches and can therefore be separated.

Similar ratcheting transport , which has been previously studied in thin film uniform pitch ratcheting platforms[34,35,36,37] , is characterized by a balance of the time averaged magnetic force, $\overline{\boldsymbol{F_{mag}}}$, with the time averaged drag force $\overline{\boldsymbol{F_{drag}}}$ (Equations 10 & 11). The time averaged magnetic force is dependent on several parameters including magnetic particle volume $\boldsymbol{V_p}$, the particle susceptibility $\boldsymbol{\chi_p}$, the permeability of free space $\boldsymbol{\mu_o}$, and the magnetic flux density $\boldsymbol{B}$.

$$\overline{\boldsymbol{F_{mag}}} = \frac{\boldsymbol{V_p\,\chi_p}}{\boldsymbol{\mu_o}}\,\overline{(\boldsymbol{B}\cdot\boldsymbol{\nabla})\boldsymbol{B}} \qquad \textbf{Equation 10}$$

Assuming a Stokes drag condition, the time averaged drag force can be described in terms of fluid viscosity $\boldsymbol{\mu_f}$, particle radius $\boldsymbol{r_p}$, and the time averaged particle speed $\overline{\boldsymbol{u_p}}$. The time averaged particle speed can be further represented in terms of the total distance traversed over one ratcheting cycle, $\overline{\boldsymbol{X_p}}$, and the ratcheting frequency $\boldsymbol{f}$ (Equation 11).

$$\overline{\boldsymbol{F_{drag}}} = \boldsymbol{6\pi\mu_f r_p}\overline{\boldsymbol{u_p}} = \boldsymbol{6\pi\mu_f r_p}\overline{\boldsymbol{X_p}}\,\boldsymbol{f} \qquad \textbf{Equation 11}$$

Assuming the magnetic and drag forces equate, a particle ratcheted at a given frequency will be able to traverse a ratcheting array of pitch $\boldsymbol{P}$ given that $\boldsymbol{P} \leq \overline{\boldsymbol{X_p}}$ and the average particle velocity becomes $\boldsymbol{Pf}$ (Movie S5). However, when the pitch reaches a

critical value $\boldsymbol{P = P_{crit} > \overline{X_p}}$, the particle does not have sufficient migration time to reach the next pillar (and potential well) and will oscillate and become trapped (Equation 12).

$$\boldsymbol{P_{crit} > \frac{V_p \chi_p}{\mu_o 6\pi\mu_f r_p} \frac{1}{f} \overline{(B \cdot \nabla)B}} \qquad \textbf{Equation 12}$$

This bimodal behavior, which has also been observed in thin film ratcheting systems[34], is dependent on driving frequency, horizontal pitch between magnetic micro-pillars, particle size, and particle magnetic content. By designing a micro-pillar array with a gradient in horizontal pitch (Figure 5-1 c), particles with varying magnetic contents will equilibrate in different spatial locations and be separated from each other; as particles with higher magnetic content will have higher critical pitches. Furthermore, particles with similar magnetic content will concentrate into quantized bands at the critical pitch under a given driving frequency.

The net magnetic force on a magnetically labeled cell can be described as a summation of forces exerted by each bound particle $\boldsymbol{N_p}$. The magnetic gradient, as well as magnetic force, decays strongly with inter-pillar distance and is concentrated locally near the magnetized pillars. We quantified this empirically by recording particle speeds across the chip at various frequencies at each pitch and deriving the magnetic force (Appendix E Figure S5). The magnetic force was best fit by a form $\alpha\ P^{-2}$, where α=550 pNμm^2 with R^2=0.85. Therefore the total magnetic force on a labeled cell becomes $\boldsymbol{\overline{F_{mag}} = \alpha N_p P^{-2}}$.

Equating the magnetic and drag forces on the cell and setting $\boldsymbol{P = P_{critcell}}$, a relationship between the number of bound particles and the critical pitch can be derived (Equation 4) where the cells critical pitch, $\boldsymbol{P_{critcell}}$, relates to $\boldsymbol{N_p}^{1/3}$.

$$P_{critcell} > \left[N_p \frac{\alpha}{6\pi\mu_f r_{cell}} \frac{1}{f} \right]^{1/3}$$ **Equation 13**

Using Equation 13 as a predictive model, gradient ratcheting arrays can be intelligently designed to achieve quantitative and highly resolved equilibrium magnetic separation of particles and cells.

To realize a magnetic ratcheting based separation system we designed and fabricated micro-pillar arrays with gradients in horizontal pitch as well as a mechatronic system (Movie S3 & Appendix E Figure S3) to generate the ratcheting field. As discussed theoretically, the pillar pitch and driving frequency can be modulated to control the trapping behavior of particles with varying magnetic content. The theoretical model informed the design of two gradient-pitch chips with linearly increasing pitch of either 10μm or 2μm increments for large dynamic range or high resolution separations.

Particle Equilibrium Separation Discretized by Iron Oxide Content

To characterize the system separation behavior, superparamagnetic particles with varying diameters and IO contents were separated under several driving frequencies. Particles ratcheted at a given frequency will traverse an array as long as the pitch, P, remains at or below that particle's critical pitch value, P_{crit}. In this regime the particle displays a linear relationship between particle speed and frequency. The particle will traverse the array until $P > P_{crit}$, where it is unable to traverse to the next micro-pillar and will equilibrate and concentrate at the edge of this pitch region (Figure 5-2a-b).

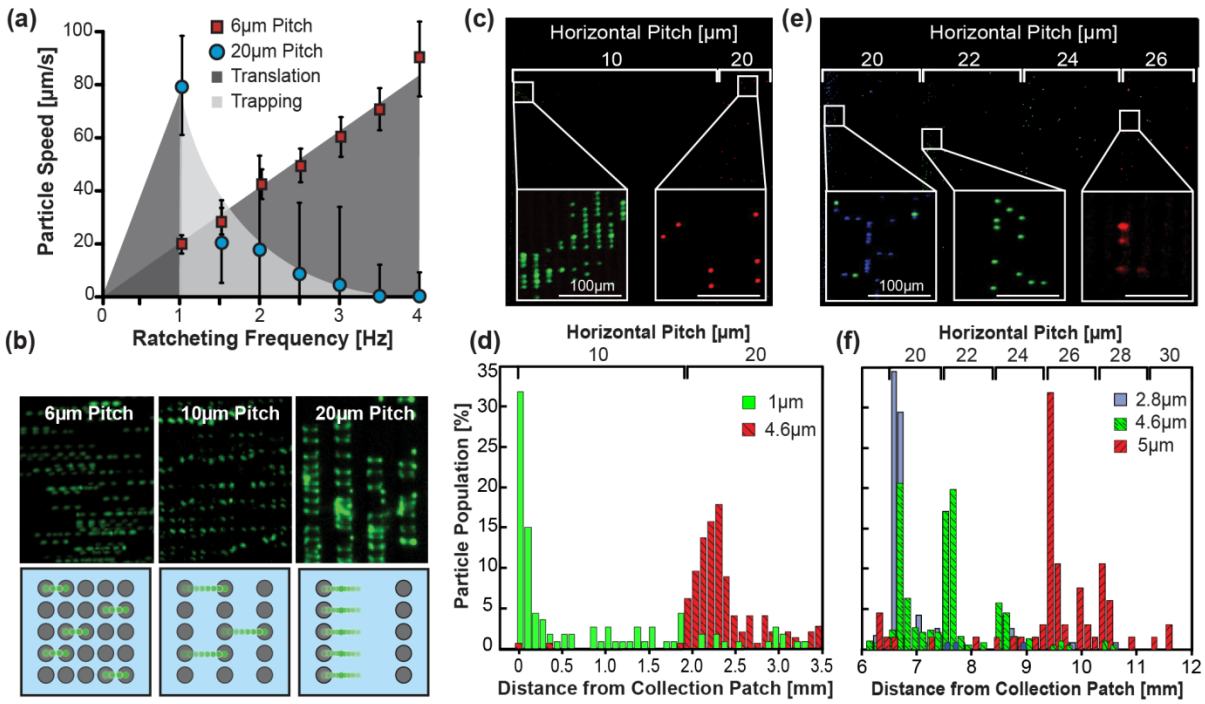

Figure 5-2: Equilibrium separation by ratcheting magnetophoresis on gradient-pitch permalloy arrays. (a) Ratcheting of 2.8µm diameter particles (IO content 10.1pg) within the chip demonstrate bimodal transport behavior dependent on the array pitch. (b) When $P \leq P_{crit}$ the particle speed correlates linearly with frequency, but when $P > P_{crit}$ particles will trap and concentrate on the pillar edge. (c &d) Fluorescently labeled particle mixtures of green 1µm diameter and red 4.6µm diameter (IO contents of 0.98 and 11.1pg respectively) were separated on a 10µm increment chip ratcheted at 30Hz. 83% of the 1µm particles equilibrated at the 10µm pitch and 92% of the 4.6µm particles equilibrated at the 20µm increment patch, demonstrating a >90% separation purity. (e & f) Particle mixtures of blue 2.8µm, green 4.6µm and red 5µm (IO contents 10.1, 11.1 and 67.4 pg respectively) were separated on a 2µm pitch increment chip at 30Hz. 77% of the 2.8 and 41% of the 4.6µm particles equilibrated in the 20µm pitch region. An additional 41% of the 4.6µm particles occupied the 22µm pitch region while 85% of the 5µm particles collected at 26 and 28µm pitches.

Successful separation of mixed 1µm and 4.6µm particles was achieved using a 10µm incremented chip at 30Hz achieving ≥90% purity and 9 pg of IO resolution (Figure 5-2c-d). Though small, some inter-population overlap was observed which we suspect is due to 1µm particle aggregates or a lack of quality control in particle size. In addition to separation, each particle population was concentrated by 500 fold from bulk solution.

As expected, the 2µm incremented chip leads to finer resolved separations with a mixture of three particle types demonstrating a resolution of 5.6 pg of IO (Figure 5-2e-f). The 2.8µm particles could be easily separated from 5µm particles with a >90% purity. Interestingly, the 4.6µm particles subdivided into three subpopulations at the 20, 22 and 24µm pitches which was unexpected as our model predicted a critical pitch of 24µm for this particle. We determined that this behavior was most likely due to variations in IO content as derived from the particle data sheet[59]. This suggests that the system can achieve resolutions bordering on 1pg of IO. After characterizing separation behavior, we employed the magnetic ratcheting separation system to measure and concentrate cell populations based on surface expression level of Epithelial Cell Adhesion Molecule (EpCAM).

Quantitative Magnetic Cell Separation Based on EpCAM Surface Expression

We first found that the quantity of 1 µm diameter, anti-EpCAM magnetic particle binding correlated with αEpCAM immunofluorescence on two prostate cancer lines with differential expression. LNCaP cells have been reported to have high but varying EpCAM expression (337,000 ± 37% molec/cell[60]), which was in agreement with our flow cytometry analysis that demonstrated a variation from mean fluorescence of ± 27% (Appendix E Figure S7). PC3 cells have comparatively lower EpCAM expression levels, ~ 52,000±78% molec/cell which we confirmed with flow cytometry analysis (Figure 5-4b, $p<<0.05$). Quantity of bound magnetic particles followed a similar trend where PC3 cells ranged between 1-41 bound particles per cell while a majority of LNCaPs ranged between 21-103 particles per cell ($N_{LNCaP}=508$, $N_{PC3}=57$, $p=5.7e-6$).

Once we confirmed that particle binding correlated positively with EpCAM expression, LNCaP cells were magnetically labeled and separated using the ratcheting system (Movie S6). Labeled LNCaPs driven with a 5Hz ratchet separated and equilibrated at critical pitches according to their bound particle quantity (Figure 5-3). Using kmeans statistical analysis, cells were binned (unpaired two-tailed t-test, $p<<0.05$) into five subpopulations with particle binding quantities of 1-25, 22-46, 40-70, 83-123 &130-180 particles per cell (PPC) each equilibrating at their corresponding critical pitches. The average PPC's for each subpopulation demonstrated the expected 1/3 power relationship between critical pitch and PPC, in agreement with the predictive (Equation 4, $R^2=0.91$). Furthermore, the system was able to resolve the cells at high resolution resolving a 13 particle differential between the 10-24µm pitch regions. Additionally, the population distribution from the ratcheting cytometry chip (Figure 5-3d) was similar to flow cytometry data on the same LNCaP population (Figure 5-3 a &b). The LNCaP distribution was centered on the 22µm pitch and had a coefficient of variation of 37%, which was close to the flow cytometry distribution with a 27% coefficient of variation.

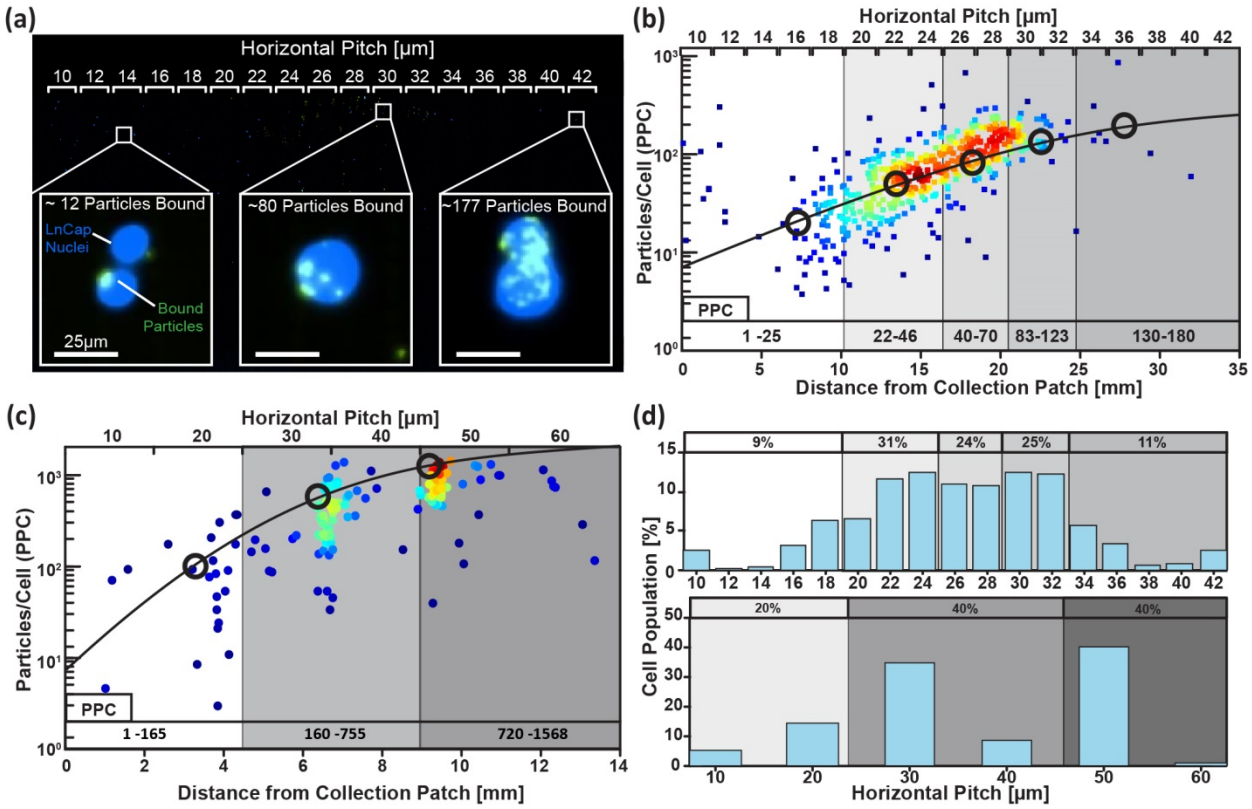

Figure 5-3: Equilibrium separation and analysis of LNCaP EpCAM distribution in a gradient pitch array. (a) A stitched image is shown of magnetically labeled LNCaP cells equilibrating at different pitches within a 2μm incremented chip driven at 5Hz frequency. Insets show cells equilibrating at pitches according to quantity of particles per cell (PPC). (b) The graph plots the PPC versus the on-chip location and critical pitch of individual cells (points). The theoretical 1/3 power relationship between PPC and pitch is shown as a solid line. Five statistically significant ($p<0.05$) populations were identified ranging from 1-25, 22-46, 40-70, 83-123 &130-180 particles per cell with corresponding averages (black circles). Each subpopulation equilibrated at increasing horizontal pitches, correlating well with the theoretical model ($R^2=0.91$). (c)The PPC distribution of magnetically labeled LNCaP cells is also plotted for a 10μm incremented chip at 5Hz, again correlating with the predicted model ($R^2=0.89$). More punctate trapping is observed due to the coarseness of the pitch gradient and additional populations of more strongly labeled cells are observed compared to the 2μm incremented chip. (d) Independent of the attached particle number, the cell distribution as a function of pitch for both chips is also shown (N=508).

To accommodate separation and enrichment of cells with larger magnetic signatures, ratcheting cytometry with labeled LNCaPs was also performed on a 10μm incremented chip driven at 5Hz (Figure 5-3c & d). Using the same kmeans and t-test

analysis, three PPC ranges of 1-165, 160-755 and 720-1598 PPC were resolved. This behavior on the 10µm incremented chip also correlated with the predictive model (R^2=0.89) and separated a subpopulation of cells that was not detected in the 2µm increment. This population, with a PPC range of 720-1598, was not observed in the 2µm incremented chip most likely due insufficient pitch length, whereby this population may have ratcheted off the end of the chip.

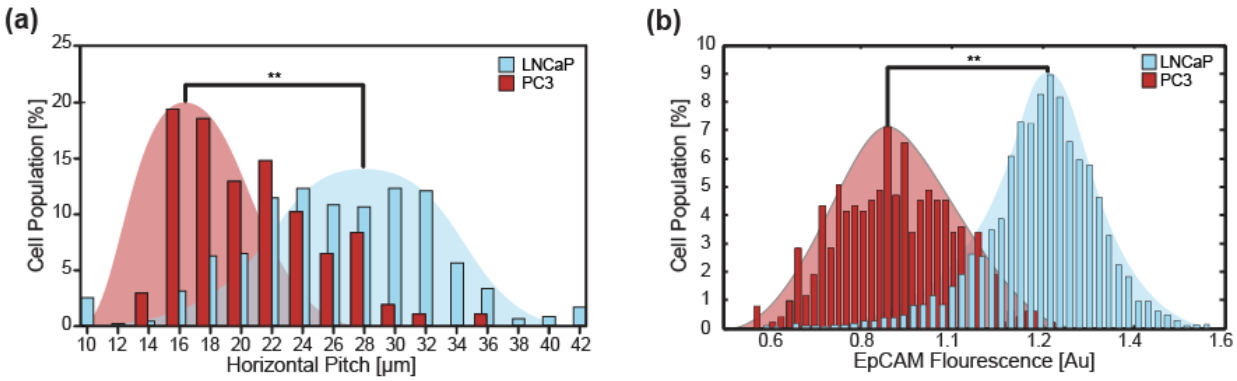

Figure 5-4: Ratcheting cytometry of PC3 and LNCaP cells showed differential population distributions consistent with flow cytometry analysis. (a) PC3 cells demonstrate lower EpCAM expression and therefore equilibrate at lower critical pitches when ratcheted at 5Hz on a 2µm incremented chip compared to the LNCaP cells. (b) Flow cytometry analysis shows a similar trend in differential expression between the PC3 and LNCaP cell populations.

In addition to LNCaP cells, ratcheting cytometry was also performed on PC3 cells to compare EpCAM expression profiles. Using a 2µm incremented chip, we were able to see differences in equilibrium pitches between LNCaP cells and PC3 cells ratcheted at 5Hz, in agreement with EpCAM expression levels (Figure 5-4a). PC3s exhibited PPC signatures of 1-23 and 19-41 (p=0.01), which equilibrated at 14-20µm and 22-26µm pitches respectively.

Ratcheting Cytometry of Prostate Circulating Tumor Cells

The system was then assessed as a rare cell cytometer using low levels of cancer cells spiked in blood, simulating prostate circulating tumor cell (CTCs) samples. Our goal was to quantify surface expression profiles on CTCs but also address the major barrier of CTC purification which has limited MACS and other CTC capture systems. Using magnetic ratcheting cytometry, highly expressing CTCs can be quantitatively separated from the leukocyte background at high purity streamlining downstream precision assays. As a control, healthy blood was labeled with 1μm αEpCAM particles and ratcheted through a 10μm incremented chip to quantify contaminating leukocyte background. Most of non-specifically labeled leukocytes occupied a pitch range from 10-60μm and equilibrated mostly at the 20μm pitch corresponding to a PPC range of 1-25 (Appendix E Figure S8). From this data we set a “cut-off” pitch at 60μm. Therefore, CTCs could be successfully purified as long as they equilibrated at a ≥70μm pitch.

To simulate patient samples low levels of LNCaP (~100 cells/mL) were spiked into healthy blood and were separated on a 10μm incremented chip at 5Hz (Figure 5-5a). The spiked cells were successfully extracted from the leukocyte background and equilibrated mostly at the 80μm pitch (Figure 5-5b). Of the spiked cells approximately 24.9±1.94% were recovered and purified. This capture efficiency is comparable to MACS based techniques targeting prostate cancer cells with EpCAM[57,58]. However, compared to standard MACS techniques the separation purity (Figure 5-5c) was significantly higher where a majority of the LNCaPs were successfully extracted from the leukocyte background. Note that for traditional MACS any amount of magnetic labeling leads to capture, ultimately resulting in lower purity.

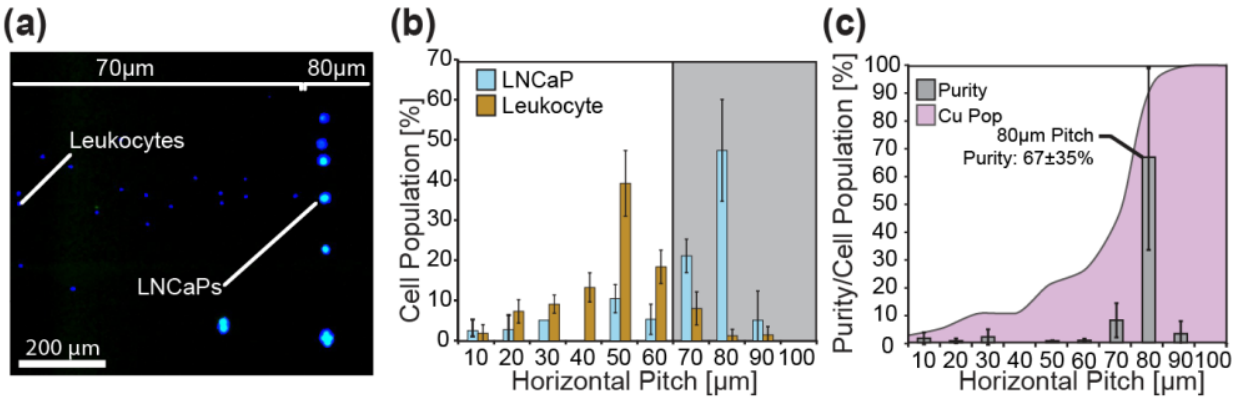

Figure 5-5: Separation of LNCaP cells from leukocytes as a function of pitch. (a) After quantification of leukocyte background and setting a cut-off pitch at 60µm, LNCaP cells spiked into blood were separated and purified from the leukocyte background on a 10µm incremented chip under a 5Hz ratchet. (b) High purity separation of LNCaPs from leukocytes was achieved despite both populations shifting to higher pitches. The LNCaP majority equilibrated at the 70-100µm pitches peaking at 80µm while the leukocytes equilibrated between the 10-60µm pitches peaking at 50µm. (c) Purity, defined as the total number of LNCaPs to total cells, for each pitch was determined showing a maximum purity of 67±35% at the 80µm pitch. The cumulative population the spiked cells was determined by sequentially summing the spiked population beginning at the 10µm pitch and showed 26% of the spiked population equilibrated below the cut-off pitch.

Interestingly, the recovered LNCaPs and non-specifically-labeled leukocytes occupied higher pillar pitches than observed in buffer. A majority of the LNCaPs, 74%, resided at the 80µm pitch which we hypothesize is attributed to an effective particle concentration increase due to the excluded volume of the red blood cells. Additionally, the non-specifically labeled leukocyte population demonstrated a shift towards the higher pitches but a vast majority, ~90%, remained at or below the cutoff pitch of 60µm and therefore did not significantly affect the 70µm-100µm pitch purities. The system demonstrated minimal loss as shown in the cumulative distribution plots (Figure 5-5c). 74% of the extracted LNCaPs were cleared past the cut-off pitch and highly purified. The purity of the extracted cells above an 80µm pitch was 67±35% and contained 47±14% of the extracted population. In total, the ratcheting cytometry system was able

to successfully concentrate and purify low concentrations of cancer cells from blood making it a tenable option as a clinical purification instrument for CTCs.

After validating the magnetic ratcheting cytometry system with spiked cancer cells, clinical blood samples of metastatic prostate cancer patients were run on the chip. We expected some prostate CTCs to exhibit high EpCAM expression (PPC 1700-3600) as observed in the spiking experiments, thereby equilibrating past the cutoff pitch under a 5Hz ratchet. Of note, we define suspected prostate CTCs as large nucleated cells (diameter ≥ 9μm) with high EpCAM expression (PPC ≥1700) and no detectable CD45 expression as quantified by florescence. Three patient samples were labeled and separated on the chip, two of which had several large, CD45 negative cells which equilibrated at the 70-100μm pitches (Figure 5-6a). These results were similar to our spiking experiments and, upon observation, demonstrated morphological characteristics consistent with CTC profiles including large nuclear to cytoplasmic ratio or multinucleated cells (Figure 5-6b). The CTC separation purity was high, where each binned purity for the 70-100μm pitches ranged between 50% to 100% for these two patients (Figure 5-6a Pat 46.1 & 10.3). Furthermore, the loss of suspicious cells was low as the cumulative populations of suspected prostate CTCs for these patients exhibited a skew towards the 70-100μm pitch values. Between 78% and 100% of the suspected CTCs were above the cut-off pitch for the two patients respectively, demonstrating high purity separation without significant loss of the captured cells.

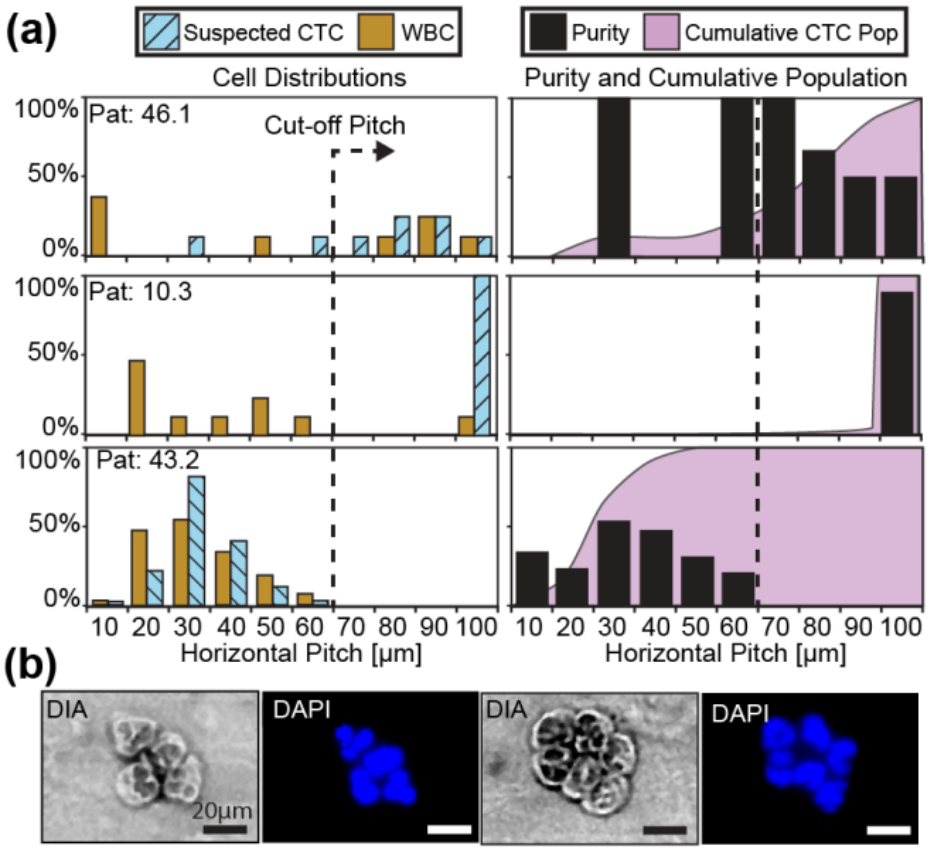

Figure 5-6: Blood biopsies (1ml volume) from prostate patients with metastatic castration resistant cancer were magnetically labeled with 1μm αEpCAM particles and cells were separated on the ratcheting cytometry system. (a) Patients 46.1 and 10.3 had several cells (N=7 and N=8 CTCs respectively) which equilibrated between the 70-100μm pitches with purity ranging from 50% to 100%. In contrast, patient 43.2 exhibited no cells in the 70-100μm pitches and a skewed cumulative population towards the lower pitches. Suspected prostate CTCs extracted from patients 10.3 (b) possessed morphological characteristics consistent with CTCs including large nuclear to cytoplasmic ratio, and large lobed or multiple nuclei in addition to being CD45 negative.

However, one patient exhibited a ratcheting profile more akin to the healthy controls where no cells occupied the 70-100μm pitch ranges (Figure 5-6 Pat 43.2). While many cells equilibrated at the lower pitches had little to no CD45 expression (N=188), they had small nuclei (< 9μm) and are therefore most likely non-specifically labeled leukocytes with low CD45 expression such as neutrophils or granulocytes [61].

In a parallel study with the same patient group, CTCs were captured using microfluidic vortex CTC isolation technology[62]. The findings from the ratcheting cytometry correlated with the vortex technology findings in two patients. The vortex chip detected high suspected CTC counts in Patient 46.1 and little to no CTCs in patient 43.1 which matched the findings of the ratcheting cytometer. Interestingly, ratcheting cytometry extracted several large suspected prostate CTCs from 10.3 where the vortex chip isolated only little to no CTCs. This discrepancy is most likely due to the clustered nature of the cells which prevented entrance into the vortex chip. Overall, the ratcheting cytometry system isolated EpCAM expressing suspected prostate CTCs from peripheral whole blood with an average purity of ~74%, a substantial improvement over traditional MACS-based techniques. The system shows promise as a high efficiency extraction method where high purity is also necessary, such as is the case for downstream sequencing for precision medicine.

Conclusion

Magnetic ratcheting cytometry enables widely used magnetic labeling techniques to be deployed for robust, efficient, and quantitative separations, while simultaneously concentrating target cells. Using 1:1 aspect ratio permalloy micro-pillar arrays we have increased the magnetophoretic force envelope 10 fold compared to thin film ratcheting systems. Increased force not only decreases processing time but enables the use of small particles which is advantageous due to their increased labeling efficiency attributed to large diffusion lengths. In developing a theoretical framework for high force magnetic ratcheting, arrays with gradient pitch can be rationally designed and constructed to achieve separation and concentration of magnetic particles and cells.

Furthermore, these gradient pitch arrays achieve separation in a temporally stable, equilibrium based manner making them more robust than kinetic or flow based separation techniques which are sensitive to dynamic physical parameters such as flow rate. Additionally, magnetic ratcheting cytometry cleanly integrates separation and quantification (on the gradient pillar slide) into a single step assay, bringing a much needed quantitative aspect to MACS systems.

As demonstrated, ratcheting cytometry is an effective tool to capture and quantitatively separate rare cell types in both laboratory and clinical settings. Particularly, the system addresses the major challenge of purity that has plagued traditional MACS based systems. In future works separation resolution can be increased by using smaller magnetic particles to reduce the effective iron content per particle which will likely increase sample purity by reducing labeling time and off-target labeling. Another future system improvement could include a combined 10μm and 2μm incremented chip to enable both high dynamic range and high resolution separation. First cell populations can undergo a coarse separation in one axis and a fine separation in an orthogonal axis, thereby accommodating samples with a large PPC range without sacrificing separation resolution. Additionally, separated cell populations can be further concentrated for simple extraction for downstream processing (Movie S7).

In addition to separation, the magnetic ratcheting system can also be used to manipulate particles and cells at high speed and high resolution (Appendix E Figure S9 & Movie S8). Therefore, the system is not limited solely to separation but can be used as a manipulation platform to develop completely integrated lab-on-a chip systems enabling assays to be performed from whole samples down to single cells directly on

the same chip. For example, target cells can first be quantitatively separated and concentrated using the gradient pitch arrays and then manipulated through fluid reservoirs to perform wash steps or various biochemical assays, or arrayed to enable single-cell interrogation. We envision the ratcheting system as a new platform for lab-on-a-chip automation, enabling sample-to-answer assays to be performed rapidly with single cell resolution.

Experimental

Automated Ratcheting System

The automated ratcheting system (Appendix E Figure S3) consists of a radial array of N52 grade rare earth neodymium ferrite magnets (KJ Magnetics), with a quasi halbach array arrangement (strength ranged from 20-200mT), driven by a custom designed mechatronic system and Labview® interface.

Chip Fabrication

Borosilicate glass (Fisher) slides were piranha cleaned and coated with a Ti-Cu-Ti metal seed layer via e beam evaporation. SPR220 resist was used to make electroplating molds, after which permalloy micro-pillars (1:1 aspect ratio ~4µm height) were electroplated. The chip was then sealed with silicon nitride and coated with spin-on polystyrene. Chips were soaked in 2% pluronic F127 solution before use. See SI Text for details.

Particles and Particle Separations

Magnetic particles of 1µm, 2.8µm, 4.6µm and 5µm were made fluorescent through a variety of surface modifications (SI Text). Particle concentrations ranged between 0.5~1

x 10^6 pts/mL. PDMS interface chips (Dow-Corning) were fabricated using scotch tape lithography[63] to create fluid access. Particle separation was observed by inverting the chip on the stage of a Nikon Eclipse Ti fluorescent microscope and positioning the mechatronic system above it. Particles were injected into the ratcheting chip, ratcheted at various frequencies, and imaged. Image analysis with ImageJ was used to identify particle distributions (Appendix E Figure S6).

Cell Labeling

1µm iron oxide particles (Invitrogen) with anti-EpCAM (abcam) were diluted with PBS + 0.5% BSA to a concentration of 10^6 parts/mL and added to a solution of fixed LNCaP or PC3 cells (4% paraformaldehyde) at a 1:100 cell to particle ratio. Labeling was performed at room temperature with gentle mixing for at least 1 hour. Anti-mouse IgG Alexa Fluor-488 secondary (Invitrogen) was added to stain and visualize the particles. The solution was then washed and resuspended into 1mL of PBS.

Flow Cytometry

For flow cytometry experiments, the same fixed cells were used. ~10^5 cells of each type was labeled using anti-EpCAM PE (BD Biosciences) and incubated for an hour. The cells where then washed and resuspended in ~1mL of PBS. Flow cytometry was performed on a BD Accuri C6 flow cytometer with sampling of at least 2000 events.

Ratcheting Cytometry Separation based on EpCAM

1µm magnetically labeled LNCaP and PC3 cells (Hoechst stained) were injected at 50µL/min via a syringe/PEEK tube assembly onto the ratcheting chip's loading patch. Note that both 2µm and 10µm chips where characterized. Simultaneously the

mechatronic system was positioned over the loading patch to concentrate the cells. Ratcheting was initiated at a frequency of 5Hz for ~ 10 minutes. The entire chip was imaged under DAPI and FITC wavelengths.

Image Analysis and Aggregate Statistics

Stitched images of ratcheted cells and particles were analyzed using an automated MATLAB script to crop each cell, sum the florescent grey value of the particles (FITC), and normalize to the total cell area (DAPI). This numerical value was proportional to the number of bound particles per cell and was calibrated for each image analyzed.

Kmeans and t-test statistical analysis was used to characterize the relationship between bound particles and pillar pitch. Using a MATLAB script with a kmeans algorithm, the number of statistically significant populations ($p \leq 0.05$) and their mean PPC was determined.

Blood Spiking, Capture Efficiency and Purity Experiments

Peripheral whole blood collected from healthy donors, including 1 age matched, were aliquoted into 1mL volumes then spiked with ~100 FITC labeled LNCaPs. The blood was then diluted 5x with PBS and labeled with 1µm anti-EpCAM particles at 10^6 particles/mL (SI Text). Ratcheting separation was carried out at 5Hz and the entirety of the chip was imaged under DAPI and FITC filter sets. Capture efficiency was determined by counting the number of FITC positive cells and comparing to a control. Purity characterization was performed similarly where ~2000 FITC labeled LNCaP cells

were spiked into 1mL of whole blood, labeled, then separated at 5Hz. Purity was defined as the ratio of spiked LNCaP cells to the total number of cells binned by pitch.

Ratcheting Cytometry with Prostate Cancer Patients

Blood was obtained from prostate patients with metastatic castration resistant cancer being treated at the UCLA medical center according to IRB approved protocol. Blood was aliquoted, stained with Hoechst & CD 45, diluted 5x in PBS and labeled with particles (SI Text). Similar to blood spiking experiments the cells were separated using a 5Hz ratchet and imaged under DAPI and TRITC filter sets.

Acknowledgements

This work was supported through the NIH Director's New Innovator grant (1DP2OD007113). We thank Dr. Eric Diebold for flow cytometry analysis, Dr. Jere Harrison for help in microfabrication, and Brian McVerry for particle functionalization. Additional thanks to the California NanoSystems Institute for ISNC microfabrication facilities.

Chapter 6 : Biofilm Disruption using Magnetic Ratcheting Scrubbing

In addition to manipulation and separation, ratcheting can be used for therapeutic uses specifically involving clearing of biofilm infections from implanted devices such as catheters. Implanted catheters are commonly utilized for both monitoring blood and administrating treatments and unfortunately are a major source for hospital acquired infections (HAIs) [64,65,66]. Often times, these infections are caused by opportunistic pathogens which are members of general bacterial skin flora such as staphylococcus epidermidis (S. epidermidis) and staphylococcus aureus (S. aureus). Upon implantation, these bacteria will begin to colonize the catheter lumen and form biofilms[66,67]. The traditional method of treatment for bacterial biofilm related infections involves the use of highly concentrated antibiotics applied locally within the catheter, a technique known as antibiotic lock therapy (ALT)[68]. However ALT has limited success with biofilm based infections as the biofilm provides a diffusive barrier from antibiotics due to the dense polysaccharide matrix that constitutes most biofilms. Due to this limited diffusion, ALT treatments will often fail to deliver the antibiotics to all of the organisms within the biofilm. To address this need, magnetic ratcheting can be used to physically disrupt the biofilm, enabling antibiotics to penetrate deep into the biofilms and eradicate the colonizing pathogens (Figure 6-1).

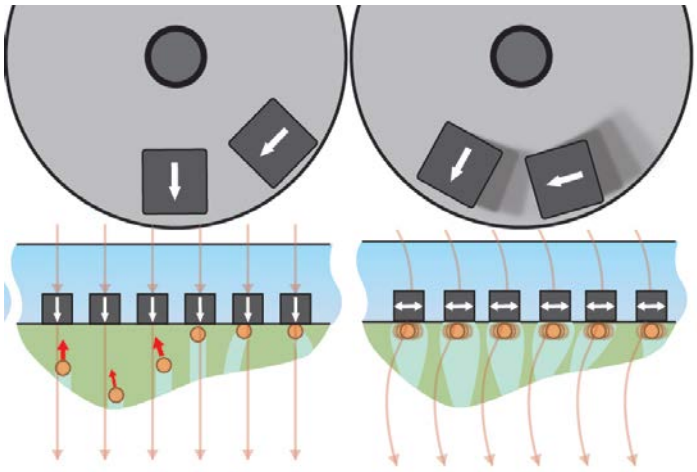

Figure 6-1: Magnetic ratcheting for biofilm disruption. Imbedded micro-pillar arrays underlying surface where bacterial biofilms can colonize can be used mechanically perturbate the biofilm structures, increasing antibiotic penetration. Using iron oxide micro or nanoscale particles, biofilm can be pulled into the biofilm under a static field and then ratchetted to further disrupt the film.

As a model strain for catheter infection, S. aureus biofilms were grown on ratcheting substrates. The ratcheting substrates were immersed in tryptic soy media, inoculated with approximately 1000 S. aureus bacteria which have been shown to constitutively form biofilm and incubated for 36 hours at 37ºC. After biofilm growth the substrates were exposed to red florescent SPIONS (100nm diameter) at a concentration of 10^6 particles per mL and exposed to a static field directed normal to the substrate plane with a strength of 0.5T. After approximately 1 hour of field application, the biofilm appeared to be deformed into discrete columns which co-localized with the micro-pillars (Figure 6-2a). This behavior is attributed to the forces imparted onto the biofilm by co-localized SPIONs. Furthermore the high forces generated by the micro-array pillars shows high porosity as the within the biofilm at the magnetic particles mechanically perturb the film as demonstrated in Figure 6-2c. Compared to a control of polystyrene (Figure 6-2d &d), the micro-pillars are able to generate substantially high

mechanical perturbation and increased porosity into the biofilm which could increase antibiotic effectiveness.

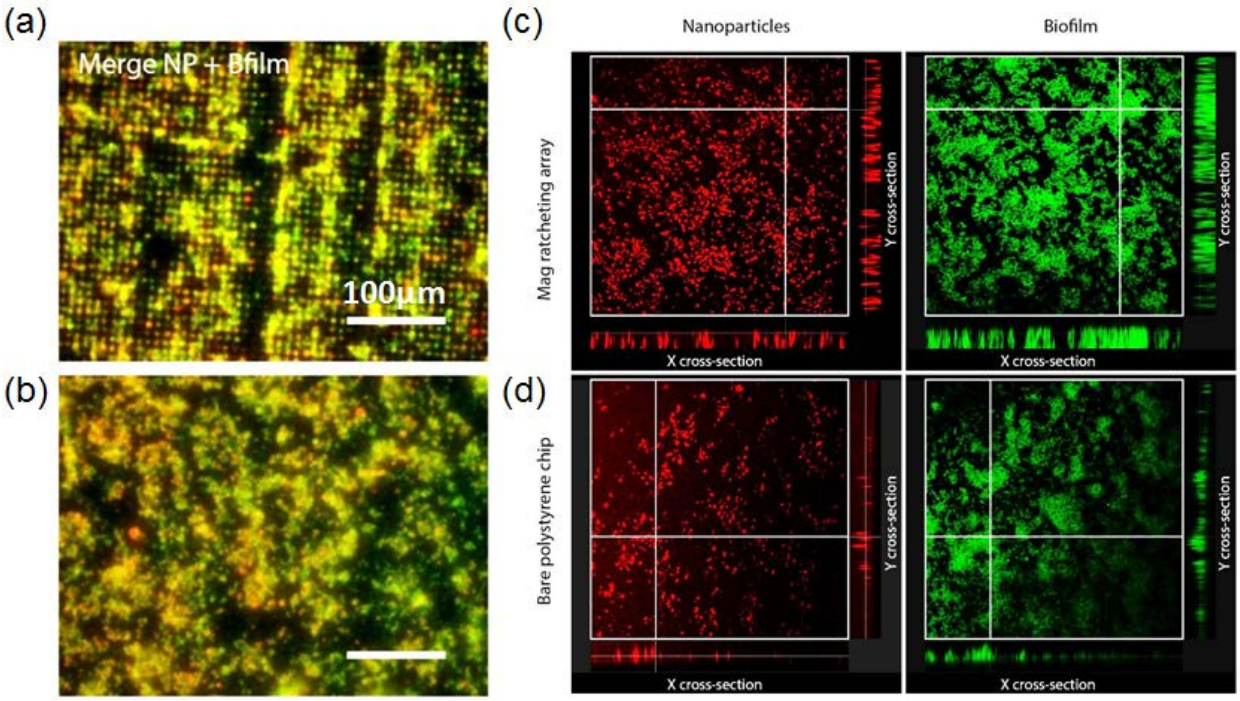

Figure 6-2: (a) S. aureus biofilm (green) with co-localized 100nm SPIONs (red) under a normally applied 0.5T magnetic field demonstrate mechanical perturbation due to local applied magnetic forces while (b) a control on polystyrene under the same field shows minimal mechanical perturbation. (c) Film portion, due to local forces, was provided by localized micro-pillar arrays but was not observed in the polystyrene control (d).

Further mechanical biofilm disruption was achieved by ratcheting biofilms under a dynamically applied field using larger (3µm) magnetic particles. First the particles were pulled into the biofilm under a static field and ratcheted at 1Hz to effectively "scrub" the surface (Movie S9). Figure 6-3 shows a biofilm inoculated substrate (magenta) before ratcheting with 3µm particles and after ratcheting 3µm particles repeatedly back and forth across the substrate for one hour.

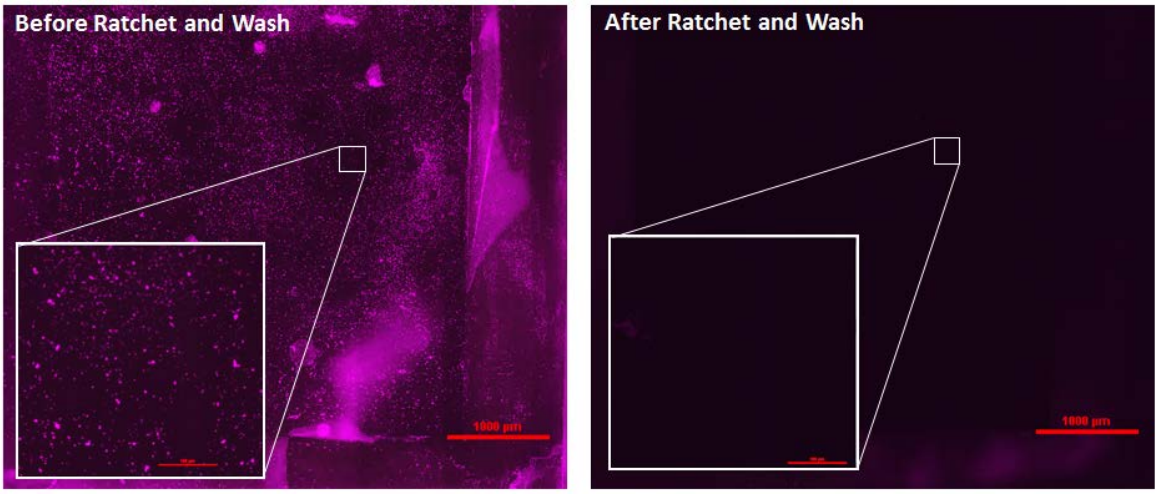

Figure 6-3: Pre-treated ratcheting substrate (left) demonstrating S. aureus biofilms (magenta). One hour of treatment with ratcheting scrubbing using 3µm particles at 10^6 particles/mL at 1 Hz shows dramatic decrease in the adhered biofilms which have been scrubbed off the surface.

The effectiveness of ratcheting scrubbing was quantified (Figure 6-4) by sonicating substrates for 8 minutes to release the colonies from the surface and re-culturing them in sterile tryptic soy broth with agar. Both the statically applied field and the ratcheting scrubbing showed a reduction of 91% compared to control showing potential as a method for therapeutic treatments of biofilm catheter infections.

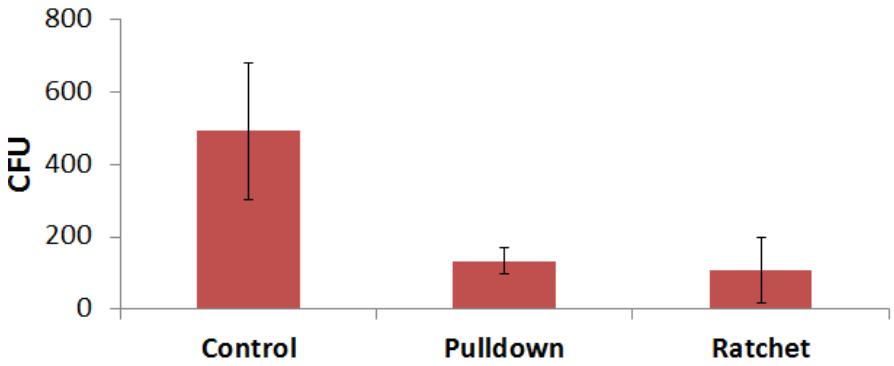

Figure 6-4: Quantification of ratcheting scrubbing with 3µm particles. Compared to control, both static and ratcheting treatments show substantial reduction in biofilms procured from ratcheting substrates.

Ratcheting treatment of biofilms presents many advantageous which can be used in conjunction with traditional treatments such as ALT. SPIONS are commonly used as injectable dyes for MRI contrast agents and are FDA approved. By imbedding micro-pillar arrays into catheter lumens, mechanical disruption in concordance with antibiotic treatment can be utilized using FDA approved reagents. Additionally, the particles themselves can be used for therapeutic means either by functionalization with a charge group to mediate attachment to biofilm surfaces or doping with antibiotics which can be released into the biofilm by a chemical trigger[69]. Furthermore, biofilm disruption can be achieved in a minimally invasive manner as magnetic fields can be used to penetrate into the body, not requiring direct contact with the catheter.

Ratcheting manipulation stands not only as a manipulation architecture but also as a therapeutic platform in treating biofilm infections. However, there are many different applications where this could be useful to achieve microscale transport within the body for use in artificial organ technology where magnetic particles have been shown to perform continuous dialysis operations[70]. Indeed ratcheting is not solely limited to in vitro operations but also has therapeutic potential.

Chapter 7 : Concluding Remarks

Ratcheting manipulation provides a highly parallelized, nanoscale resolved, biocompatible manipulation platform that can be used to develop fully integrated systems to perform miniaturized biological assays. While ratcheting manipulation has been studied in the past, it has been limited in its ability to apply high force to perform high throughput operations on small magnetic particles. This work demonstrates an innovative solution to these shortcomings by utilizing unity aspect ratio micro-pillar arrays amplify magnetic force; extending throughput by an order of magnitude and allowing advantageous the use of nanoscale magnetic particles. An analytical model for traveling wave ratcheting transport was also developed to provide design rules for intelligent design of these systems. To provide repeatable and robust manipulations, a mechatronic system was developed to allow for automated or manual control through an intuitive graphic user interface and joystick. The ratcheting system was able to achieve highly parallelized manipulations with 500nm-1μm resolved motion control with a 93% fidelity. This highly parallelized motion control demonstrated proof of concept for subcellular interface and also high throughput piloting of magnetically labeled cells in any arbitrary path.

Using the system's high force envelope, assays such as magnetically activated cell sorting could be improved enabling the use of small magnetic particles with high cell labeling efficiency. Using a concentrating ratcheting array, endothelial cells were extracted from bulk solution in as little as 10 minutes, demonstrating the systems applicability in point of care applications. In addition to rapid concentration, separation based on magnetic content was also achieved by introducing gradient pitch arrays.

Using the gradient pitch arrays iron oxide content encoded separation was achieved with high resolution, which can enable multiplexed magnetic precipitation assays of multiple targets in complex biosamples. In addition to particles, LNCaP cells were separated based on EpCAM surface expression using the quantity of bound magnetic particles as a metric. This quantitative magnetic separation on ratcheting arrays was utilized to measure surface expression profiles on LNCaP and PC3 cells but was also to purify EpCAM expressing cells from spiked and clinical samples, showing applicability as an integrated clinical instrument.

In addition to in vitro development, we demonstrated ratcheting in a therapeutic use case for treatment of bacterial biofilm infections of catheters. Using particles to physically prorate or scrub the system was able clear a majority of the biofilm from the surface. Combined with traditional antibiotic based therapies, this technique stands to improve current treatment options and help alleviate the burden of biofilm related infections on the healthcare system.

In conclusion, we have shown the power and applicability of magnetic ratcheting as a tool in building miniaturized systems. Ratcheting provides a vehicle to extend our reach into the microscopic length scale to solve problems or gain knowledge; providing us a million tiny hands to reach into, explore, and engineer in the microscale world.

Appendices

Appendix A

Magnetic activated cell sorting involves the use of superparamagnetic particles conjugated with a ligand, such as an antibody, to specifically label a target cell population within a fluid sample. The magnetic particle solution is added to a fluid sample where the magnetic particles will be conjugated onto the desired cell type via the antibody. Using a large magnetic field or magnetic column, the labled cells can be extracted and concentrated for further processing

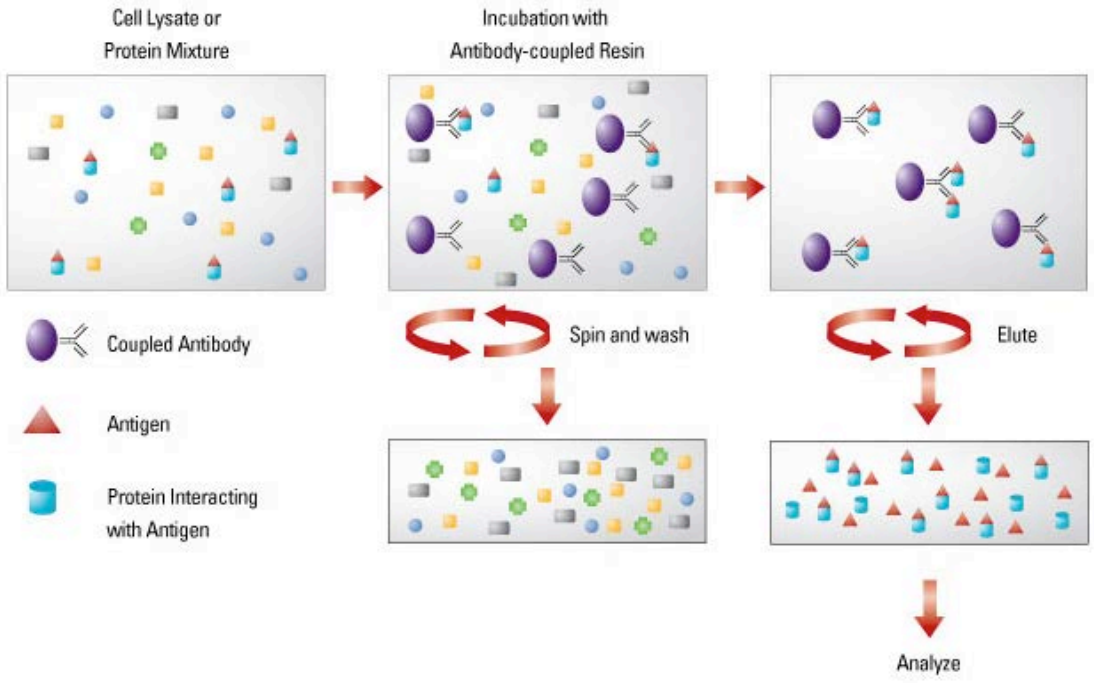

Procedural schematic of a standard immunoprecipitation assay (Credit: Pierce Protein Biology Products, http://www.labome.com/method/Antibody-Applications.html, accessed 8/6/2015)

Appendix B

Adapted from M. Glickman, T. Niblock, J. Harrison, I. Goldberg, P. Tseng, and J. Jud y. "High Permeability Permalloy for MEMS." *Solid State Sensors and Actuators Workshop* (2010).

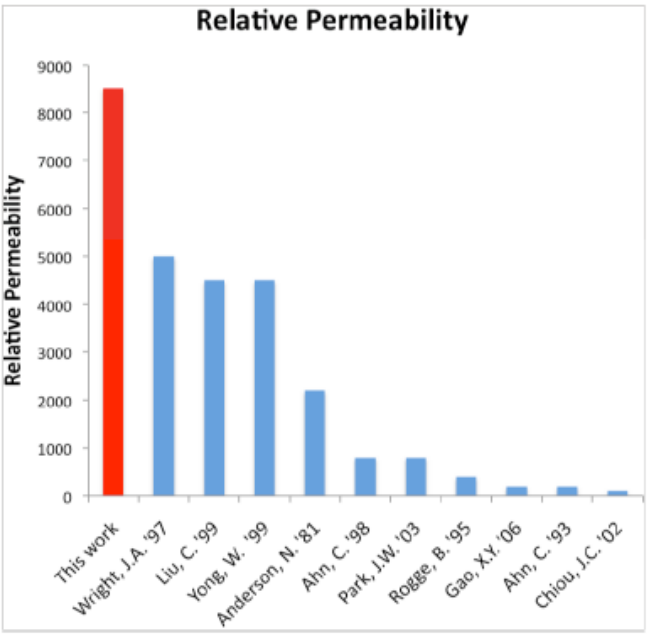

Figure 1: Comparison of maximum permeability of various published work.

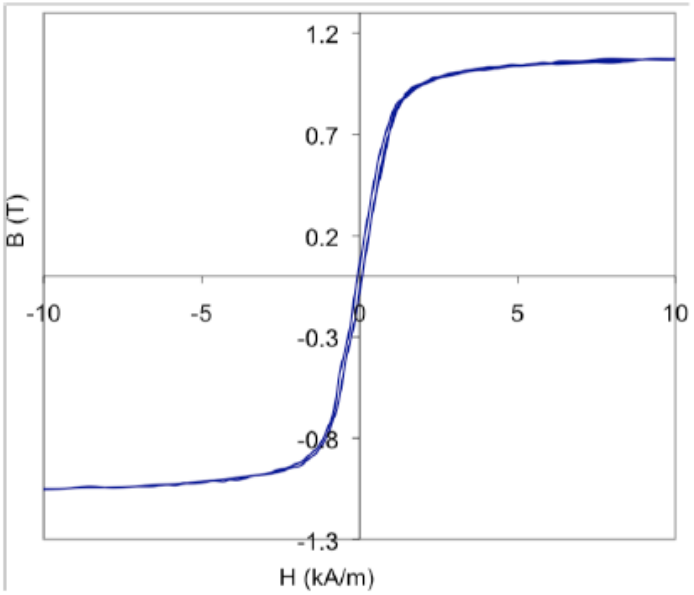

Figure 5: NiFe 80/20, not corrected for demagnetization factor.

Appendix C

Magnetization Shape coefficients:

Adapted from Jiles, D. , *Introduction to Magnetism and Magnetic Materials*

Source: UCLA Course MAE 282, Professor Eric Chiou. *Magnetic Actuators II* (2012)

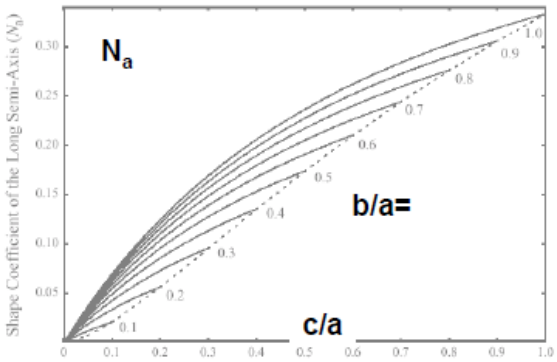

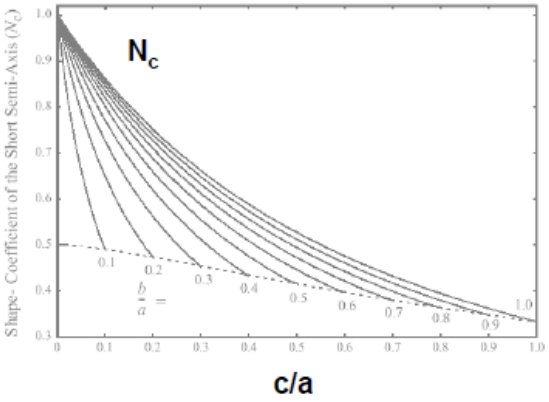

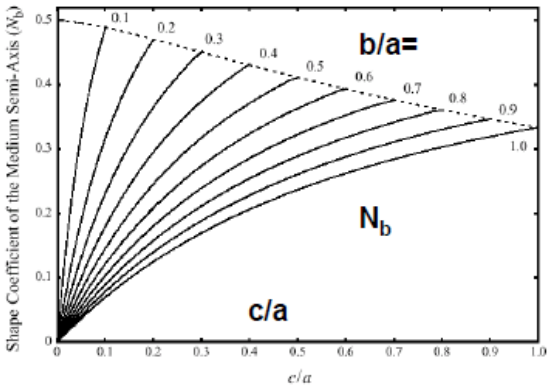

N_a, N_b, N_c depends on shape parameters a, b, c (convention: a ≥ b ≥ c)

For example, a = 50 um, b = c = 5 um
→ b/a = 0.1, c/a = 0.1
→ N_a = 0.02, N_b = 0.48, N_c = 0.48

Appendix D

Magentic field mesasured by a gausmeter on the magentic wheel. Br and Bt correspond to the radial and tangential field as measured with respect to the wheel.

Point	Angle [º]	R [mm]	Br [mT]	Bt [mT]
A	0	2	-22	-19
B	11.25	2	-20	-22
C	22.5	2	-12	-36
D	33.75	2	23	-55
E	45	2	122	-43
F	56.25	2	183	6
G	67.5	2	140	42
H	78.75	2	80	26
I	90	2	76.1	25
J	101.25	2	88	61
K	112.5	2	23	67
L	123.75	2	22	64
M	135	2	-55	-9
N	146.25	2	-69	-11
O	157.5	2	-42	-15
P	168.75	2	-29	-18
Q	180	2	-23	-21

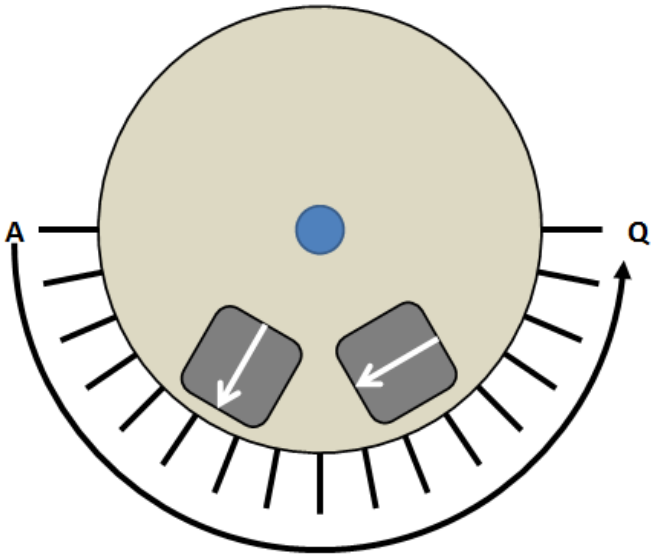

Appendix E

Supporting Information: Quantitative Magnetic Separation of Particles and Cells using Gradient Magnetic Ratcheting

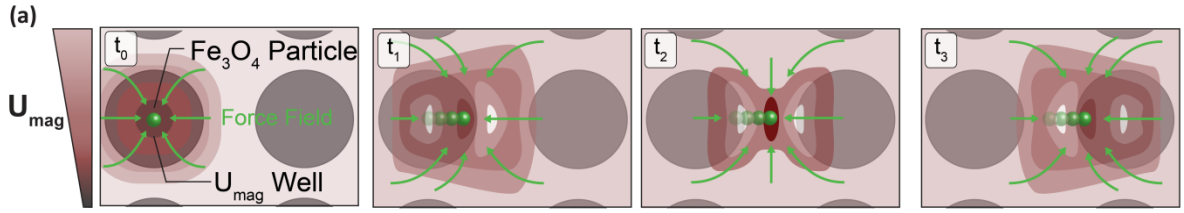

Figure. S1: Magnetic ratcheting utilizes arrays of electroplated permalloy micro-pillars to create dynamic potential energy wells which can be used to trap and manipulate superparamagnetic particles. When a bulk magnetic field is applied, the micro-pillars magnetize in alignment to the bulk field and modify the magnetic potential energy landscape introducing dynamic potential wells in which superparamagnetic particles become trapped. As the field orientation is cycled particles will follow the changing potential wells and ratchet through the pillars if the frequency and pitch between neighboring pillars is low enough and iron oxide content is high enough.

Comsol Simulation: Permalloy Micro-pillar Aspect Ratio vs. Force Application

One of the peak challenges for translating magnetic ratcheting into biomedical application is attributed to the minimal force envelope. Traditional ratcheting platforms consist of thin magnetic structures (aspect ratios ~ 0.05) which are usually fabricated using metal evaporation. However, thin film structures are limited in the forces they can apply due to minimal amount of volume in the ratcheting elements. As shown in Figure S2, numerical simulations of the micro-magnetic field with various pillar aspect ratios were performed using the Magnetostatics Module Comsol 4.2. As shown in Figure S2c, the peak magnetic force decreases rapidly with aspect ratio.

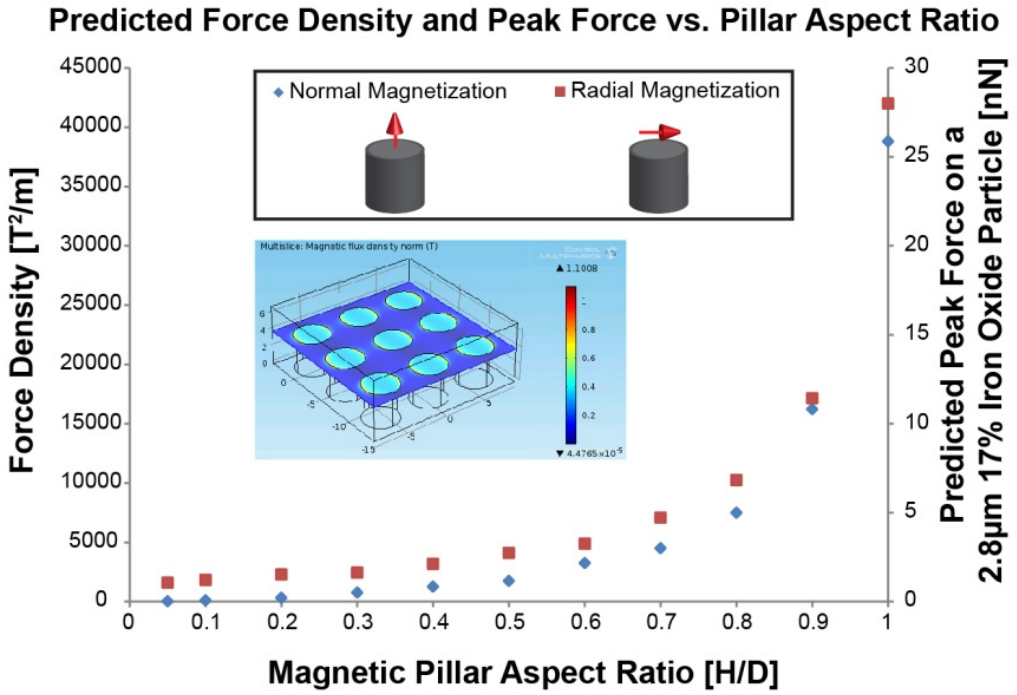

Figure. S2: Predicted peak force on a 2.8µm magnetic particle (Vp=1.95µm^3, 17% Fe_3O_4, χ=0.007,μ_o=4π 1e-7) as a function of pillar aspect ratio was simulated using Comsol 4.2 Magnetostatics Module. In the simulation the pillars were set to have a relative magnetic permeability of 8500, a diameter of 4µm, an orthogonal pitch of 6µm and a height derived from the corresponding aspect ratio (a &b). Boundary conditions included a 304mT inward flux density with either a normal orientation (parallel to the pillar axis) or tangential (parallel to the pillar radii). The force density, defined as $(B \bullet \nabla)B$, was numerically calculated at the surface of each pillar and the magnetic force derived for a 2.8µm magnetic particle (c).

The limitation on the force envelope has limited thin film ratcheting to use larger magnetic particles (2.8µm and above) to compensate. However, larger particles are less ideal for magnetic labeling applications due to their limited diffusivity which results in low labeling efficiency. The presented system overcomes these challenges, with aspect ratios ~1, thereby allowing the use of smaller particles (1µm and under) and enabling magnetic ratcheting to be used as a quantitative separation technology.

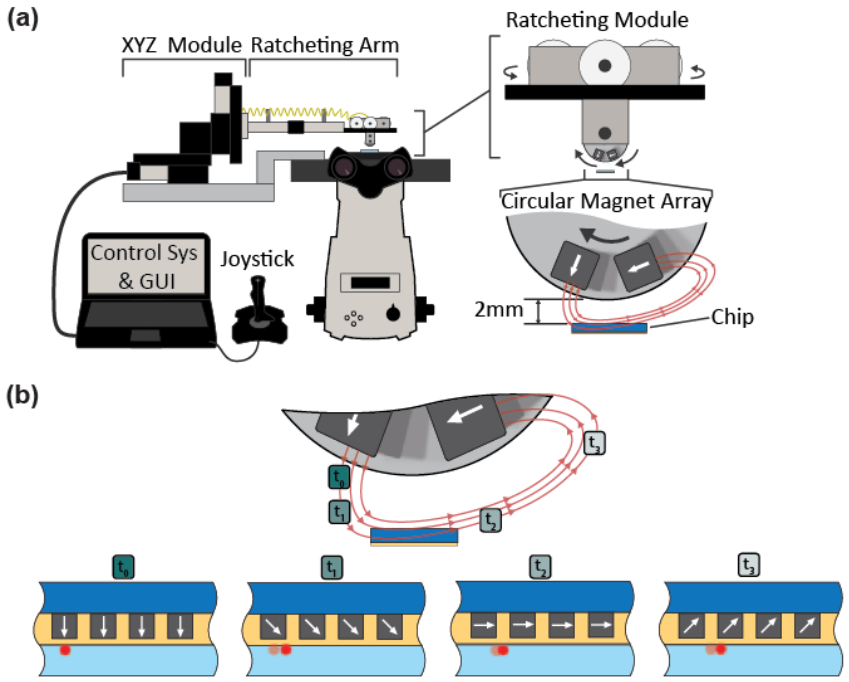

Figure. S3: Automated and scope mounted ratcheting system consists of an XYZ module for positioning and a ratcheting module for angular and ratcheting speed control (a). The chip is first inverted onto a PDMS well containing aqueous buffer, placed on the scope, and then the ratcheting system is positioned over it with an offset of 2mm (a & b). The system was able to operate a full cycle of the radial array at frequencies between 0.1 to 50 Hz.

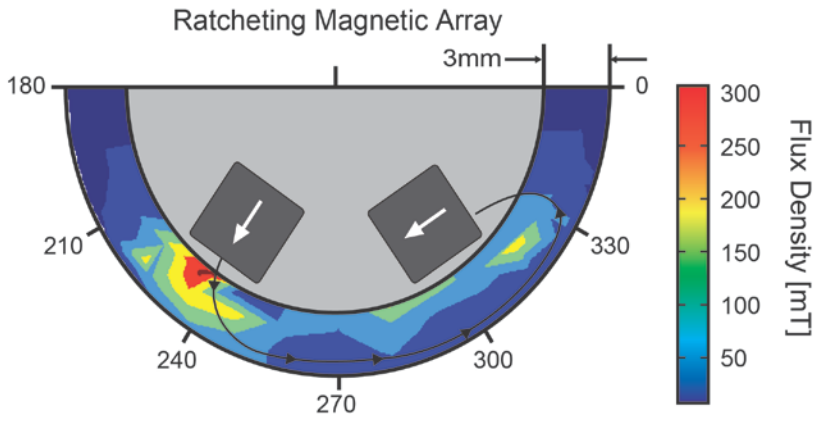

Figure. S4: Magnetic wheel with a partial halbach array of N-52 grade rare earth magnets. As shown the peak flux density is 300mT with an average flux density of ~ 100mT with a max radial distance of 3mm from the surface of the drum.

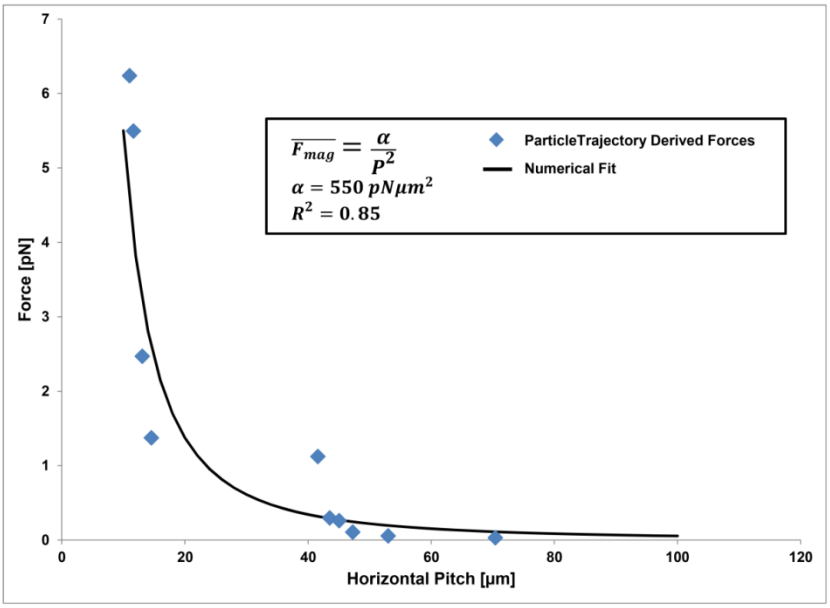

Figure. S5: Calculated magnetic force on a 1µm particle vs. horizontal pitch which was determined empirically by tracking ratcheting trajectories of 1µm Fe_3O_4 particles at various frequencies on 10µm incremented chip by balancing with drag force. A power law best fit the data, specifically αP^{-2}, where $\alpha = 550 pN\ \mu m^2$. Pearson's fit coefficient for this data was 0.85.

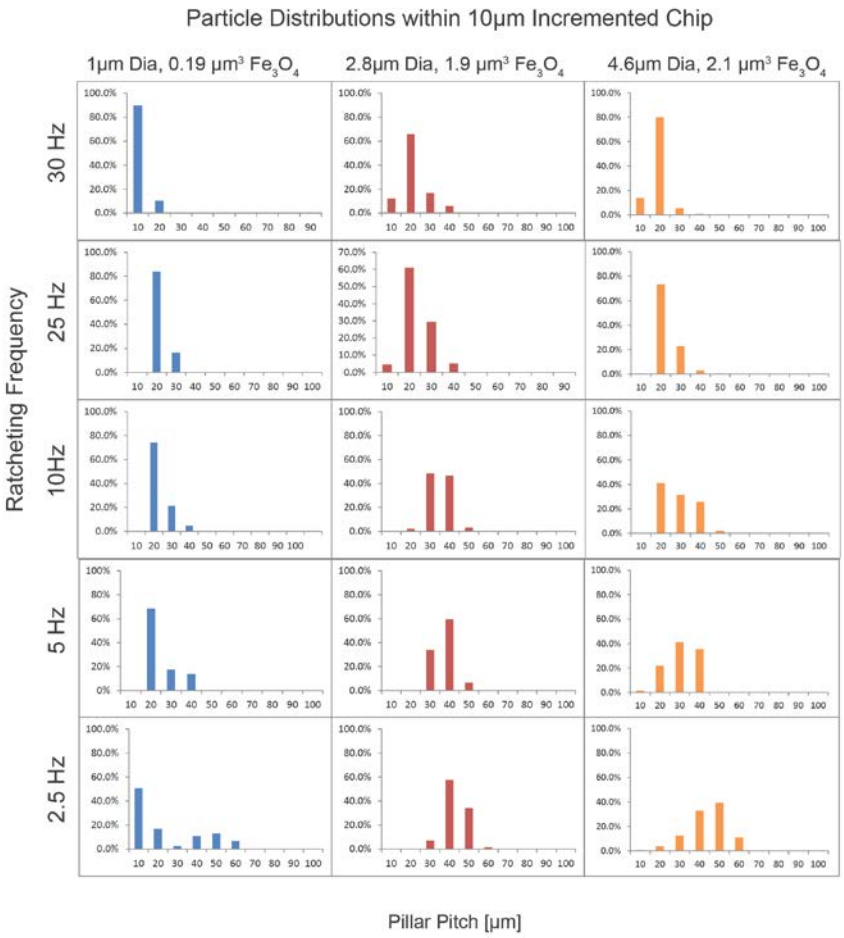

Figure. S6: Shown above are distributions of several particle types (1µm, 2.8µm and 4.6µm diameter) driven at 30, 25, 10, 5 and 2.5 Hz ratcheting. As expected, particles with higher iron oxide content equilibrate at larger pillar pitches. As frequency decreases, the particle population migrates to higher pitches.

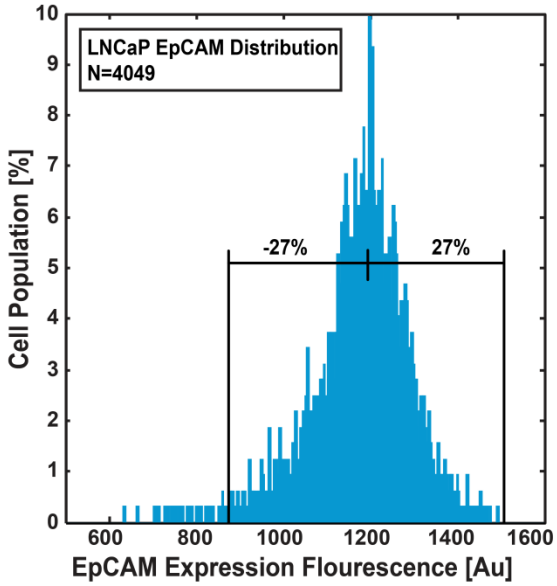

Figure. S7: Flow cytometry analysis for EpCAM expression on LNCaP cells. The EpCAM expression shows a near normal distribution with approximately a 27% coefficient of variation.

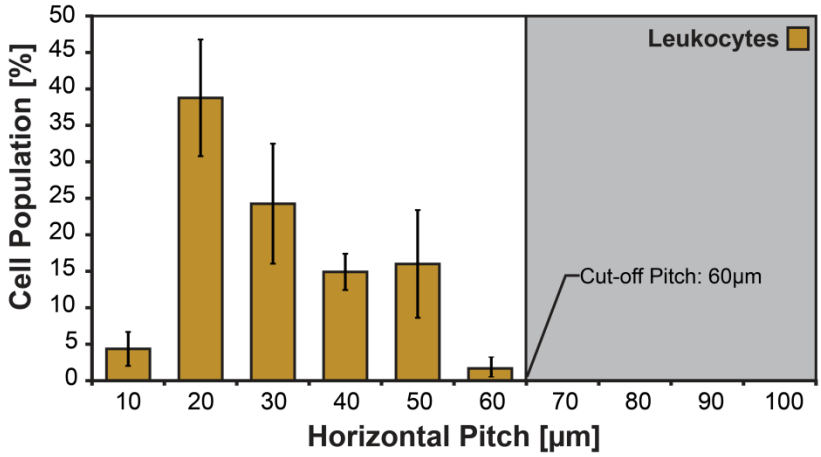

Figure. S8: : Healthy control samples (N=3), including 1 age matched sample, was run through the chip to develop a healthy patient profile and determine cutoff pitch for leukocyte background. The non-specifically labeled leukocyte population occupied the 10-60μm pitches under a 5Hz ratchet, therefore the cut-off pitch was set as ≤60μm and cells equilibrating at ≥70μm under a 5Hz ratchet were past the leukocyte background.

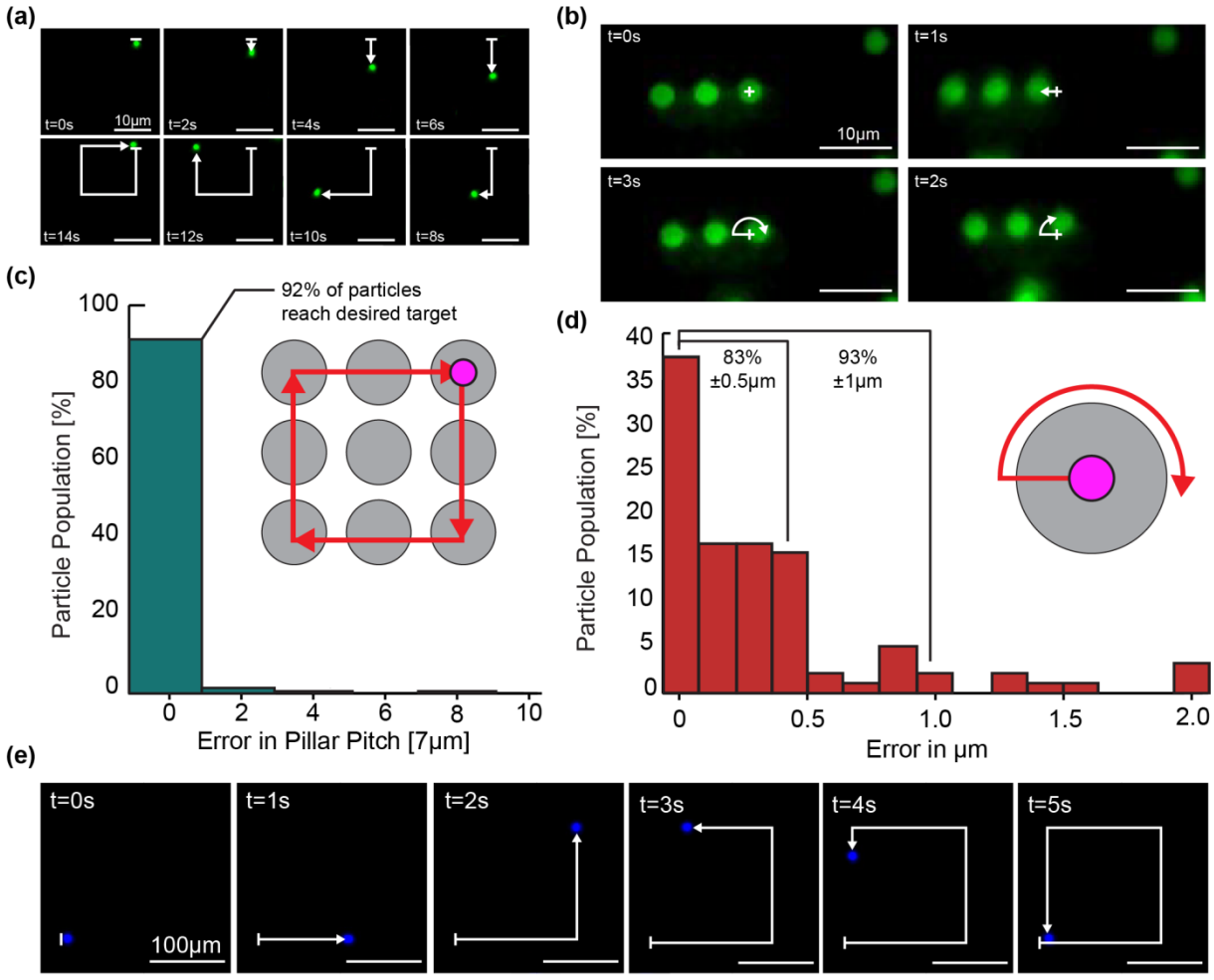

Figure. S 9: Using the automated ratcheting system parallelized and high resolution manipulation of particles and cells can be achieved. (a) Coarse mode manipulations of 2.8μm particles in a square trajectory can be achieved by translating particles between pillars and (b) fine mode, nanometer scale manipulations can be achieved by piloting the particle radially and tangentially on a single pillar. (c) Coarse mode manipulations have high consistency where 92% of particles were successfully piloted to a desired location. (d) Fine mode manipulations demonstrated nanometer scale error with 83% of the particles having a ±500 nm error and 93% of the particle population had a ±1μm error. (d) Cells can also be piloted in an arbitrary trajectory in a parallelized and repeatable manner.

Supplementary Information: Materials and Methods

Chip Fabrication

Polished borosilicate glass (Fisher) were cleaned with piranha solution (30 min), washed in DI water and dried before deposition of 50-nm-Ti, 200-nm-Cu and 50-nm-Ti seed layer using a CHA Mark 30 E Beam Evaporator. SPR 220 photoresist was spun and processed according to specification to form electroplating molds for nickel-iron alloy. Ti was etched in 1% HF, and NixFey was electroplated in a custom plating setup to a ~ 4µm thickness. Photoresist was stripped and both the Ti and Cu layers were etched completely. The chip was sealed by deposition of 100 nm SiN (PECVD). Spin on polystyrene was spun to a thickness off ~1µm above the pillars. Before use, substrates were immersed in 2% by volume Pluronic F127 for 45 minutes.

Particles and Particle Separations

Streptavidin coated 1µm and 2.8µm IO particles, 37% and 17% IO content respectively (Invitrogen), were functionalized with biotinylated fluorescent probes (Invitrogen). 4.6µm biotinylated particles (Spherotech 4.5% IO) coated with streptavidin then with fluorescent biotin. 5µm polystyrene magnetic particles (Sigma, 20% IO) were aminated via perfloroazide and made florescent with Alexa Fluor hydrazide (Invitrogen). Particles were diluted to working concentrations between 0.5~1 x 10^6 pts/mL. PDMS interface chips (Dow-Corning) were fabricated using scotch tape lithography and clamped to the ratcheting chips using a custom made polycarbonate clamp. Separation experiments were executed by inverting the chip on the stage of a Nikon Eclipse Ti fluorescent microscope and positioning the ratcheting system above it. Particles were injected into

the ratcheting chip, ratcheted at various frequencies, and imaged under 10X objective using the DAPI, FITC and TRITC filter sets. Image analysis using ImageJ was used to identify equilibrium particle distributions on the chip for varying frequencies.

Blood Spiking, Capture Efficiency and Purity Experiments

Peripheral whole blood was collected from healthy donors, including 1 age matched donor, and aliquoted into 1mL volumes. ~100 LNCaP cells were pre-labeled with Celltracker Green (Invitrogen) and spiked into the blood. The blood was then diluted 5x with pbs and 1µm anti-EpCAM particles were added to a final concentration of 10^6 particles/mL. The samples were incubated at room temperature for 2 hours with gentle agitation and stained with Hoescht to visualize cell nuclei. The total volume was injected through the magnetized chip at 50µL/min. Ratcheting separation was carried out at 5Hz and the entirety of the chip was imaged under DAPI and FITC wavelengths. Capture efficiency was determined by counting the number of FITC positive cells and comparing to a control. Purity characterization was performed similarly where ~2000 FITC labeled LNCaP cells were spiked into 1mL of whole blood, labeled, then separated at 5Hz. Purity was defined as the ratio of spiked LNCaP cells to the total number of cells binned by pitch.

Ratcheting Cytometry with Prostate Cancer Patients

Blood from patients with metastatic castration resistant prostate cancer was aliquoted into 1mL volumes in Falcon tubes. 12 µL of anti-CD45 PE was added to label all white blood cells and 2µL of Hoechst stain was added to label all nuclei and allowed to incubate for at 30 minutes. The sample was then diluted to 5X with PBS, 1µm anti-

EpCAM particles were added to the blood at 10^6 particles/mL, and allowed to incubate for 2 hrs under gentle agitation. The solution was then injected over the magnetized chip loading patch using a syringe pump set to 50µL/min. Once injected through the chip, the cells were separated using a 5Hz ratchet and the chip was imaged at 10x magnification under DAPI and TRITC wavelengths.

Bibliography

1. Feynman RP. There ’ s Plenty of Room at the Bottom. *J Microeleciromechanical Syst*. 1992;1(1):60-66. doi:10.1109/84.128057.

2. Wang D, Bodovitz S. Single cell analysis: The new frontier in “omics.” *Trends Biotechnol*. 2010;28(6):281-290. doi:10.1016/j.tibtech.2010.03.002.

3. Liu X, Long F, Peng H, et al. Analysis of Cell Fate from Single-Cell Gene Expression Profiles in C. elegans. *Cell*. 2009;139(3):623-633. doi:10.1016/j.cell.2009.08.044.

4. Miltenyi Biotec - Biomedical instruments, reagents, and services. http://www.miltenyibiotec.com/en/. Accessed April 22, 2015.

5. CellSearch. No Title. https://www.cellsearchctc.com/. Accessed April 9, 2015.

6. Campbell JDM. Detection and enrichment of antigen-specific CD4+ and CD8+ T cells based on cytokine secretion. *Methods*. 2003;31(2):150-159. http://www.ncbi.nlm.nih.gov/pubmed/12957573. Accessed July 31, 2015.

7. Kunze A, Tseng P, Godzich C, et al. with Nanomagnets on a Chip. *ACS Nano*. 2015. doi:10.1021/nn505330w.

8. Tseng P, Judy JW, Di Carlo D. Magnetic nanoparticle–mediated massively parallel mechanical modulation of single-cell behavior. *Nat Methods*. 2012. doi:10.1038/nmeth.2210.

9. Chou R, Cuevas C, Fu R, et al. Imaging Techniques for the Diagnosis of Hepatocellular Carcinoma: A Systematic Review and Meta-analysis. *Ann Intern Med*. 2015;162(10):697-711. doi:10.7326/M14-2509.

10. Choi J-W, Oh KW, Thomas JH, et al. An integrated microfluidic biochemical detection system for protein analysis with magnetic bead-based sampling capabilities. *Lab Chip*. 2002;2(1):27-30. doi:10.1039/b107540n.

11. Tokarev A, Aprelev A, Zakharov MN, Korneva G, Gogotsi Y, Kornev KG. Multifunctional magnetic rotator for micro and nanorheological studies. *Rev Sci Instrum*. 2012;83(6):065110. doi:10.1063/1.4729795.

12. Malouin BA, Vogel MJ, Olles JD, Cheng L, Hirsa AH. Electromagnetic liquid pistons for capillarity-based pumping. *Lab Chip*. 2011;11(3):393-397. doi:10.1039/c0lc00397b.

13. Van Reenen A, de Jong AM, den Toonder JMJ, Prins MWJ. Integrated lab-on-chip biosensing systems based on magnetic particle actuation--a comprehensive review. *Lab Chip*. 2014;14(12):1966-1986. doi:10.1039/c3lc51454d.

14. Zhu G-P, Hejiazan M, Huang X, Nguyen N-T. Magnetophoresis of diamagnetic microparticles in a weak magnetic field. *Lab Chip*. 2014;14(24):4609-4615. doi:10.1039/c4lc00885e.

15. Jain KK. Nanodiagnostics: application of nanotechnology in molecular diagnostics. *Expert Rev Mol Diagn*. 2003;3(2):153-161. doi:10.1586/14737159.3.2.153.

16. Jain KK. Nanotechnology in clinical laboratory diagnostics. *Clin Chim Acta*. 2005;358(1-2):37-54. doi:10.1016/j.cccn.2005.03.014.

17. Meier S, Pütz G, Massing U, et al. Immuno-magnetoliposomes targeting activated platelets as a potentially human-compatible MRI contrast agent for targeting atherothrombosis. *Biomaterials*. 2015;53:137-148. doi:10.1016/j.biomaterials.2015.02.088.

18. Saritas EU, Goodwill PW, Croft LR, et al. Magnetic particle imaging (MPI) for NMR and MRI researchers. *J Magn Reson*. 2013;229:116-126. doi:10.1016/j.jmr.2012.11.029.

19. Calhoun R, Yadav A, Phelan P, Vuppu A, Garcia A, Hayes M. Paramagnetic particles and mixing in micro-scale flows. *Lab Chip*. 2006;6(2):247-257. doi:10.1039/b509043a.

20. Kose AR, Koser H. Ferrofluid mediated nanocytometry. *Lab Chip*. 2012;12(1):190-196. doi:10.1039/c1lc20864k.

21. Kim KS, Park J-K. Magnetic force-based multiplexed immunoassay using superparamagnetic nanoparticles in microfluidic channel. *Lab Chip*. 2005;5:657-664. doi:10.1039/b502225h.

22. Zigeuner RE, Riesenberg R, Pohla H, Hofstetter A, Oberneder R. Isolation of circulating cancer cells from whole blood by immunomagnetic cell enrichment and unenriched immunocytochemistry in vitro. *J Urol*. 2003;169:701-705. doi:10.1016/S0022-5347(05)63996-1.

23. Abts H, Emmerich M, Miltenyi S, Radbruch A, Tesch H. CD20 positive human B lymphocytes separated with the magnetic cell sorter (MACS) can be induced to proliferation and antibody secretion in vitro. *J Immunol Methods*. 1989;125(1-2):19-28. doi:10.1016/0022-1759(89)90073-2.

24. Curti G, Skowronek F, Vernochi R, et al. Morphological evaluation of sperm from infertile men selected by magnetic activated cell sorting (MACS). *Reprod Biol*. 2014;14(4):289-292. doi:10.1016/j.repbio.2014.07.002.

25. Shevkoplyas SS, Siegel AC, Westervelt RM, Prentiss MG, Whitesides GM. The force acting on a superparamagnetic bead due to an applied magnetic field. *Lab Chip*. 2007;7:1294-1302. doi:10.1039/b705045c.

26. Dynabeads® CD34 Positive Isolation Kit. https://tools.lifetechnologies.com/content/sfs/manuals/dynabeads_CD34_cellsection_man.pdf. Accessed May 16, 2015.

27. Pamme N, Wilhelm C. Continuous sorting of magnetic cells via on-chip free-flow magnetophoresis. *Lab Chip*. 2006;6(8):974-980. doi:10.1039/b604542a.

28. Adams JD, Kim U, Soh HT. Multitarget magnetic activated cell sorter. *Proc Natl Acad Sci U S A*. 2008;105(47):18165-18170. doi:10.1073/pnas.0809795105.

29. Lou X, Qian J, Xiao Y, et al. Micromagnetic selection of aptamers in microfluidic channels. *Proc Natl Acad Sci U S A*. 2009;106(9):2989-2994. doi:10.1073/pnas.0813135106.

30. Oh SS, Ahmad KM, Cho M, Kim S, Xiao Y, Soh HT. Improving aptamer selection efficiency through volume dilution, magnetic concentration, and continuous washing in microfluidic channels. *Anal Chem*. 2011;83(17):6883-6889. doi:10.1021/ac201269f.

31. Janssen XJA, van IJzendoorn LJ, Prins MWJ. On-chip manipulation and detection of magnetic particles for functional biosensors. *Biosens Bioelectron*. 2008;23(6):833-838. doi:10.1016/j.bios.2007.08.023.

32. Rinklin P, Krause H-J, Offenhäusser A, Wolfrum B. On-Chip 3-dimensional control of microparticles for lab-on-a-chip applications. In: *NanoBio Europe 2013*.; 2013. http://www.researchgate.net/publication/270576165_On-Chip_3-dimensional_control_of_microparticles_for_lab-on-a-chip_applications. Accessed May 18, 2015.

33. Chen P, Huang Y-Y, Hoshino K, Zhang JXJ. Microscale Magnetic Field Modulation for Enhanced Capture and Distribution of Rare Circulating Tumor Cells. *Sci Rep*. 2015;5:8745. doi:10.1038/srep08745.

34. Yellen BB, Erb RM, Son HS, Hewlin R, Shang H, Lee GU. Traveling wave magnetophoresis for high resolution chip based separations. *Lab Chip*. 2007;7:1681-1688. doi:10.1039/b713547e.

35. Yellen BB, Virgin LN. Nonlinear dynamics of superparamagnetic beads in a traveling magnetic-field wave. *Phys Rev E - Stat Nonlinear, Soft Matter Phys*. 2009;80. doi:10.1103/PhysRevE.80.011402.

36. Gao L, Tahir MA, Virgin LN, Yellen BB. Multiplexing superparamagnetic beads driven by multi-frequency ratchets. *Lab Chip*. 2011;11:4214. doi:10.1039/c1lc20683d.

37. Tahir MA, Gao L, Virgin LN, Yellen BB. Transport of superparamagnetic beads through a two-dimensional potential energy landscape. *Phys Rev E - Stat Nonlinear, Soft Matter Phys*. 2011;84. doi:10.1103/PhysRevE.84.011403.

38. Chen A, Vieira G, Henighan T, et al. Regulating Brownian fluctuations with tunable microscopic magnetic traps. *Phys Rev Lett*. 2011;107. doi:10.1103/PhysRevLett.107.087206.

39. Henighan T, Chen A, Vieira G, et al. Manipulation of magnetically labeled and unlabeled cells with mobile magnetic traps. *Biophys J*. 2010;98(3):412-417. doi:10.1016/j.bpj.2009.10.036.

40. Murray C, Kong J, Tseng P, Carlo D Di. Microfabricated Magnetic Potential Well Arrays and Mechatronic System for Joystick-Based Massively Parallel

Manipulation of Magnetic Particles. In: Zengerle R, ed. Freiburg: μTAS; 2013:38-40. http://www.rsc.org/images/loc/2013/PDFs/Papers/014_0128.pdf.

41. Lim B, Reddy V, Hu X, et al. Magnetophoretic circuits for digital control of single particles and cells. *Nat Commun*. 2014;5:3846. doi:10.1038/ncomms4846.

42. Global Biochip Markets: Microarrays and Lab-on-a-Chip - BIO049E. http://www.bccresearch.com/market-research/biotechnology/biochip-markets-microarrays-bio049e.html. Accessed April 22, 2015.

43. Flow-cytometric analysis of rare antigen-specific T cells. *Cytometry A*. 2013;83(8):692-701. doi:10.1002/cyto.a.22317.

44. Vieira G, Chen A, Henighan T, Lucy J, Yang FY, Sooryakumar R. Transport of magnetic microparticles via tunable stationary magnetic traps in patterned wires. *Phys Rev B - Condens Matter Mater Phys*. 2012;85. doi:10.1103/PhysRevB.85.174440.

45. Dignat-George F, Sampol J. Circulating endothelial cells in vascular disorders: new insights into an old concept. *Eur J Haematol*. 2000;65(4):215-220. doi:10.1034/j.1600-0609.2000.065004215.x.

46. Schmidt DE, Manca M, Hoefer IE. Circulating endothelial cells in coronary artery disease and acute coronary syndrome. *Trends Cardiovasc Med*. 2015. doi:10.1016/j.tcm.2015.01.013.

47. Lozano R, Naghavi M, Foreman K, et al. Global and regional mortality from 235 causes of death for 20 age groups in 1990 and 2010: a systematic analysis for the Global Burden of Disease Study 2010. *Lancet*. 2012;380(9859):2095-2128. doi:10.1016/S0140-6736(12)61728-0.

48. Kolansky DM. Acute coronary syndromes: morbidity, mortality, and pharmacoeconomic burden. *Am J Manag Care*. 2009;15(2 Suppl):S36-S41. http://www.ncbi.nlm.nih.gov/pubmed/19355807. Accessed May 12, 2015.

49. Sbarbati R, De Boer M, Marzilli M, Scarlattini M, Rossi G, Van Mourik JA. Immunologic detection of endothelial cells in human whole blood. *Blood*. 1991;77(4):764-769. http://www.scopus.com/inward/record.url?eid=2-s2.0-0026013010&partnerID=tZOtx3y1.

50. Smith RJ, Koobatian MT, Shahini A, Swartz DD, Andreadis ST. Capture of endothelial cells under flow using immobilized vascular endothelial growth factor. *Biomaterials*. 2015;51:303-312. doi:10.1016/j.biomaterials.2015.02.025.

51. Chen K-C, Lee T-P, Pan Y-C, et al. Detection of circulating endothelial cells via a microfluidic disk. *Clin Chem*. 2011;57(4):586-592. doi:10.1373/clinchem.2010.157404.

52. Weaver WM, Tseng P, Kunze A, et al. Advances in high-throughput single-cell microtechnologies. *Curr Opin Biotechnol*. 2014;25:114-123. doi:10.1016/j.copbio.2013.09.005.

53. Edwards BS, Sklar LA. Flow Cytometry: Impact on Early Drug Discovery. *J Biomol Screen*. 2015. doi:10.1177/1087057115578273.

54. Königsberg R, Obermayr E, Bises G, et al. Detection of EpCAM positive and negative circulating tumor cells in metastatic breast cancer patients. *Acta Oncol*. 2011;50(5):700-710. doi:10.3109/0284186X.2010.549151.

55. Robert D, Pamme N, Conjeaud H, Gazeau F, Iles A, Wilhelm C. Cell sorting by endocytotic capacity in a microfluidic magnetophoresis device. *Lab Chip*. 2011;11(11):1902. doi:10.1039/c0lc00656d.

56. Ozkumur E, Shah AM, Ciciliano JC, et al. Inertial focusing for tumor antigen-dependent and -independent sorting of rare circulating tumor cells. *Sci Transl Med*. 2013;5(179):179ra47. doi:10.1126/scitranslmed.3005616.

57. Dharmasiri U, Balamurugan S, Adams AA, Okagbare PI, Obubuafo A, Soper SA. Highly efficient capture and enumeration of low abundance prostate cancer cells using prostate-specific membrane antigen aptamers immobilized to a polymeric microfluidic device. *Electrophoresis*. 2009;30(18):3289-3300. doi:10.1002/elps.200900141.

58. Punnoose EA, Atwal SK, Spoerke JM, et al. Molecular biomarker analyses using circulating tumor cells. *PLoS One*. 2010;5(9):e12517. doi:10.1371/journal.pone.0012517.

59. COATED MAGNETIC MICROPARTICLES and NANOPARTICLES - Spherotech. http://www.spherotech.com/coa_mag_par.htm. Accessed May 3, 2015.

60. Rao CG, Chianese D, Doyle G V, et al. Expression of epithelial cell adhesion molecule in carcinoma cells present in blood and primary and metastatic tumors. *Int J Oncol*. 2005;27(1):49-57. http://www.ncbi.nlm.nih.gov/pubmed/15942643. Accessed June 2, 2015.

61. Kuijpers TW, Tool AT, van der Schoot CE, et al. Membrane surface antigen expression on neutrophils: a reappraisal of the use of surface markers for neutrophil activation. *Blood*. 1991;78(4):1105-1111. http://www.bloodjournal.org/content/78/4/1105.abstract. Accessed May 18, 2015.

62. Sollier E, Go DE, Che J, et al. Size-selective collection of circulating tumor cells using Vortex technology. *Lab Chip*. 2014;14(1):63-77. doi:10.1039/c3lc50689d.

63. Shrirao AB, Hussain A, Cho CH, Perez-Castillejos R. Adhesive-tape soft lithography for patterning mammalian cells: application to wound-healing assays. *Biotechniques*. 2012;53(5):315-318. doi:10.2144/000113928.

64. Levy I, Bendet M, Samra Z, Shalit I, Katz J. Infectious complications of peripherally inserted central venous catheters in children. *Pediatr Infect Dis J*. 2010;29(5):426-429. doi:10.1097/INF.0b013e3181c94d9e.

65. Dimick JB, Pelz RK, Consunji R, Swoboda SM, Hendrix CW, Lipsett PA. Increased resource use associated with catheter-related bloodstream infection in

the surgical intensive care unit. *Arch Surg*. 2001;136(2):229-234. http://www.ncbi.nlm.nih.gov/pubmed/11177147. Accessed July 1, 2015.

66. Weaver WM. Investigating the Role of Mechanical Forces in the Catheter-Related Pathogenesis of Staphylococci, From Adhesion to Biofilm Formation. 2013. https://escholarship.org/uc/item/0749169d. Accessed August 6, 2015.

67. Chauhan A, Lebeaux D, Decante B, et al. A rat model of central venous catheter to study establishment of long-term bacterial biofilm and related acute and chronic infections. *PLoS One*. 2012;7(5):e37281. doi:10.1371/journal.pone.0037281.

68. Mirijello A, Impagnatiello M, Zaccone V, et al. Catheter-related bloodstream infections by opportunistic pathogens in immunocompromised hosts. *Eur Rev Med Pharmacol Sci*. 2015;19(13):2440-2445. http://www.ncbi.nlm.nih.gov/pubmed/26214780. Accessed August 6, 2015.

69. Hwang AA, Lee B-Y, Clemens DL, Dillon BJ, Zink JI, Horwitz MA. pH-Responsive Isoniazid-Loaded Nanoparticles Markedly Improve Tuberculosis Treatment in Mice. *Small*. 2015. doi:10.1002/smll.201500937.

70. Reardon S. Artificial spleen cleans up blood. *Nature*. 2014. doi:10.1038/nature.2014.15917.